CHAPTER 1: INTRODUCTION

1.1 Optics Communication

The total internal reflection principle which is responsible for guiding of light in optical fibers has been demonstrated since 1840s (Bates, 2001). The practical applications of this phenomena such as image transmission through tubes and then optical glass fiber is only realized in the 1950s (Hecht, 1999), when the glass fiber can be coated with a transparent cladding layer to suggest a more suitable refractive index in its guiding characteristics. Optical fibers have been demonstrated in 1970 for a short distance light transmission with an enormous loss of ~1000 dB/km for possible application in communication. However, by removing the impurities in the fiber material and offering pure silica, loss can be reduced to less than 20 dB/km in the same year (Kapron, *et al.*, 1970). This opens the possibility to use an optical fiber for long haul communication with many repeaters at spacing, which is comparable to that of electrical copper cable systems. Further progress in providing low-loss optical fibers led to the era of fiber-optic communications.

From 1978 onwards, single mode fiber (SMF) became available commercially (Sanferrare, *et al.*, 1987) for long distance communication application, which operates at the wavelength of ~800 nm. During the second generation of optical fiber, it had been realized that the repeater spacing could increase significantly by shifting the operating wavelength to the 1300 nm region, which has a lower loss of less than 1 dB/km and minimum dispersion. It had led to the using of InGaAsP hetero-junction laser diodes as optical sources. In the third generation system which operating in 1550 nm region, optical fiber operates at even a lower loss of about 0.2 dB/km (Miya, *et al.*, 1979). Due to the large dispersion in such wavelength region, the dispersion-shifted fiber was designed to have minimum dispersion. In addition, single-longitudinal-mode lasers operating near 1550 nm region was also introduced commercially in year 1990 to increase the system capacity up to 10 Gb/s bit rate (Nakagawa, 1995). Light wave systems operating at 1550 nm region has a problem that the signal had to be regenerated every 60-70 km distance by using electronic repeaters. In the fourth generation, optical amplifiers were used to replace the electronic repeaters. This amplifier was fabricated by doping an optical fiber with rare-earth elements such as Erbium to provide amplification in 1550 nm region via stimulated emission process. Then, the whole transmission and reception in communication system can be performed optically without any conversions to electrical signal. Optical amplifiers not only increased the repeater spacing but also introduced wavelength-division-multiplexing to raise the bit rate. It led to a so much cheaper inter-continental communication system an optical amplifier-based system. All in all, these developments has made it feasible that silica fiber carries large amount of information over long space and caused optical communication system as a backbone of today's telecommunication network system.

The emergence of multimedia systems, its various type of data transmission, and the internet had led to an explosion in traffic and bandwidth demand. One solution is using new fibers to increase the bandwidth of optical telecommunications network, but it is not cost effective. Another alternative in increasing the bandwidth is raising the capacity of fibers by the number of channel wavelength. Dense wavelength division multiplexing (DWDM) has the potential in transmitting large number of relatively closely spaced channels along an optical SMF. Employing optical amplifiers as a regenerator of channels without requiring de-multiplexing of individual channels in multi-channel light wave systems makes a revolution in the design of multi-wavelength optical systems. This creates a need for multi-wavelength light source.

The development of multi-wavelength fiber lasers based on nonlinear effects (Cowle, *et al.,* 1996) has indicated significant outcomes that it could be implemented as a laser source of DWDM (dense wavelength division multiplexing) system in optical telecommunication network system. Fiber laser applies an optical fiber doped with rare earth elements as the active gain medium. This optical fiber doped with elements such as erbium, thulium, and ytterbium also provides light amplification without lasing which is known as the doped fiber amplifier. Today, Bismuth-based Erbium doped fiber (Bi-EDF) can be employed as the gain medium for both amplifiers and fiber lasers instead of the conventional silica-based erbium doped one. This is attributed to the Bi-EDF, which is capable to be doped with high Erbium ions concentration without causing any deleterious ion quenching and clustering effects (Harun, *et al*., 2008a). Recently, many new fibers such as photonic crystal fibers (PCFs), highly nonlinear fibers, Bi-EDFs and dispersion compensating fibers were developed and studied for various applications. In these fibers, zero dispersion wavelength shifts toward the visible band and their nonlinearity increased due to the relatively small core size (Knight, *et al.,* 1996; Broeng, *et al.,* 1999; Monro, *et al.*, 1999 and Koyamada, *et al.,* 2004).

PCF is a microstructure fiber which is constructed based on a single material with a periodic array of air and holes running along the entire length (Russel, 2003). PCFs are designed with small core size and large air-filling fraction so that it can confine light tightly in the core. Therefore they have an extremely small effective mode area A_{eff}. The research on these fibers has attracted a great attention recently due to their special optical properties such as dispersion, polarization and nonlinearity. High nonlinearity per length can be observed by launching enough high intensity of light within the core of these fibers which is 10-100 times higher than that of the conventional fiber (Monro, *et al.,* 1999). The utilization of PCF would enable various nonlinear effects to happen by using only a relatively short length of fiber and at a modest pump power level. Fiber nonlinearities effects, such as stimulated Brillouin scattering (SBS) or four-wave-mixing (FWM) are also able to provide gain and hence, incorporated as a gain medium in a fiber laser configuration. Moreover, fiber optic amplifiers based on FWM have been also developed with an attractive attention because of its potential for ultrafast signal processing (Yaman, *et al.,* 2006). As multi-wavelength fiber lasers are devices which can be generated based on the nonlinear effects, incorporating PCFs as nonlinear gain media would be beneficial in the construction of efficient and compact fiber lasers in the real optical world applications. Therefore, nonlinear fiber optics has made a remarkable progress and it is expected to be considered as an effective and a significant research area in optical telecommunication network system.

1.2 Stimulated Brillouin scattering and its applications

When the light is propagating along the fiber, it can be scattered with same frequency as elastic scattering or with different frequency of inelastic scattering process. Rayleigh scattering is an elastic scattering which is one of the main loss factors in optical fiber (Born *et al.,* 1999 and Jenkins, *et al.,* 2001). There are other famous inelastic scatterings such as Brillouin and Raman scattering with the downshifted frequencies (Boyd, 2008). From quantum aspect, these inelastic scatterings can be explained as the conversion of a launched photon of the pump wave to a scattered photon with lower frequency regarding the Stokes wave. The energy difference appears as a phonon of induced acoustic wave to conserve the energy and momentum. The main difference between Raman and Brillouin scattering is on their generation process, which involves different types of phonons. Acoustic phonons originated by moving grating incorporate in Brillouin scattering whereas optical phonons caused by vibrations of medium molecules participate in Raman scattering. A different type of incorporating phonons in scattering process makes a basic difference; Raman scattering occurs in both forward and backward directions whereas Brillouin scattering happens mainly in the backward direction. These nonlinear effects are negligible if the incident pump power and interaction length are insufficient. However, the nonlinear effects such as SBS and stimulated Raman scattering (SRS) will be generated if the pump power is above the threshold level, which also dependent on the interaction length. The threshold power of SRS is normally much higher than that of SBS. Since the higher pump power wasn't available during this study, this research is concentrating on only the SBS nonlinear effect.

Brillouin scattering was discovered by Brillouin in 1922 through his report on the light scattering process resulted from thermally excited acoustic waves (Brillouin, 1922). Later Gross (1930) experimentally confirmed the Brillouin's prediction by using liquids and crystals as the Brillouin gain media. The observation of SBS effect also became possible by the reinforcing of the backscattered Brillouin light after lasers invention in 1964 (Chiao, *et al.*, 1964). Nonlinear effects such as SBS can be detrimental with a considerable effect on the performance of the optical systems. SBS effect generates Stokes wave by depleting the launched light pump power. It also can make Brillouin induced cross talk effect in an optical multi-wavelength communication system. In SBS phenomenon, these effects happens by converting the portion of incident channel power to the neighboring longer wavelength channel with wavelength difference of about 0.08 nm spacing (about 11 GHz). However, the channel spacing must be almost the Brillouin shift of around 11 GHz in silica fiber and the channels also must counter propagates to cause the Brillouin-induced cross talk. Therefore, Brillouin crosstalk can be easily avoided with employing a proper structure of multi-wavelength communication systems (Christodoulides, *et al.,* 1996 and Ho, 2000). Although SBS with generating crosstalk doesn't effect on the channels propagating in the same direction, it can be harmful by the way of depleting the transmitted channel power due to the very low threshold power. This is attributed to the Brillouin threshold power, which is only about a few miliwatts, within the output power of the communication laser diodes. Several methods have been applied for suppressing SBS by raising the Brillouin threshold power that are rely on increasing either the Brillouin gain bandwidth or the spectral width of the optical channel waves (Horiuchi, *et al.,* 1998 and Lee, *et al.,* 2001 (b)).

On the other hand, SBS phenomenon can be used to advantage. For example, it can be used to amplify an optical light wave by converting energy from a pump beam to the light wave, whose wavelength is properly chosen (Headly, *et al.,* 2005 and Strutz, *et al.,* 2001). Indeed SBS can also be applied for constructing fiber sensors to measure temperature and strain variations over a relatively long distance. This is attributed to the fact that the Brillouin shift is dependent on refractive index of the fiber which varies with the local environment changes such as temperature and pressure (Parker, *et al.,* 1998 and Cho, *et al.,* 2005). Another most interesting applications of SBS is Billouin fiber lasers (BFL) or Brillouin Erbium fiber lasers (BEFL) which have been studied with a great attention since it was proposed as early as 1976 (Hill, *et al.,* 1976; Bayvel, *et al.,*1989; Smith, *et al.,* 1991 and Geng, *et al.,* 2008). In these type of lasers, a standard SMF or a highly nonlinear fibers was used as the nonlinear Brillouin gain medium. In some cases, the lasers are constructed by applying any optical fiber doped with rare-earth elements of erbium (Tausenev, *et al.,* 2008), and ytterbium (Shen, *et al.,* 2004) as both nonlinear and linear gain medium. A laser with Erbium doped fiber (EDF) or hybrid of EDF and SMF i is denoted as BEFL. The laser signals generated by a BEFL operate just in a special wavelength region provided by optical doped fiber characteristics in the cavity. The BEFL normally operates at 1550 nm wavelength region; hence it can be used for communication application. Since BFL and BEFL generates laser with extremely narrow linewidth which could be a few Hz (Smith, *et al.,* 1991 and Geng, *et al.*, 2006) and due to the low intensity noise, low frequency noise specifications it can also used in coherent lidar detection, interferometric sensing material processing, and medicine (Hack, 2003; Koroshetz, 2005; Polynkin, *et al.,* 2007 and Polynkin, *et al.*, 2007). The main advantages of BFLs are their very high coherency, low threshold, and high efficiency besides the directional sensitivity of the Brillouin gain, which are important for many applications. Among all these applications, the generation of multiwavelength laser by cascading process of Brillouin Stokes is one of the most popular topic in current research. This source has a potential application in wavelength-division-multiplexing (WDM) transmission optical systems.

1.3 Brillouin Fiber Lasers (BFLs)

Fiber lasers are lasers where the active gain medium is an optical fiber , although some lasers with a semiconductor gain medium (a semiconductor optical amplifier) and a fiber resonator have also been known as fiber lasers (or semiconductor fiber lasers). Fiber laser is pumped by a laser denoted as a pump with a spectral wavelength selection of radiation. The gain medium can be an optical fiber doped with rare-earth ions such as Erbium (Er^{3+}), Neodymium (Nd^{3+}), Thulium (Tm^{3+}), and Ytterbium (Yb^{3+}) pumped by some laser diodes to amplify as a gain media in these fibers. The Brillouin nonlinear gain can also be used to provide fiber laser known as BFL which can be radiated any wavelength once the Brillouin pump is prepared. The BFL oscillates once the Brillouin pump (BP) power exceeds a certain power called the SBS threshold power. A suitable design must be considered for adding a feedback to a SBS system in the form of a Fabry-Perot (linear) cavity or a ring cavity (Agrawal, 2007 and Cowle, *et al*., 1997). In order to provide a proper BFL oscillation inside the cavity, Brillouin Stokes amplification must over-compensate the cavity loss. The BFL will radiate at a frequency shifted from the BP frequency due to the Doppler effect in the backward scattered light through moving grating acoustic waves generated in electrostriction phenomenon.

Another fiber laser is the hybrid of Brillouin and Erbium incorporated in the fiber laser construction denoted as BEFL which manipulates the nonlinear Brillouin gain in a fiber with the linear gain from EDF as an amplifier to yield laser source with the BFL specifications and the large output power from EDFA (Cowle, et al., 1996a). BEFLs are capable of generating optical multiwavelength, which is also known as multi-wavelength Brillouin Erbium fiber lasers (MBEFLs), with channel spacing about 10 GHz at room temperature due to the Brillouin Stokes-shifted frequency from the incident Brillouin pump. Such combs with higher number of lines in comparison with MBFLs (multiwavelength Brillouin fiber laser) have been used as sources for DWDM systems (Cowle, *et al*., 1996b and Zhan, *et al*., 2005).

1.4 FWM effect and FWM-based fiber laser

FWM phenomenon arises from the interaction of two or more coherent optical waves through the third order nonlinear susceptibility denoted as the optical Kerr effect such that produces the fourth signal. Generally FWM happens when light of two or three different wavelengths is launched into a fiber, giving rise to a wave of new

wavelength known as an idler. This effect is a strongly dependent on the relative phases of all incident signals. This process can efficiently accumulate along the optical fibers only if a phase-matching condition is satisfied. This condition can be feasible if the frequencies involved of launched signals are close to each other, or if the chromatic dispersion spectra has a suitable shape. Moreover, it is difficult to fulfill the phase matching condition over a relatively long length of fiber. Therefore, the FWM-based devices focus on incorporating highly nonlinear fibers such as dispersion-shifted fiber (Gross, *et al.*, 1930), highly nonlinear fiber and photonic crystal fiber (Yusoff, 2004; Belardi, *et al.*, 2002 and Aso, *et al.*, 2000). Since these types of fibers have a considerable nonlinear coefficient, using just a short length can be sufficient to provide an efficient FWM effect.

Although FWM is detrimental for signal transmission in the DWDM network systems, but it provides an effective technological basis for optical fiber devices. This phenomenon has capability of the basic technology to measure the nonlinearity and chromatic dispersion of fiber. This phenomenon have also proven to be of utility in many numbers of applications in optical systems, phase conjugate optics, and the measurement of atomic energy structures and decay rates. FWM effect is a kind of optical parametric oscillation and it is also able to generate multi-wavelength laser for WDM applications (Sharping, *et al.*, 2001). Multi-wavelength fiber laser can be obtained with a more stable output and wider tenability using highly nonlinear fibers.

1.5 Multi-wavelength Laser

Transmitting data at lower rates over multiple fibers can be converted to the transmitting at higher rates over a single fiber by applying channel multiplexing technique which makes a larger capacity of the transmission. One of the major concerns in optical transmission systems is the ultimate transmission capacity which critically depends on the temporal and spectral characteristics of light. This dependence leads to a time-division multiplexing (TDM) and WDM technology. There are some more physical limitations in applying WDM technique such as nonlinear effects of self-phase modulation (SPM), cross-phase modulation (CPM), SBS, SRS, FWM and parametric generation (Kim et al., 1993).

Early WDM system, denoted as wideband WDM, started the applying of the two widely spaced in the 1310 nm and 1550 nm wavelengths. Later, the narrow-band WDM as the second generation of WDM system was provided by incorporating two to eight wavelengths spaced at an interval of nearly 400 GHz in the 1550 nm region in 1990s (Derickson, 1998). Today, using multimedia applications such as TV, video conferencing and internet causes an unprecedented need for having higher capacity. Therefore, a DWDM system has to be introduced with a higher capacity which enables to provide a considerable number of wavelengths with precise wavelength spacing, every wavelength with very narrow bandwidth, and extremely little drift due to environmental condition tolerance during the multi-wavelength operation (Fiber System-Technology survey, 1999).

Several researchers have studied Erbium doped fiber lasers (EDFLs) to produce multiwavelength lasers with a constant wavelength spacing. One process was that EDF were cooled by liquid nitrogen to prevent mode competition between the adjacent laser lines and homogeneous broadening of lasing modes (Desurvive, *et al.*, 1990). In order to obtain inhomogeneous broadening, twin-core EDF has been used to produce a triple frequency EDFL (Graydon, *et al*., 1996). The other method which has attracted a great attention is generating a comb of laser lines knows as multiwavelength laser based on Brillouin or FWM nonlinear effects, known as multi-wavelength Brillouin fiber laser (MWBFL) or multi-wavelength fiber laser (MWFL) (Sun, *et al*., 2000), multi-wavelength Raman lasers (Yamada, *et al*., 2001 and Koch *et al*., 2001) and multi-wavelength generation incorporating semiconductor optical amplifiers (SOA) (Pleros, *et al*., 2002). To meet the mentioned demand of WDM system, the proposed multiwavelength laser has to operate with a high signal to noise ratio and flat channel power with a considerable stability. Generally, in order to produce the multiwavelength, we have to employ intra-cavity filter in the EDFL cavity. In some works, a polarization controller (PC) is applied inside the cavity to control both the number of lasing lines and spacing of the multiwavelength channels (Desuvire, *et al.*, 1987 and Hill, *et al.,* 1976). All in all, multiwavelength laser is highly desirable due to the cost and size reduction, development of the system integration and compatible with optical communication networks.

1.6 Research Objectives

The main objective of this research is to investigate and demonstrate MWFLs based on nonlinear effects employing either Bi-EDF or PCF, or a hybrid of both for possible applications in DWDM systems. The Bismuth host glass is used in Bi-EDF which enables the fiber to be doped heavily with Erbium ions for use in a compact optical amplifier design. The Bi-EDF exhibits a relatively high fiber nonlinearity, which has the potential for realizing new nonlinear based devices such as multi-wavelength fiber laser with narrow linewidth. Therefore, one of the aims of this research is to study the Bi-EDF amplification characteristic as well as nonlinear characteristic so that it can be used to improve the performance of the nonlinear based multi-wavelength fiber lasers. Besides Bi-EDF, PCF also has proved unique guiding and enhancing optical nonlinear properties led to the demonstration of a number of nonlinearity-based devices. PCFs are a class of micro-structured fiber which possesses a solid core surrounded by a cladding region that is defined by a fine array of air holes that extend along the full fiber length. Hence, the other aim of this work is to propose new configurations for Brillouin and FWM based fiber laser configurations by employing a short length of PCF. To achieve this goal, a comprehensive study on the PCF nonlinear characteristics has also been done. At the end of this work, enhanced configurations of the multi-wavelength fiber laser are demonstrated to produce a flat and stable output lines as well as a constant spacing based on either SBS or FWM effects using either Bi-EDF or/and PCF.

1.7 Thesis Overview

This thesis comprehensively studies the PCF and Bi-EDF for applications in BEFL, BFL and FWM-based fiber laser which consists of 6 main chapters. The current chapter of this thesis presents a brief introduction on the fiber optics field which also includes the motivations and the objectives of this research. Chapter 2 gives an overview background on the fundamentals of the nonlinear fiber optics such as SBS and FWM effects as well as their applications in multi-wavelength fiber laser generation. It also introduces briefly the main characteristics of the Bi-EDF and PCF.

Chapter 3 describes numerically and experimentally nonlinear characterization of both PCF and Bi-EDF using a basic configuration. The pump power requirements, attainable gain and saturation characteristics of the SBS process are evaluated in PCF. The amplification and nonlinear characteristics of Bi-EDF are then investigated. In the end of this chapter, nonlinear effect of FWM is numerically and experimentally studied by incorporating two tunable laser sources in the configuration. The FWM efficiencies in both PCF and Bi-EDF are then estimated using the most common and basic experimental setup.

Chapter 4 demonstrates various new architectures for BFL using either PCF or Bi-EDF as the gain medium to reduce the threshold power of the SBS effect as well as to increase the efficiency of the BFL. A compact fiber laser set-up is also demonstrated using a 49 cm long Bi-EDF as the gain medium. Dual wavelength laser is then demonstrated applying 100 m long PCF. Fiber laser based on FWM is discussed at the end of this chapter using a Bi-EDF as the gain medium. Chapter 5 proposes advanced compact multi wavelength fiber laser structures based on SBS and FWM effects using both PCF and Bi-EDF. Compact configurations of BFL are investigated to achieve channels with different order of Brillouin spacing. Then, to provide the efficient and enhanced multi-wavelength laser, the hybrid nonlinear gain media of PCF and Bi-EDF has also been investigated and demonstrated. The results and analysis of these studies are summarized and concluded in chapter 6. The recommendation for further research work is also presented in this chapter. In appendix, some selected published papers during the PhD in which the author had actively involved is also included.

CHAPTER TWO: NONLINEAR EFFECTS IN OPTICAL FIBERS

2.1 Introduction

The tremendous growth of the data traffic and the internet has caused an enormous demand for transmission bandwidth for dense wavelength-division-multiplexed (DWDM) optical communication systems. Deployment of multi-channel laser source has become one of the prominent and possible solutions to meet the strong demand of higher capacities in optical network systems. The usable spectral band for a WDM system strongly depends on the linear and nonlinear gain provided by the fiber amplifiers. The linear and nonlinear terms in optics, mean intensity independent and intensity dependent phenomena, respectively. When high intensity light passes through optical fibers or bulk materials, various nonlinear effects may be observed (Agrawal, 2001). The nonlinear effects commonly observed are second harmonic generation (SHG), third harmonic generation (THG), four-wave mixing (FWM), stimulated Raman scattering (SRS), stimulated Brillouin scattering (SBS), and many others. Nonlinear effects are related to the inharmonic motion of the bound electrons under the influence of an applied electromagnetic field.

Since the silica-based transmission fibers have a wide-band operating window ranging from 1400 - 1700nm, optical amplifiers with a wider amplification bandwidth are required to cover all these ranges for DWDM systems. In order to extend the wavelength range, several glass hosts such as tellurite (Wang, *et al.* 2008), multi-component silicate (Ellison, *et al.* 1999), and Bismuth oxide based glass (Tanabe, *et al.* 2000) have been developed. Now a days, Bismuth-based Erbium-doped fibers (Bi-EDFs) have been extensively studied for use in compact amplifiers with short gain medium lengths. These fibers incorporate Lanthanum (La) ions to decrease the concentration quenching of the Erbium ions in the fiber (Shahia, 2009), which in turn allows the Erbium ion concentration to be increased to above 1000 ppm. A fiber with such a high Erbium dopant concentration is expected to have enormous potentials in realizing compact EDFAs and EDFA-based devices. Additionally, the advent of small-core photonic crystal fibers (PCFs) with their unique guiding properties and increased optical nonlinearities led to the demonstration of a number of nonlinear-based devices (Ju, 2004; Wang, 2008). In PCFs with a solid silica core, the guidance mechanism is somewhat similar to the total internal reflection that occurs in conventional fibers, except that the effective cladding index is an appropriate average of the air and silica refractive indices. The PCF is used to significantly reduce the length of nonlinear gain medium. The nonlinear based fiber lasers configurations can be implemented based on the Erbium gain or without Erbium in the main structure.

In this chapter, the physics governing the process of nonlinear effects in optical fiber is presented especially SBS and FWM effects in optical fiber waveguides starting with Maxwell’s equations. One of the main applications of nonlinear effects in optical fiber is fiber laser to generate a laser source. The operation principle and the characteristics of fiber laser based on nonlinear effects will be investigated in this chapter with presenting a literature survey on the experimental analysis, measurements, and applications of nonlinear fiber laser. Generally, this chapter reviews the nonlinear effects that occur in a typical SMF and some background information about Bi-EDF and PCF.

2.2 Origin of Nonlinear effects in optical fiber

The nonlinear phenomena are studied by considering the electromagnetic wave theory in optical waveguides as dispersive nonlinear media. The wave equations of light propagating in a medium can be obtained by Maxwell's equations in a dielectric material with no free currents or charges as follows (Jackson, 1998):

$$\nabla . \mathbf{B} = 0 \tag{2.1}$$

$$\nabla . \mathbf{D} = 0 \tag{2.2}$$

$$\nabla \times \mathbf{H} = \frac{\partial \mathbf{D}}{\partial t} \tag{2.3}$$

$$\nabla \times \mathbf{E} = -\frac{\partial \mathbf{B}}{\partial t} \tag{2.4}$$

Where **B**, **E**, **D** and **H** denote magnetic field, electric field, Electric displacement field, magnetizing field, respectively. A dielectric medium exposed in the presence of an electric field can be anticipated as a grouping of dipoles bound together for representing electrons with ion nuclei. Along the field propagation through the material, negatively charged electrons move against the launched field while positively charged ions move with the field. The lattice forming the solid dielectric constrains the charged particles which can be evenly distributed in any directions or in some certain direction stronger than others to form an anisotropic material.

As the incident field interacts with the material, oscillation among the bound dipoles happens. The polarization **P** of the material is denoted as the dipole moment per unit volume, and the electric displacement is then defined as:

$$\mathbf{D} = \varepsilon_0 \mathbf{E} + \mathbf{P} \tag{2.5}$$

where ε_0 is the permittivity of free space. The polarization of the material influenced by the radiation in optical region dominantly and strongly arises from the motions of the electrons, because the nuclei are much more massive than the electrons. In case that the incident field amplitude is small, electrons oscillates with the same frequency of the incident field. As high enough field amplitude interacts with material, the electrons motions begin to deviate from the used field and the polarization vector consists of frequencies not included in the launched field (Boyd, 2003). The material's polarization is represented by an expansion series of the electric field as follow:

$$\mathbf{P} = \varepsilon_0 \left[\chi^{(1)} + \chi^{(2)}\mathbf{E} + \chi^{(3)}\mathbf{E}\mathbf{E} + \ldots \right] \mathbf{E} \tag{2.6}$$

where $\chi^{(1)}$ represents the linear susceptibility of the material, and the nonlinear susceptibilities are denoted by $\chi^{(2)}$, $\chi^{(3)}$, and successive higher orders. The first-order polarization represents a linear material response to the applied field as follows:

$$\mathbf{P}^{(1)} = \varepsilon_0 \chi^{(1)} \mathbf{E} \tag{2.7}$$

The resulting electric displacement from a linear material polarization is

$$\mathbf{D} = \varepsilon_0 (1 + \chi^{(1)}) \mathbf{E} \tag{2.8}$$

The relation between the induced polarization **P** of the material and the incident electric field **E** is expressed in the following equation as a function of the electric field,

$$\mathbf{D} = \varepsilon_0 (1 + \chi^{(1)} + \chi^{(2)}\mathbf{E} + \chi^{(3)}\mathbf{E}\mathbf{E} + \ldots) \mathbf{E} \tag{2.9}$$

where $\chi^{(1)}$ is a 2nd rank tensor, $\chi^{(2)}$ is a 3rd rank tensor, $\chi^{(3)}$ is a 4th rank tensor, etc.

The value of $\chi^{(2)}$ is zero in any isotropic and centrosymmetric material such as glasses, liquids, and gases which is left invariant in the form under inversion. The electric displacement is caused by the first and third-order susceptibility terms. Consequently, $\chi^{(2)}$ diminishes in silica glasses made by symmetrical molecules of SiO_2. For more simplification, terms higher than fourth order can be neglected and $\chi^{(1)}$ converts to a scalar function represented by the index of refraction where $n^2 = 1 + \chi^{(1)}$ (Boyd, 2003). With vanishing of both $\chi^{(2)}$ and $\chi^{(4)}$, the nonlinear susceptibility in an isotropic material can be approximated by the lowest order nonlinear effects originate from $\chi^{(3)}$ term in the expansion of Equation (2.6). With these approximations, Equation (2.9) becomes

$$\mathbf{D} = \varepsilon_0 (1 + \chi^{(1)} + \chi^{(2)}\mathbf{E} + \chi^{(3)}\mathbf{EE})\mathbf{E} = \varepsilon\mathbf{E} + \mathbf{P}^{(3)} \tag{2.10}$$

where $\mathbf{P}^{(3)} = \varepsilon_0 \chi^{(3)}\mathbf{EEE}$, and ε is the first-order permittivity of the material. Then for materials exhibiting a non-negligible Kerr effect, the 3rd order susceptibility, $\chi^{(3)}$, is responsible for the phenomena such as third harmonic generation, nonlinear refraction and FWM.

The nonlinear effects happened based on the 3rd order susceptibility $\chi^{(3)}$ that are divided in two named categories. Firstly, this mentioned phenomena will be elastic such that there is no energy exchanged between the matter and the incident electromagnetic field. Since, the refractive index of the material depends on the incident light intensity, some nonlinear effects as self-phase modulation (SPM), cross-phase modulation (XPM) and FWM happens depending on the type of input signal, as shown in Figure 2.1. Secondly, the inelastic scattering effect can also occur due to the third-order effects. This category of nonlinear effects are known as SBS and SRS in which part of the optical field energy is transferred to the nonlinear medium.

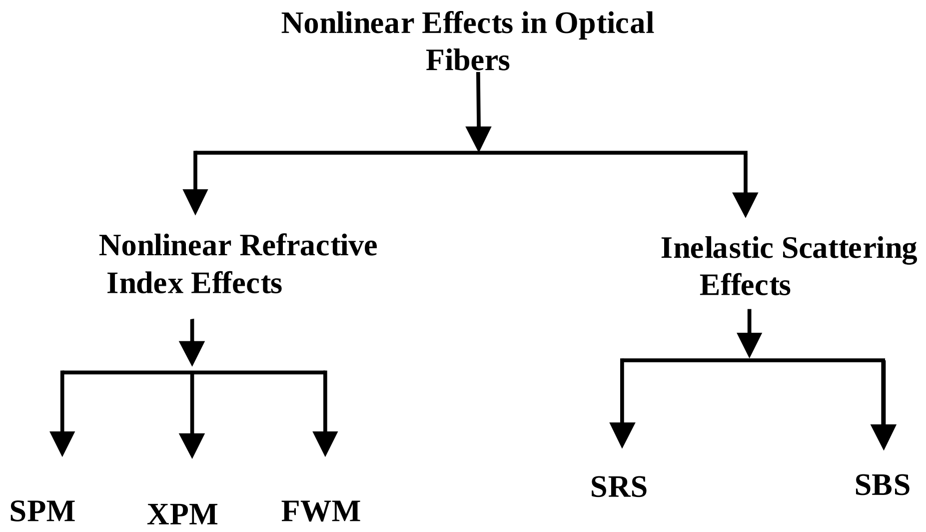

Figure 2. 1**:** Schematic of the nonlinear effects in fiber optics.

These phenomena can be explained quantum-mechanically as a scattering of a pump photon to a lower energy photon called a Stokes photon by generating a phonon with energy equal to the energy reduction of the initial photon. There are some main differences between these two inelastic scatterings of SBS and SRS which are strongly caused by the type of the involved interval modes. Firstly, SRS arises from the light interaction with the non-propagating vibration and rotational transitions in a single molecule as optical phonons modes in the lattice whereas SBS involves low-frequency propagating wave phonons as acoustic modes in it through electrostriction process. Second and fundamental difference is that major SBS is coherent and in the backward direction with respect to the incident launched light. However, SRS happens in both forward and backward directions incoherently although it dominates in the forward direction in the same way as the incident light direction. The third difference is that the downshifted scattered light frequency is approximately 10 GHz for SBS but 13 THz for SRS with respect to the incident light frequency in the single mode fibers. Finally, the Brillouin-gain spectrum bandwidth is less than 100 MHz which is very narrow when comparing with the Raman-gain spectrum bandwidth which is more than 20 to 30 THz (Diament, 1990) Since the threshold power of SBS in long haul fibers is low, SBS provides some harmful effects in optical fiber telecommunication network systems, however it has also been observed as a useful applications in Brillouin amplifiers, Brillouin/erbium fiber lasers (BEFL), Brillouin fiber lasers (BFL) which are of particular interest in this thesis and temperature sensors. The SRS requires a relatively high incident power as a threshold power which was not available in our lab. In the next sections, the nonlinear effects such as SBS and FWM which are relevant to this study are especially explained.

2.3 Principles of Stimulated Brillouin Scattering (SBS)

SBS is one of the important nonlinear effects in a SMF which can shift the input laser wavelength with certain frequency of the Brillouin shift. SBS is able to produce Brillouin Stokes cascading process such that it can generate a laser comb with dense constant spacing (Digonnet, 1993; Lamminpaa, 2003). Such laser comb is attractive and has potential to become a laser source in future DWDM development. SBS can be explained physically by a nonlinear interaction between the incident light as a Brillion pump wave, Stokes wave or Brillouin backscattered light, and an acoustic wave generated via electrostriction process. Through the electrostriction process, the pump signal give rise to acoustic wave by periodically modulating the refractive index of the medium**.** The principle of SBS generation in optical fibers is illustrated in Figure 2.2. The SBS was first discovered by Leon Brillouin in 1922 in bulk media (Brillouin, 1922) and then in 1972 in optical fibers and it has been considered extensively since then due to its effects for optical systems (Agrawal, 2001). Similar to SRS, Brillion scattered light also denotes as a Stokes wave whose frequency is downshifted from the incident launched wave with a mount depending on the type of nonlinear medium (Cotter, 1983). Hence, the energy of the launched high-frequency channel can be transferred to a low-frequency by SBS process with the channel spacing of the Brillouin shift.

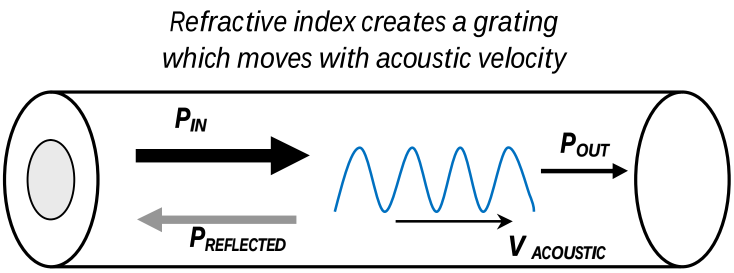

Figure 2. 2: Schematic plot of the SBS generation in optical fibers.

According to this fact that the scattered light frequency is very close to the incident signal frequency, acoustic phonons provides a relatively small frequency shift of about (~10 GHz or ~0.08 nm at 1550 nm) (Cotter, 1983). This small difference between the backscattered light and incident signal frequency is due to the Doppler shift associated with an induced grating propagating in the fiber at the acoustic velocity (Agrawal, 2001). Therefore, classically, the SBS process can be described as the Bragg grating reflection of light by a wave traveling through fiber, and ultimately incident light frequency is downshifted due to the optical Doppler effect. The acoustic wave is propagating along the medium or fiber at a velocity of V_a corresponding to a frequency of ω_a with the induced refractive index grating period. The pump frequency ω_p with the wave number of k_p will propagate through Bragg reflection grating which will be diffracted in a certain direction θ with frequency of ω_s, as shown in Figure 2.3.

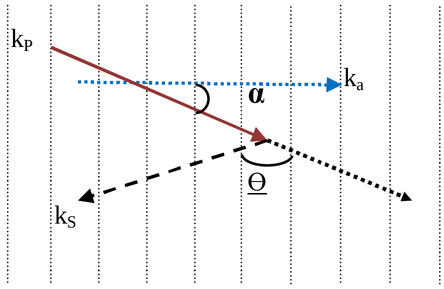

Figure 2.3: Diagram describes the principle in which SBS is generated.

Since during the Brillouin scattering the energy and linear momentum must be conserved, the frequencies and wave vectors can be related by the following equations:

$$\omega_{\mathrm{p}} = \omega_{\mathrm{s}} + \omega_{\mathrm{a}} \tag{2.11}$$

$$\mathbf{k}_{\mathrm{p}} = \mathbf{k}_{\mathrm{s}} + \mathbf{k}_{\mathrm{a}} \tag{2.12}$$

where the indices p, s, and a responsible for pump, scattered, and acoustic waves, respectively. As acoustic frequency is very small compared to the incident light frequency, $\omega_{\mathrm{a}} << \omega_{\mathrm{p}}, \omega_{\mathrm{s}}$, this simplification can be considered that $\omega_{\mathrm{p}} \approx \omega_{\mathrm{s}}$, $\mathrm{k}_{\mathrm{p}} = \mathrm{k}_{\mathrm{s}}$ and based on Figure 2.3 it can be concluded that:

$$\mathrm{k}_{\mathrm{a}}^2 = 4\mathrm{k}_{\mathrm{p}}^2 \sin^2\frac{\theta}{2} \tag{2.13}$$

where θ denotes the angle between the pump and scattered wave vectors.

According to the wavenumber and frequency relation as $k_a = \frac{\omega_a}{v_a}$, and $k_p = \frac{\omega_p}{v_p}$, it can be obtained as:

$$\omega_s = \omega_p (1 - 2\frac{v_a}{v_p} \sin\frac{\theta}{2}) \qquad (2.14)$$

where v_p refers to the pump light wave velocity. It is clear that the backscattered Brillouin frequency depends on the angle θ, the scattering angle. Hence, Brillouin frequency shift diminishes when the pump and scattered fields propagate in the same direction and has its maximum value of $2\frac{v_a}{v_p}\omega_p$ when the scattered Brillouin Stokes propagates in the opposite direction $(\theta = \pi)$ corresponding to the incident light propagation in optical fibers. When the incorporated medium is a typical type of single mode fiber, only the backward scattering is monitored in which the Brillouin frequency shift v_B is given by

$$v_B = \frac{\omega_a}{2\pi} = \frac{2n_e V_a}{\lambda_p} \qquad (2.15)$$

where n_e is the refractive index of the medium. For the typical kind of silica fiber which is made from SiO_2 mainly, it can be assumed that V_a = 5.96 km/s, n_e = 1.45 and λ_p =1.55μm, then from Equation 2.3, ν_B =11.2 GHz or Δλ≈ 0.09 nm as the Brillouin wavelength shift. To simulate the SBS nonlinear effect, the propagating signals equations studied along the fiber. This will be discussed in the remaining part of this section.

A material density function ρ [kg/m^3] which is satisfying the wave equation driven via electrostrictive process in position z and at time t can be written as (Boyd, 1990):

$$\frac{\partial\rho}{\partial t} + \frac{\Gamma_a}{2}\rho = i\Lambda E_p E_s^* \qquad (2.16)$$

where ρ (z, t) is responsible for the complex amplitude of the variation from the mean value ρ_0 in the fiber. The phonon intensity decay rate is referred to the Γ_a and the Brillouin coupling constant Λ will be introduced below. $E_s(z, t)$ and $E_p(z, t)$ are the complex optical fields amplitude of the backscattered Stokes and the pump waves along the Brillouin-active medium, which can be identified with the following equations:

$$\frac{\partial E_P}{\partial z} + \frac{n}{c}\frac{\partial E_P}{\partial t} = -\frac{\alpha}{2}E_p + ik\rho E_S \tag{2.17}$$

$$\frac{\partial E_S}{\partial z} - \frac{n}{c}\frac{\partial E_S}{\partial t} = -\frac{\alpha}{2}E_S - ik\rho^* E_P \tag{2.18}$$

The refraction index is n, the light speed is c, and α is the attenuation coefficient. It is worth noting that Stokes field is propagating in the negative z direction as assumed in this equation and the transverse variation of the pump and Stokes fields have been ignored (Agrawal, 2001). According to the reference (Boyd, 1990), the constants k and Λ are then defined as

$$k = \frac{\gamma_e \omega}{4\rho_0 nc} \tag{2.19}$$

$$\Lambda = \frac{\gamma_e q^2}{2nc\Omega} \tag{2.20}$$

The acoustic or sound wave frequency is related to the wave vectors of the pump and Stokes waves k_P and k_S by the relationship $\Omega = qv$, where $q = k_P + k_S \approx 2k = 2\omega n/c$ is the acoustic wavenumber (Boyd, 1990). The parameter $\gamma_e = \rho\ (\delta\varepsilon_r / \delta\rho)$ is denoted as the electrostrictive constant, where ε_r is the relative permittivity (Melloni, 1998).

In the steady state, all explicit derivatives respect to time t are set to zero so that the material density is modified as:

$$\rho = \frac{2}{\Gamma_a}(i\Lambda E_P E_S^*) \tag{2.21}$$

In order to solve the equations (2.17 - 2.18) and (2.16), it is common to consider that the pump, Stokes, and acoustic waves are plane waves traveling in the z direction along the fiber length (Yeniay, 2002).

$$\mathrm{E_p}(z,t) = \frac{1}{2}\mathrm{E_{0p}}(z)e^{i(\omega_p t - k_p z)} + c.c. \tag{2.22}$$

$$\mathrm{E_s}(z,t) = \frac{1}{2}\mathrm{E_{0s}}(z)e^{i(\omega_s t + k_s z)} + c.c. \tag{2.23}$$

in which c.c. denotes the complex conjugate of the first term with the assumption that the amplitudes E_{0p}, E_{0s} are not functions of time according to the steady-state regime. Substituting the pump and Stokes intensities, I_P and I_S which are defined based on the Equations (2.22 and 2.23) by substituting in Equations (2.17 and 2.18) results in the following coupled differential equations:

$$\frac{\mathrm{dI_p}}{\mathrm{dz}} = -g_B \mathrm{I_p I_s} - \alpha_\mathrm{p} \mathrm{I_p} \tag{2.24}$$

$$\frac{\mathrm{dI_s}}{\mathrm{dz}} = -g_B \mathrm{I_p I_s} + \alpha_s \mathrm{I_s} \tag{2.25}$$

where g_B, known as the Brillouin gain coefficient is:

$$g_B = \frac{4k\Lambda}{\Gamma_a} = \frac{\gamma_e^2 \omega^2}{\rho_0 n c^3 \nu \Gamma_a} \tag{2.26}$$

In a conventional single mode optical fiber, the Brillouin gain coefficient g_B will be divided by a factor of 1.5 due to randomly variation of the relative polarization angle between the pump and Stokes wave (Deventer, *et al*. 1994). By solving the SBS coupled equations, the most important factors characterizing SBS effect such as the threshold input power and sufficient active length of fiber can be obtained. Therefore, finding a technique or method to estimate the proper conditions of input pump power and fiber length is very significant and critical. In order to solve analytically the coupled equations of representing SBS effect, these transformations can be used as the following (Jenkins *et al.*, 2007) terms:

$$V = \mathrm{I_p} - \mathrm{I_s} \quad , \quad U = \mathrm{I_p} + \mathrm{I_s} \tag{2.27}$$

and

$$S = U^2 - V^2 \tag{2.28}$$

Such that the differential equations can be modified as

$$\frac{\mathrm{d}V}{\mathrm{dz}} = -\alpha U \tag{2.29}$$

$$\frac{\mathrm{d}U}{\mathrm{dz}} = -\frac{g_B}{2} S - \alpha V \tag{2.30}$$

Noting that $dS/dV = 2U(dU/dV) - 2V$, the coupled equations can be modified to the following equation:

$$\frac{\mathrm{dS}}{\mathrm{dz}} = \frac{g_B}{\alpha} S \frac{\mathrm{d}V}{\mathrm{dz}} \tag{2.31}$$

By a direct integration the last equation over the fiber length, a conservation relation will be considered as:

$$\mathrm{Ln(S)} - \frac{g_B}{\alpha} V = \left\{ \mathrm{Ln(S)} - \frac{g_B}{\alpha} V \right\}_{z=0} = \text{constant} \tag{2.32}$$

Therefore, U can be obtained in terms of V by transferring the Equation (2.31) to the exponential function as:

$$U = \sqrt{(U_0^2 - V_0^2)\exp[\frac{g_B}{\alpha}(V - V_0)] + V^2} \qquad (2.33)$$

where $V_0 = V(z=0)$ and $U_0 = U(z=0)$. Finally, from Equations (2.29) and (2.32), it is revealed that V can be obtained exactly by solving the following integration

$$\int_{x(0)}^{x(z)} \frac{\mathbf{dx}}{\sqrt{(U_0^2 - V_0^2)\exp[\frac{g_B}{\alpha}(x - V_0)] + x^2}} = -\alpha z \qquad (2.34)$$

Since it has not been any closed form solution for this integral so far, it should be solved numerically (Jenkins *et al.*, 2007). To solve these equations, it is convenient to consider some assumptions as ignoring the pump depletion term. In this approximation known as the no depletion pump, the pump intensity I_P is only a function of fiber loss. Due to the relatively small amounts of the acoustic wave frequency ω_a, it is assumed that $\omega_P \approx \omega_S$ and then $\alpha_p \approx \alpha_s \equiv \alpha$. In the case of a weak nonlinear coupling, such that $I_s << I_p$, the solutions of the coupled SBS Equations (2.75) and (2.76)

$$I_p(z) = I_p(0)\exp(-\alpha\ z) \qquad (2.35)$$

and

$$I_s(0) = I_s(L)\exp[(g_B P_0 L_{\text{eff.}} / A_{\text{eff.}}) - \alpha L)] \qquad (2.36)$$

In this relation, $P_0 = I_p(0)A_{\text{eff}}$ is denoted as the incident pump power, $A_{\text{eff.}} = \pi r^2$ is the effective core area of the Stokes wave in the optical fiber where <u>2r</u> is the mode field diameter of the beam, and L_{eff} is the effective interaction length defined as

$$L_{\text{eff.}} = \frac{1}{\alpha}[1 - \exp(-\alpha L)] \qquad (2.37)$$

The effective interaction length, L_{eff}, is slightly smaller than the actual fiber length L due to fiber linear loss. In the case that the fiber is very long, the approximation $\exp(-\alpha L) << 1$, for instance, the effective interaction length of a SMF with 25 km long is about

$$L_{\mathrm{eff}} \approx 1/\alpha \approx 22.86 \ (\mathrm{km}) \qquad (2.38)$$

where $\alpha = 0.19 \ (\mathrm{dB/km}) = 0.0437 \ (\mathrm{km})^{-1}$. The Equation (2.36) indicates how a Stokes signal grows exponentially in the backward direction along the active nonlinear medium due to the Brillouin amplification that happens as a result of SBS scattering. Hence, the described phenomenon is a SBS process in which the backward Brillouin Stokes input originates from spontaneous Brillouin scattering and Rayleigh scattering occurring within the fiber. It is evident that the assumption of ignoring the pump depletion breaks when the amount of I_s becomes a comparable level with that of the input pump intensity I_p.

One of the most significant features of the characterizing Brillouin scattering process is the SBS threshold power. For a common case, there is no Stokes input by another external laser at the end of the fiber. Brillouin scattering arises from thermal fluctuations in the density as spontaneous Brillouin scattering, threshold power defined analytically by Smith's definition. This definition assumes in the absence of pump depletion, threshold power is the input pump power at which the backscattered Stokes power is equal to the incident pump power (Smith, 1972):

$$\mathrm{P_{th}} \approx 21 \frac{\mathrm{A_{eff}}}{\mathrm{g_B^{(0)} L_{eff}}} \qquad (2.39)$$

In optical communication systems at 1550nm, the conventional values for optical single mode fibers are $\mathrm{A_{eff}} = 50\mu m^2$, $\mathrm{L_{eff}} \approx 21km$, and $g_B^{(0)} = 5\times10^{-11} \mathrm{m/W}$, Equation (2.39) results in $\mathrm{P_{th}} \approx 1\mathrm{mW}$. It is such a low threshold power that makes SBS a dominant nonlinear phenomenon in optical fibers.

2.4 Nonlinear refractive index effects

As described above, optical fiber responds nonlinearly under the influence of the high intensity due to the inharmonic motion of the medium bound electrons (Agrawal, 2007; Saleh *et al.*, 1999). A change in the refractive index of a medium in responding to an incident intense electric field is called Kerr effect. As it is relevant to this study, namely SPM, XPM and FWM caused by nonlinear Kerr effect will be described briefly.

SPM is one of the nonlinear optical effects caused by Kerr effect or the intensity dependence of the refractive index of medium. Indeed, SPM is defined as the self-induced phase shift which an ultrashort pulse signal experiences by travelling in a medium**.** To understand how the travelling electric field gives rise to the nonlinear phase shift, the incident electric field generally can be approximated as a plane wave in this form:

$$\mathbf{E}(\mathrm{r},\mathrm{t}) = \frac{1}{2}\hat{\mathrm{x}}\left[\mathbf{E}(\mathbf{r},\mathrm{t})\mathrm{e}^{-\mathrm{i}(\omega_0 \mathrm{t})} + \mathrm{c.c.}\right] \qquad (2.40)$$

where c.c. denotes complex conjugate, $\hat{\mathrm{x}}$ is the polarization unit vector of the incident light (considered as linearly polarized) and $\mathbf{E}(\mathbf{r}, t)$ is a slightly changing function of time.

The polarization related to the incident electric field can be indicated as follows:

$$\mathbf{P}_{\mathbf{L}}(\mathbf{r},\mathrm{t}) = \varepsilon_0 \chi^{(1)}.\mathbf{E}(\mathbf{r},\mathrm{t}) \qquad (2.41)$$

$$\mathbf{P}_{\mathbf{NL}}(\mathbf{r},\mathrm{t}) = \varepsilon_0 \chi^{(3)} \vdots \mathbf{E}(\mathbf{r},\mathrm{t})\mathbf{E}(\mathbf{r},\mathrm{t})\mathbf{E}(\mathbf{r},\mathrm{t}) \qquad (2.42)$$

It can be observed that $\mathbf{P}_{NL}$ has two main terms at frequencies of ω_0 and third harmonic frequency of $3\omega_0$ when Equation (2.40) is substituted into the Equation (2. 42). Since it is difficult to obtain the phase matching condition, the term of third harmonic frequency is ignored. Consequently, $\mathbf{P}_{NL}$ can be shown based on the other terms as follow:

$$\mathbf{P_{NL}}(\mathbf{r}, \mathrm{t}) \approx \varepsilon_0 \varepsilon_{NL} \mathbf{E}(\mathbf{r}, \mathrm{t}) \tag{2.43}$$

where ε_{NL} is the nonlinear term of the dielectric constant defined by :

$$\varepsilon_{NL} = \frac{3}{4} \chi^{\mathbf{3}}_{\mathbf{xxxx}} \left|\mathbf{E}(\mathbf{r}, \mathrm{t})\right|^2 \tag{2.44}$$

As a result, the total dielectric constant can be described as follow:

$$\varepsilon = \varepsilon_L + \varepsilon_{NL} \tag{2.45}$$

The dielectric constant can be substituted to describe the refractive index $n(\omega)$ and the absorption coefficient $\alpha\ (\omega)$ incorporating the definition of $\varepsilon = (\mathrm{n} + \mathrm{i}\ \alpha/2k_0)^2$ **.** As mentioned above, $n\ (\omega)$ depends on the launched light intensity due to the ε_{NL} and can be described as:

$$n(\omega) = n_0 + n_2 \left|E\right|^2 \tag{2.46}$$

And so the nonlinear phase shift is obtained by

$$\varphi_{NL}(t) = \frac{2\pi L_{eff}\, n_2}{\lambda} \left|E\right|^2 \tag{2.47}$$

where L_{eff} is effective fiber length by Equation (2. 37), n_2 is the nonlinear-index coefficient which its value can be around of 2.16×10^{-20} $\mathrm{m^2/W}$ (Agrawal, 2001). According to this equation the nonlinear phase shift is a function of effective area and incident pump power as well by this relation

$$\left|E\right|^2 = P / A_{eff} \tag{2.48}$$

Hence, higher value of φ_{NL} can be obtained by incorporating a fiber with smaller value of A_{eff} , longer L_{eff} and/or higher launched pump power. To find a suitable fiber, these factors play significant roles for generating nonlinear effects.

According to the equation (2.47) the time varying of nonlinear phase shift leads to a spectral modification of the transmitted pulse which typically makes the pulse shape broader. To look how the transmitted pulse spectrum is modified, the instantaneous frequency *ω (t)* of the pulse will be described by:

$$\omega(t) = \omega_0 + \delta\omega(t) \qquad (2.49)$$

in which

$$\delta\omega(t) = \frac{d}{dt}\varphi_{NL}(t) \qquad (2.50)$$

where *δω(t)* stands for the variation of the instantaneous frequency. Therefore, it can be observed that the spectrum frequency of the transmitted pulse will be modified by SPM nonlinear effect originated from Kerr effect. This nonlinear effect which causes the spectral broadening in optical fibers can realize many nonlinear devices as a nonlinear loop optical mirror (Petropoulos *et al.*, 2001), and optical 2R regenerator(Lee, *et al.*, 2001(a)).

In addition to the SPM which is a self-induced phase shift, there are some other nonlinear effects caused by the Kerr effect as XPM and FWM effects. XPM refers to the induced phase shift of an optical field propagating in a fiber caused by another optical field having either a different wavelength, or direction, or polarization form (Agrawal, 2001). However, in this explanation, the case of optical fields with different wavelengths is considered with the same state of the polarization and direction. FWM is also another nonlinear effects which occurs when two or more frequencies of optical fields propagate through a medium (Inoue, 1992). Provided that phase matching condition is satisfied, incident optical power can be converted and generate new frequencies. From the quantum mechanics perspective, FWM occurs when photons from one or more waves are annihilated and new photons are created at different frequencies such that the net energy and momentum are conserved (Agrawal, 2001). FWM caused by the third-order optical nonlinearity term can be explored by considering four optical fields at frequencies ω_1, ω_2, ω_3 and ω_4 which are linearly polarized and propagating along the same direction as the z axis. Then, the total electric fields propagating in the medium can be written as

$$\mathbf{E} = \hat{x}\frac{1}{2}\sum_{j=1}^{4} \mathrm{E}_{\mathbf{j}} \exp\left[i(k_j z - \omega_j t)\right] + c.c. \tag{2.51}$$

where $k_j = n_j \omega_j / c$, which n_j is the refractive index while c.c. refers for complex conjugate. By substituting Equation (2.51) in Equation (2.42), nonlinear polarization indicates the following form

$$\mathbf{P}_{NL} = \hat{x}\frac{1}{2}\sum_{j=1}^{4} \mathrm{P}_{\mathbf{j}} \exp\left[i(k_j z - \omega_j t)\right] + c.c. \tag{2.52}$$

where P_j includes a large number of terms which is involving the three terms of electric fields production. For example, P_4 can be represented as

$$\begin{aligned} \mathrm{P}_{\mathbf{4}} = \frac{3\varepsilon_0}{4}\chi^{3}_{xxxx}\,(&\left[\left|E_1\right|^2 + 2(\left|E_1\right|^2 + \left|E_2\right|^2 + \left|E_3\right|^2)\right]E_4 \\ &+ 2E_1E_2E_3\exp(i\theta_+) + 2E_1E_2E_3\exp(i\theta_-) + \ldots) \end{aligned} \tag{2.53}$$

$$\theta_+ = (k_1 + k_2 + k_3 - k_4)z - (\omega_1 + \omega_2 + \omega_3 - \omega_4)t \tag{2.54}$$

$$\theta_- = (k_1 + k_2 - k_3 - k_4)z - (\omega_1 + \omega_2 - \omega_3 - \omega_4)t \tag{2.55}$$

It is worth noting that the terms proportional to E_4 in Equation (2.53) stand for SPM and XPM nonlinear effects. The remaining terms which represent new waves at different frequencies are responsible for FWM effect. Since FWM is a phase-sensitive phenomenon, the efficiency strongly depends on the phase matching of the relative phases of E_4 and P_4 as shown by θ_+, θ_-. The term that includes θ_+ is responsible for a condition that three photons converting energy to a single photon at frequency $\omega_4 = \omega_1 + \omega_2 + \omega_3$. The term with θ_-

represents the case that two photons at frequencies ω_1 and ω_2 converting energy to the other photons at frequencies ω_3 and ω_4 such that

$$\omega_3 + \omega_4 = \omega_1 + \omega_2 , \tag{2.56}$$

Consequently, it leads to the phase-matching requirement as follow

$$\Delta k = k_3 + k_4 - k_1 - k_2 = (n_3\omega_3 + n_4\omega_4 - n_1\omega_1 - n_2\omega_2)/c = 0 \tag{2.57}$$

Dispersion is the key parameter that plays a significant role in satisfying the phase matching condition. Providing that zero-dispersion wavelength is localized in the middle among the four interacting waves, the phase matching condition will be fulfilled for a uniform zero-dispersion wavelength along the fiber (Inoue, 1992a). Besides the fiber dispersion, channel spacing of incident lights also affects the FWM efficiency. According to the dispersion variation with wavelength, the incident and generated waves are found to have different group velocities. This fact causes phase mismatching of the interacting waves and reduces the efficiency of the converting power to the new generated waves. The higher value of the group velocity and the wider value of the channel spacing provide the lower FWM efficiency. The generation of new frequency waves through FWM effect can induce crosstalk in WDM network system and limit its performance especially around the zero-dispersion wavelength. However, this process can also be useful to build nonlinear fiber devices such as wavelength converters (Inoue, *et al.*, 1992; Dorman *et al.*, 1999), phase conjugators (Yariv, *et al.*, 1979), optical parametric oscillator (OPO) (Sharping *et al.*, 2002) squeezing (Slusher *et al.*, 1985 and Levenson *et al.*, 1985), frequency metrology (Washburn *et al.*, 2004; Diddams *et al.*, 2001 and Jones *et al.*, 2000) and spectroscopy. Four-wave mixing in a dispersion-shifted fiber was used for yielding comb-like spectra (Chen *et al.*, 2010), and a rational harmonic fiber ring laser was successfully constructed

(Yu *et al.,* 2001). In this thesis, FWM will be applied to build a multi wavelength generation (comb-like spectrum) and will be discussed in the following chapters.

2.5 Nonlinear effects applications in optical fibers

The fiber optics research has progressed well recently especially in field of laser, communication network and sensors (Yu *et al.,* 2001; Huang *et al.,* 2010 and Sun *et al.,* 2010). Recently, the most common and significant nonlinear effects such as SBS and FWM plays key roles as possible solutions to meet the strong demand of higher capacities in WDM communication network. One of the main solutions is multi-wavelength (multi-channel) laser source to make the WDM cost-effective. Multi-wavelength fiber laser has many possible applications such as in DWDM systems and sensors. Today, Brillouin Erbium fiber lasers (BEFL) have been investigated extensively using various configurations to produce multiple wavelengths in both the C band and L band regions (Zhao *et al.,* 2010; Li *et al.,* 2010 and Liu *et al.,* 2009). Although it suffers the disadvantage of low tuning range due to homogenous effect in the Erbium doped fiber (EDF) that caused free running modes to oscillate in the laser's cavity. A number of different configurations of multi-wavelength BEFL in a ring and in a linear cavity have been proposed and demonstrated by many researchers (Doug *et al.,* 2010 and Liu *et al.,* 2009). To mitigate the limitation of tuning range, multi-wavelength Brillouin fiber laser (BFL) can be used, even though the use of BFLs has not been considered seriously because of the limited number of lasing lines and undesirable power flatness. To look how this laser source can be generated, firstly the characteristics of fiber laser should be investigated. In the next section, it will be discussed about the basic principle of the linear gain provided by EDF and nonlinear gain originated from the cascading of the SBS and FWM in a conventional single mode fiber.

2.5.1 Fiber laser principle

The primary and main purpose of optical fiber fabrication firstly was only about light transmission. This low loss light guiding property quickly results in other applications such as optical amplifiers and fiber lasers. Optical fiber utilized as a laser gain medium was first introduced in 1964 (Koester *et al.,* 1964), shortly after the first laser appeared (Maiman Koester *et al.*, 1960), the first fiber lasers were realized in the 1970s in both pulsed (Stone, *et al.*, 1973) and continuous-wave (CW) (Stone, *et al.*, 1974) forms. Fiber lasers (FLs) are lasers with an optical rare-earth doped fibers as the active gain medium. These rare earth ions incorporated as the active gain medium in FLs are mostly Erbium, Neodymium, Thulium and Ytterbium which can make laser over a wide wavelength range from 0.4 μm to 4 μm.

Fiber lasers configurations can be designed based on the various schematics of laser cavities. The most common sort of these cavities are Fabry-Perot (linear), ring and figure-of-eight configuration which includes three basic elements as the pump source, gain medium and oscillation cavity (France, 1991). Figure 2.4 illustrates a simple schematic of conventional fiber laser cavities set-up.

The Fabry-Perot cavity (resonator) illustrated in Figure 2.4(a) contains a gain medium which is localized between two highly reflecting mirrors. In optical fibers, the mirrors of cavity can be fiber Bragg grating (FBG) or loop mirrors made from optical circulators and optical couplers as shown Figure 2.4(a). In case that optical circulators or optical couplers are being used as reflectors, the loss might be higher than the FBG usage case. This can be attributed to this fact that FBG can reflect special band of wavelength and with less power losses in splicing and connections.

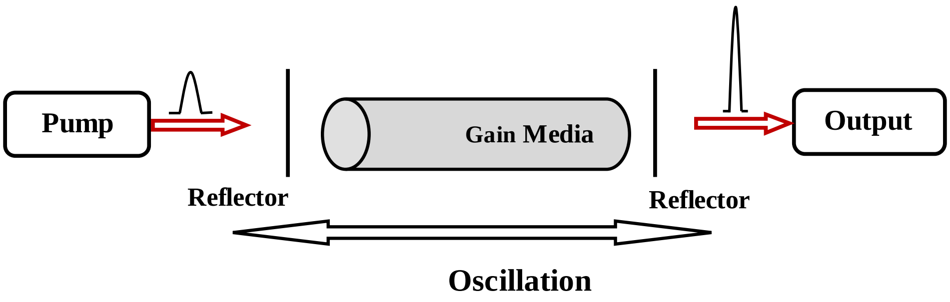

(a) Fabry-Perot (linear) Cavity

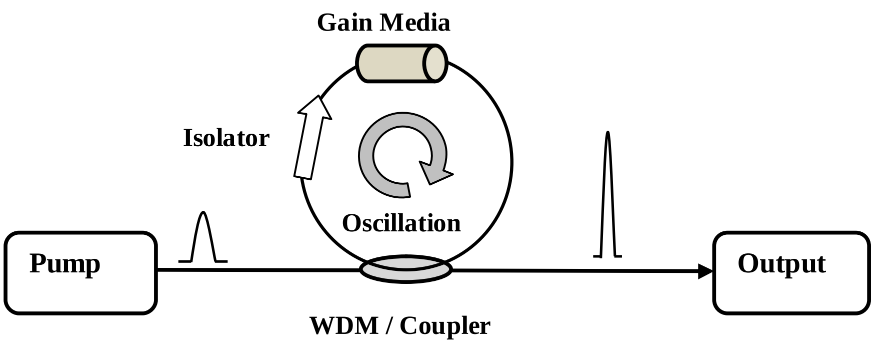

(b) Ring Cavity

Figure 2. 4: Schematic plots of Fiber lasers cavities.

Ring cavities are the other choice of fiber laser configurations which often used to provide unidirectional oscillation of a laser. In the case of optical fiber lasers, a main and useful feature of ring cavity is that it can be designed without utilizing any mirrors. In the simplest configuration, two ports of an optical coupler are connected together to form a ring oscillation including the doped fiber as the gain medium as shown in Figure 2.4(b). An isolator is incorporated within the loop to realize the unidirectional operation. One significant advantage of the ring cavity configuration is that it can be made-up of all fiber optics components, and then making such designs is much easier to be set-up.

The advances in optical fiber lasers are targeted to be utilized today as high average power CW lasers, high quality low power seed lasers, and compact lasers. Fiber lasers as used in the mentioned applications have many advantages compared to the bulk lasers. In the case of high power use, the cooling process is easier as well as they are compact and easy to build, to manipulate and align, and to transport. Fiber laser architectures can be also robust when they are made of fibers only. They are easy to integrate and do not require any complicated alignment or coupling. Indeed, fiber lasers are starting to replace the bulk and solid state lasers in many areas.

Another type of fiber lasers known as Brillouin /Raman fiber lasers (BFLs and RFLs) are relying on inelastic nonlinear effects associated with using nonlinearity of the gain medium such as Brillouin and Raman scatterings. Raman fiber laser can realize a relatively high power laser about a few Watt with considering also requirement of high input pump power. However, Brillouin fiber lasers can happen with a relatively low threshold power with a small linewidth output. According to the limitation of high power Raman pump in our laboratory and it is not relevant to this thesis, only Brillouin fiber laser will be described in the following section.

2.5.2 Brillouin fiber laser and Brillouin Erbium Fiber Lasers

BFLs have been studied with increasing attention and interests since 1976 (Hill *et al.,* 1976 and Montes *et al.,* 1999). The generated Brillouin scattering can be controlled and amplified within a cavity to realize a suitable Brillouin laser wave. The transmission fiber and specially designed nonlinear fiber can be used as the nonlinear gain medium to overcome the cavity loss by providing sufficient Brillouin gain function g_B within the cavity. As described earlier, one of the significant features of SBS generation is its threshold power introduced as Equation (2.39). In order to measure the threshold power, a very conventional and basic configuration was used which will be discussed with more details in chapter 3. As described earlier, the Brillouin gain is a function of fiber characteristics and then according to Equation (2.39), its value effects on the SBS threshold power. In most cases, threshold power is very high within basic and conventional measurement backward configurations. Note that when the threshold power should be measured, a basic and common set-up must be used. However, in some cases we want to reduce the threshold power because insufficient length of the gain medium, an advanced configuration can be used. In this case, the configuration design functions to compensate the input power and/or the fiber length shortages. Furthermore, the type of cavities mentioned earlier can be used to design an efficient Brillouin fiber laser. It is worth noting that the output laser should be monitored in the backward direction according to the SBS characteristic.

Other important characterizing features of SBS effect are the Brillouin shift frequency and linewidth. The Brillouin frequency shift is denoted as the difference in the Brillouin Stokes generated of BFL and launched Brillouin pump (BP) frequencies (Smith *et al.*, 1991 and Shirazi *et al.*, 2007). It is depended on the operating wavelength region as described in Equation 2.15. The Brillouin Stokes linewidth is very narrow compared to the other fiber lasers. It becomes significantly narrower than the Brillouin pump linewidth with reductions of up to a few Hertz (Smith *et al.,* 1991).

Brillouin Stokes lasers can be produced by either BFL or BEFL. Each of lasers has their own specific advantages and drawbacks. Generally, it is preferable to use a medium with a higher Brillouin gain coefficient to lower the required power and also to shorten the incorporated fiber length. Cowle and Stepanov (1996) had introduced BEFL using a hybrid gain media; nonlinear fiber and EDF to assist in laser generation. Further developments of this laser have been carried out by many researchers (Harun *et al.,* 2003 and Lim *et al.,* 1998). The 980/1480 nm pumped EDF generates amplified spontaneous emission, which oscillates in the BEFL cavity to produce free running modes. In order to amplify the Brillouin scattered waves generated by single mode fiber within the cavity, the BP wavelength will be launched at the same wavelength of free running modes. Therefore, only a certain Brillouin Stokes wavelengths can be amplified according to the free running modes. It causes a limitation in the Brillouin scattered tuning wavelength range. On the other hand, BFL has no limitation on the wavelength tuning range but requires a higher BP power and lower loss cavity compared to BEFL to efficiently generate single and cascaded Brillouin laser. Both types of Brillouin lasers will be thoroughly investigated in this thesis.

2.5.3 Multi-wavelength operation

Multi-wavelengths laser sources have attracted a great interest in many applications such as WDM transmission systems, optical sensors, and spectroscopy (Han, *et al.,* 2005 and During *et al.,* 2002). Many researches have been done on nonlinear fiber lasers to generate multiple wavelengths with an equal constant wavelength spacing (Desurvive *et al.,* 1990 and Graydon *et al.,* 1996) using SBS or FWM nonlinear effects. For instance, a comb of laser lines can be generated by a BFL via a cascading process of the Stokes. In this process, each Stokes wave acts as a Brillouin pump for generation of successive Stokes. The laser cavity should be efficient enough to provide the Stokes with a sufficient power to fulfill the requirement of threshold power. This can be easily achieved by providing an Erbium gain in the laser cavity to assist the cascading process as in a BEFL. During this process, anti-Stokes waves with higher frequency are also generated via FWM effect occurring between co-propagating pump and Stokes waves and increases the number of laser lines.

As explained in the previous section, BEFL manipulates the nonlinear Brillouin gain in an optical fiber to produce a narrow linewidth laser at the higher output power with assistance of Erbium gain (Cowle, *et al.,* 1996). The new BEFLs with a short piece of Bi-EDF as the gain medium will be demonstrated in Chapter 5 of this thesis. The comb lasers can also be produced by FWM effect as long as the phase match conditions will be satisfied. In this case the wavelength spacing value is not fixed as happening in SBS cascading effect which is around 0.08 nm. In FWM laser, multi-wavelength spacing depends on many conditions such as used fiber nonlinear coefficient and configuration design. This topic will be further discussed in the next following chapters.

2.6 Nonlinear Optical Fibers

2.6.1 Bi-EDF

Many works have been done to study the properties of Bismuth Borate glass in many conditions such as un-doped (Becker, *et al.,* 2003), Er^{3+}-doped (Chen *et al.,* 2004) or Nd^{3+}-doped (Chen *et al.,* 2005). For instance, Tanabe et al., (2000) indicated that the luminescence lifetime and efficiency of Er^{3+} doped Bi_2O_3 and SiO_2 glasses reduce with B_2O_3 content increment. Similar results were also reported by Yang et al., (2004) for Bi_2O_3 glasses. Becker et al. (2003) reported that the refractive index of the Bismuth Borate glass can be widely varied, which is useful in fiber fabrication.

The fabrication of Bismuth oxide fiber was demonstrated by incorporating three main former elements, Bismuth oxide Bi_2O_3, silicon oxide SiO_2 and alumina Al_2O_3. The core and cladding refractive index of this fiber are nearly 2.03 and 2.02, respectively at 1.55 μm, whereas these are about 1.45 for SMF. This fiber has a relatively small core size, which can confine the light in the center of fiber core for a better pump and signal absorption and thus improves amplification process. This feature also increases the nonlinearity of the fiber, which creates another application in the nonlinear fiber laser. This fiber also has a capability to be doped with higher Er^{+3} ions concentration compared to the conventional silica-based EDF. The utilization of Bismuth glass as fiber elements allows the erbium ion concentration to be more than 3000 ppm (Sugimoto *et al.*, 2004) without experiencing the ion clustering and quenching effects compared to SiO_2 glass. This type of fiber also has a wider amplification bandwidth due to suppression of excited state absorption.

Indeed, the larger values of Judd-Ofelt intensity coefficients, $\Omega_{2,\ 4,\ 6}$, of Bi_2O_3 results in higher peak emission cross-section and wider emission bandwidth (Sugimoto *et al.*, 2006). According to the optical fluorescence emission and absorption measurements, Bi-EDF possesses a higher peak coefficient of 7.58×10^{-25} m^2 and broader full width half maximum (FWHM) value of nearly 80 nm in comparison with silica based EDFA (Si-EDFA) especially at a longer wavelength region. Figure 2.5 shows the schematic plot of the gain bandwidth of Si- and Bi-EDFA against fiber length and Er^{+3} ions concentration. As shown in this figure, the Bi-EDFA in comparison with Si-EDFA performs better in term of bandwidth and compactness. The Bi-EDFA has a broad band gain profile covering 1530 to 1620 nm and a short gain medium length, which 1/100 to 1/10 shorter than a Si-EDF due to high Er^{+3} ions concentration.

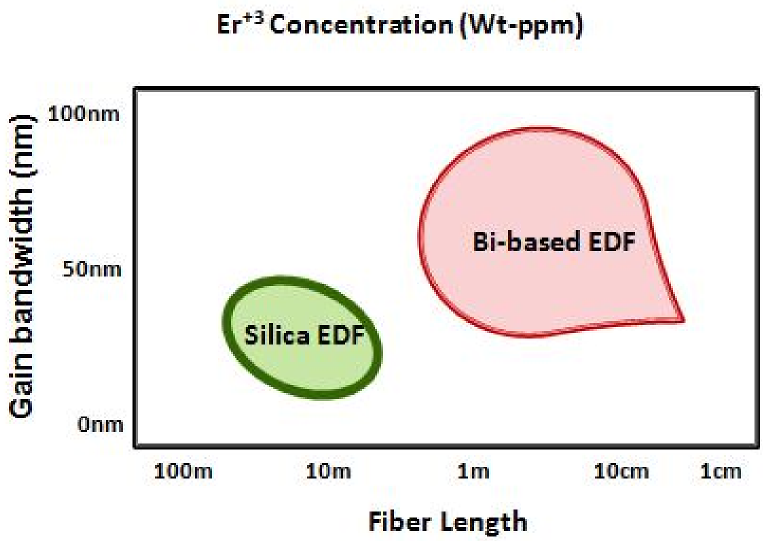

Figure 2. 5: Schematic plot of the gain bandwidth of silica and Bismuth EDF against fiber length and Er^{+3} ions concentration.

The base structure of Bi-EDF is illustrated in Figure 2.6, which contains the yellowish powder of Bismuth oxide atoms with melting temperature point of 817°C. In this study, the Bi-EDF used has Er^{+3} ions concentration of 3250 wt.ppm (weight parts per million) and La ion concentration of 4.4wt%. Lanthanum ion is used to suppress the ions quenching as the erbium ions concentration is increased (Sugimoto *et al.*, 2004). The Bi-EDF used is a commercially available from Asahi Glass Co. with different lengths of 49 and 215 cm. The cross section of the Bi-EDF is presented in Figure 2.7. The Bismuth fiber also has a large content of the group velocity dispersion (GVD), which is mainly caused by the material dispersion of the high refractive index of the glass (Agrawal, 2001).

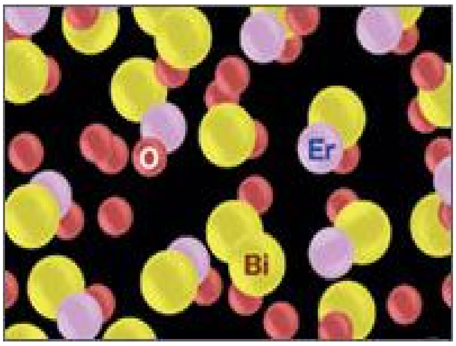

Figure 2. 6: Schematic plot of the distribution of erbium ions in bismuth-based glass (Jusoh, 2008).

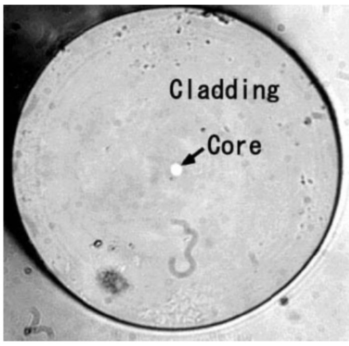

Figure 2. 7: The cross-section image of the Bi-EDF, provided by AGC.

Since the melting point of Bi-EDF (~ 800^{o}C) is much lower than that silica fiber (nearly more than 1000^{o}C), the fusion splicing of Bi-EDF is the main problem to splice the Bi-EDF to standard telecommunication fiber. Therefore, the Bi-EDF used is angled-spliced with a standard high numerical aperture (NA) silica fibers (as Nufern 980-HP) as depicted in Figure 2.8. The mixed angled-cleaving fusion splicing is applied to suppress the reflection effect, which arises from the large refractive index difference between the Bi-EDF and silica fiber (Sugimoto, 2005). Fresnel reflection loss which is caused due to the large refractive index difference (approximately 0.5~0.6) between Bi-EDF and SMF fiber is approximately estimated 2.8%. To suppress back reflected light to the fiber, the incident angle θ_2, must be larger than θ_1, introduced by the following equation (Sugimoto, 2005)

$$\theta_1 = 45^o - \frac{1}{2}\arcsin\left[\frac{n_{clad}}{n_{core}}\right] \tag{2.58}$$

where n_{clad} and n_{core} are cladding and core areas refractive index, respectively. Note that the incident angle cannot be too large, because it would increase the splicing loss between the SMF and Bi-EDF in the connection point. As shown in Figure 2.8, the angles of θ_1 and θ_2 are fixed at 6 and 8 degree, respectively. This splicing also resulted in an increase of insertion loss. The value of the insertion loss of the Bi-EDF is estimated to be about 0.82 dB at 1550 nm.

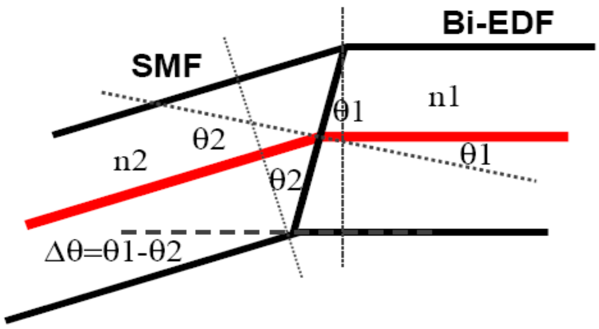

Figure 2. 8: Schematic diagram angled splicing between Bi-EDF and SMF which angle (θ2) is 8.2◦ optimum for Bismuth fiber with the angle (θ1) of 6◦ (Sugimoto, 2005).

NA essentially indicates the difference between the core and the cladding index, is estimated to be 0.2. It is a key parameter determining the mode-field diameter (MFD) and then the effective area of the fundamental mode, with the direct implication on the characterizing parameter of threshold power for SBS occurrence (Sanghera *et al.*, 2008). The value of V_{number} for a step-index SMF is 2.405 such that for larger V_{number}, corresponds with higher potential for the number modes. Using these parameters of NA and $V_{\text{-number}}$, the MFD of the BI-EDF is calculated to be approximately 6.12 μm using the Marcuse empirical formula (Marcuse, 1977). Consequently, the effective area A_{eff} of the fiber is obtained at about 29.4 $(\mu m)^2$ when it is evaluated by $(\pi/4)(MFD)^2$. The Bi-EDF also exhibits another striking feature which is its ultrahigh nonlinear coefficient due to its high refractive index and Erbium ion concentration characteristics. The nonlinear coefficient of the Bi-EDF is approximately 100 times larger than that of silica-based highly nonlinear fiber (HNLF) (Sugimoto *et al*., 2004). Hence, it can be utilized as a promising nonlinear gain material for realizing nonlinear based devices (Harun *et al.*, 2008; Ahmad *et al.,* 2009) which will be explored more in detail in the following chapters of this thesis.

2.6.2 Photonic crystal fiber

PCF which is also known as holey fibers (HF) or microstructure fibers (MF) is a new class of fibers with novel and unique properties. PCFs are able to confine light in hollow core and provide high effective nonlinearity and managed dispersion characteristics (Sinha *et al.,* 2003). Since PCFs have specifications that are not achievable with the conventional standard fiber technology, PCFs has been attracted a remarkable attention in the research community. Therefore, among the other fibers, these interesting abilities have resulted in many applications in communications, spectroscopy and metrology. For instance, a small size of core of this fiber is useful for fiber laser and super-continuum generation applications (Genty *et al.,* 2002).

PCFs are designed as an array of air holes in the fiber's cladding region surrounding the silica core such that run along the entire fiber length (Russell, 2003). Figure 2.9

illustrates a standard structure of the PCF. The air holes reduce the cladding's refractive index and lead to light confinement inside the core. In fact, the size and arrangement manner of air holes arrays, and also core size determine the guidance property of the PCF. The main parameters governing guidance properties of PCF are the hole size d, the distance between adjacent holes Λ (which is nearly on the light wavelength scale) and their ratio d / Λ, named as the air fill fraction to indicate the air percentage inside the PCF. A schematic profile of a common PCF's refractive index is shown in Figure 2.9.

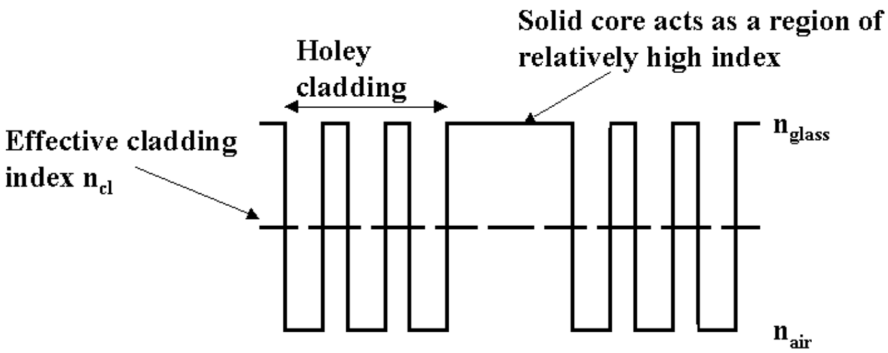

Figure 2. 9: Refractive index profile of the PCF with silica core.

The effective refractive index n_{eff} of the cladding needs to be calculated for each PCF. Since the n_{eff} is determined with the air existence, it can be considered that light is confined to the core by the holes and the guidance is much more efficient. The most common choices of materials to fabricate PCF are pure silica glass and some percentage Germanium doped silica glass (Zou *et al.*, 2005). Figure 2.10 illustrates scanning electron microscope images (SEM) of various types of PCFs which can be classified into two fundamental categories, solid-core and hollow-core.

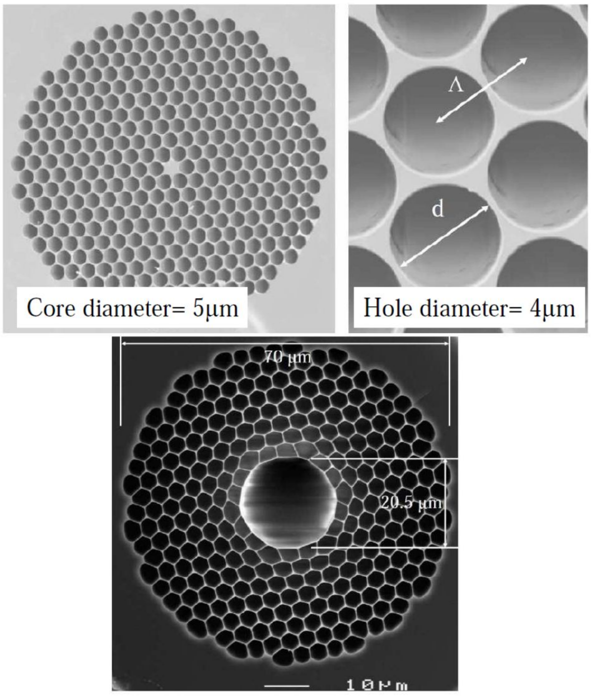

Figure 2. 10: SEM micrographs of a photonic-crystal fiber with silica core (upper figure) and hollow core (lower figure).[Russel, 2003]

V-number defines the number of modes supported by fiber which depends on air hole diameter d, pitch Λ and wavelength in PCFs cases as following equation:

$$V = \frac{2\pi D}{\lambda}\sqrt{n_{core}^2 - n_{cladding}^2} \tag{2.59}$$

where D is core radius, n_{core} is refractive index of silica and $n_{cladding}$ is effective index of the space filling mode. It has been studied that for $V<4.2$, PCF propagates only the single fundamental mode while V-number for conventional standard fibers is 2.405 (Russell, 2006). Therefore, PCF is suitable for single mode operation in short wavelengths region. Indeed the PCF's structure practically determines the modal behavior of the fiber. Providing that PCF is with air-hole diameter $d/\Lambda<0.48$, it operates as a single mode fiber for a wide range of wavelength which are suitable for high power delivery in telecommunication system (Knight, *et al.*, 1998 and Baggett, *et al.*, 2001).

Tight light confinement within the PCF's core region leads to a high intensity and high nonlinearity effects in this fiber. The parameter determining optical nonlinearity of fibers is normally measured in terms of its effective nonlinear coefficient

$$\gamma = \frac{n_2 \omega}{c A_{eff}} \tag{2.60}$$

where c is the light speed, A_{eff} is the effective area of traveling mode, ω is the frequency of propagating optical field and n_2 is responsible for the nonlinear refractive index as defined in Kerr effect intensity which is dependent on the incident intensity. Small pitch size Λ and large d/Λ in PCFs confines light strongly within the core region so that results in small effective mode area (Finazzi *et al.*, 2003). Such a small A_{eff} leads to a high nonlinear coefficient and then low level of incident intensity will be required for a certain nonlinearity value. For instance, PCF based on pure silica core has $n_2 = 2.16 \times 10^{-20}$ m^2/W and γ up to 168 $W^{-1}km^{-1}$ (known as NL-1.5-670 Blaze Photonics), which is nearly 150 times greater than standard silica fiber with γ equals 1.1 $W^{-1}km^{-1}$. Noting that there is a limitation for decreasing the core size for higher nonlinearity, because it leads to higher loss and then it has to be a tradeoff between these effects.

CHAPTER THREE: NONLINEAR CHARACTRIZATION OF PHOTONIC CRYSTAL FIBRE AND BISMUTH BASED ERBIUM DOPED FIBRE

3.1 Introduction

Photonic crystal fibres (PCFs) exhibit unique and dramatic nonlinear optical effects due to their periodic microstructure which forms the core and cladding (Russell *et al*., 2006 and Laude *et al*., 2005). For instance, one of the most interesting classes of PCFs is composed of a small-scale solid core with multiple air holes typically arranged in a hexagonal lattice around the core acting as the cladding. With the combination of a large refractive index contrast between the silica core and the air field microstructure, PCFs can be designed to enable tight mode confinement that results in a low effective mode area and thereby high nonlinear characteristics. Nonlinear effects in PCFs have been reported in many recent literatures which show that the fibre can achieve dramatic nonlinear effects, even with short fibre lengths (Di Teodoro *et al*., 2005; Chremmos *et al*.,2005; Geng *et al*., 2007 and Beugnot *et al*., 2007).

Bismuth-based-erbium-doped fibres (Bi-EDFs) have been extensively investigated as a short gain medium length in compact optical amplifiers. This fibre incorporates lanthanum (La) ions to provide heavily doped Erbium ions with decreasing the concentration quenching in the fibre (Desurvire *et al.*, 1990), which allow compact optical amplifier design. Therefore, it is expected that this fibre has enormous potential in realizing EDFA based devices. The Bi-EDFAs can provide a flat and high value of gain by a short length of a few ten cm long fibre in C and/or L band region from 1520 nm to 1620 nm for optical communication networks. In addition to the amplification characteristics, Bi-EDF also exhibits a very high fibre nonlinearity, which can be used to generate nonlinear devices such as Brillouin Erbium Fibre Laser (BEFL) (Harun *et al.,* 2008).

Recently, various works have been reported on Stimulated Brillouin scattering (SBS) and Four Wave Mixing (FWM) effects in optical fibres. SBS and FWM are very important nonlinear effects in optical fibres which may limit the performance of optical communication system. These effects also have a possible application in developing nonlinear devices such as fibre lasers, fibre amplifiers and sensors. SBS has a significant influence on the operation of optical transmission systems as well as many applications such as in distributed fibre sensors using narrow-linewidth single frequency lasers (Harun *et al*., 2009). Many recent works have also been reported on the development of Brillouin fibre lasers (BFLs) using a highly nonlinear fibre as a gain medium(Wu *et al.,* 2010; Guan *et al,.2010)*.The highly nonlinear fibres such as PCF and Bi-EDF can also be applied to realize optical soliton (Yulin *et al.,* 2004), wavelength conversion (Andersen *et al.,* 2004), and with the proper design of dispersion these fibres have been used to generate new frequency resulting from four-wave mixing (FWM) (Chow *et al.,* 2005). In comparison with conventional optical fibres, the significant FWMs in PCFs can occur at relatively low peak powers and over short propagation distances.

In this chapter, nonlinear effects are investigated numerically and experimentally in both PCF and Bi-EDF using a basic configuration. The power budget requirements (threshold pump power), the achievable gain and saturation characteristics of Brillouin amplifiers, precise and quantitative treatment of the SBS process are evaluated in PCF. The amplification and nonlinear characteristics of Bi-EDF are then studied. In the last part of this chapter, a FWM effect is numerically studied and experimentally demonstrated using two tunable laser sources. The FWM efficiencies in both PCF and Bi-EDF are then estimated using the simplest experimental arrangement.

3.2 Performance of Stimulated Brillouin Scattering in Optical Fibres

As described in chapter 2, the acoustic phonons involved in the Brillouin scattering and the interactions occurs typically over a narrow order of tens of MHz of Brillouin gain linewidth, such as 35 MHz for fused silica, with the downshifted frequency nearly 10 GHz from the Brillouin pump (BP) wave in the wavelength 1550 nm (Smith *et al*., 1972; Shibata *et al*., 1987; Azuma *et al*., 1988 and Shibata *et al*., 1989) The shift is determined by the velocity of the acoustic grating along the fibre and is therefore dependent on the mechanical properties of the fibre such as the elasto-optic coefficient, applied strain and ambient temperature (Nobuyuki *et al*., 1993 and Nicklès *et al*., 1996). SBS provides gain in the opposite direction of the direction of the BP wave source. The pump power is depleted to be converted to a potentially strong Brillouin Stokes wave propagating backward to the pump direction. The Brillouin Stokes (BS) distorts communication signal in optical communication systems, which may harmful in some cases. Therefore, an optical isolator is normally deployed in the system to eliminate the back-propagating signals.

Figure 3.1 shows the simplest experimental setup to demonstrate SBS effect. In this setup, BS propagates in the backward direction which can be monitored through the port 3 of the optical circulator (OC) by using optical spectrum analyzer (OSA) with the resolution of 0.01 nm. In the experiment, a piece of 25 km long standard single mode fibre (SMF) is used as the gain medium. OC functions to protect the tunable laser source (TLS) from any backward reflected powers as well as to isolate and route the Brillouin signal to be monitored by OSA. In this experiment, TLS with the maximum peak power approximately 5 dBm and linewidth of about 15 MHz is used as the BP. An amplifier (Erbium doped fibre amplifier, EDFA) can be incorporated after the TLS to amplify the pump power when the higher power is needed in Brillouin fibre lasers (BFLs) structures. With the amplifier, the BP has the maximum output power of about 15 dBm. The evolution of the anti-Stokes, the BP reflection, and the Brillouin Stokes waves are investigated at various pump powers. Index matching gel is applied at the free end side of the fibre under test to eliminate Fresnel reflection and thus ensure that the back-propagating light constitutes only the Brillouin Stokes.

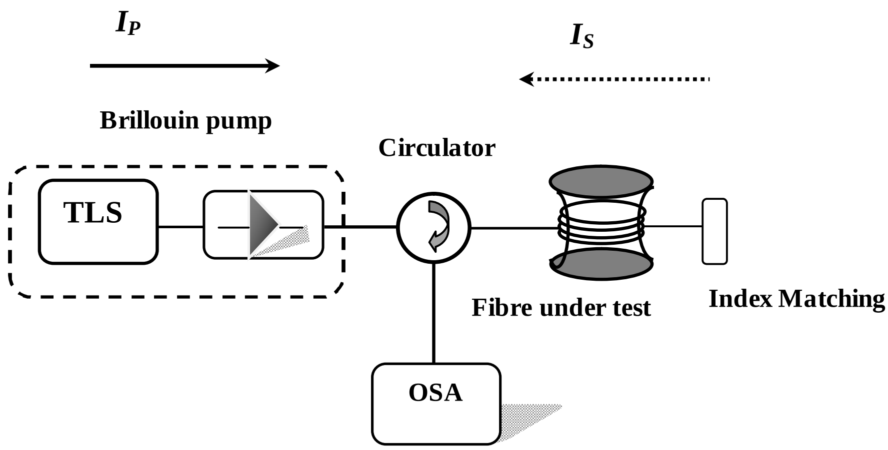

Figure 3. 1: Experimental setup for generating Brillouin scattering in the backward direction. I_p and I_s denote the intensities of the pump and Brillouin signal lights, respectively.

Figure 3.2 compares the launched BP and back-propagating Brillouin when the BP is fixed at 1560 nm. The anti-Stokes, the BP Rayleigh reflection and the Brillouin Stokes are observed at powers of around -54 dBm, -5.1 dBm, and -30.5 dBm, respectively. The Brillouin Stokes light wavelength is shifted upward by 0.088 nm from the BP wavelength whereas the anti-Stokes wavelength is downshifted by the same spacing. The BS is obtained due to the interactions between the gain media and BP. According to the SBS theory, the beat frequency between the Brillouin scattered wave and the incident BP light is equal to the frequency of the acoustic wave. As long as the Brillouin laser pump and the Brillouin Stokes wave interactions reinforce the acoustic waves, it amplifies the scattered Brillouin Stokes wave so that the stimulated Brillouin scattering (SBS) occurs. Rayleigh scattering in the fibre causes some portion of BP is reflected back as shown in the figure 3.2. The anti-Stokes is caused by the degenerate four-wave mixing effect which happening between the BP and Brillouin Stokes waves.

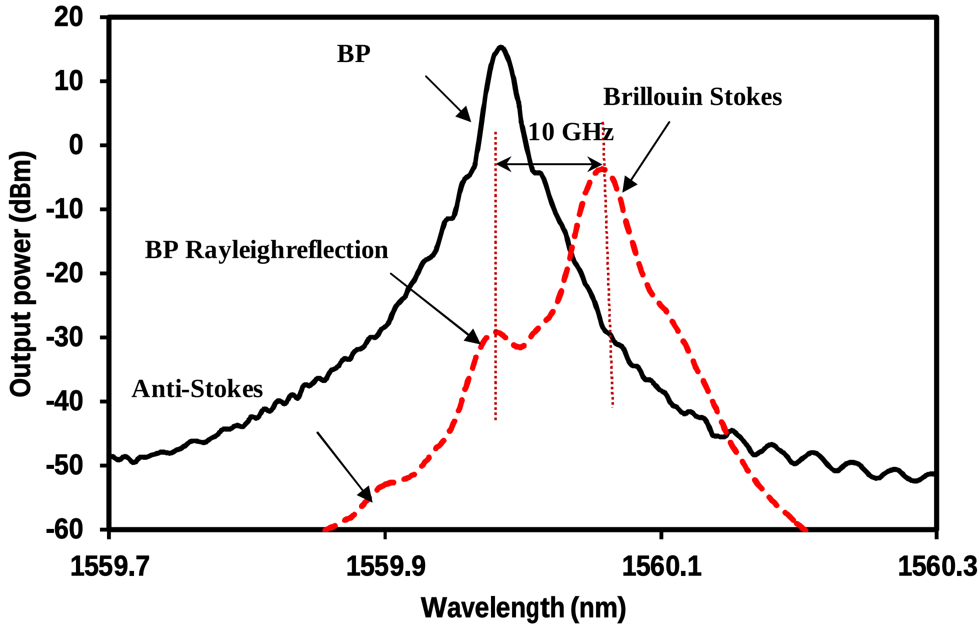

Figure 3. 2: The spectra of the launched BP and the back propagating Brillouin Stokes.

Figure 3.3 shows the evolution of the BS spectrum with BP power. By increasing BP power from 6 dBm to 15 dBm, the BS power is observed to increase from -61.7 dBm to -5.1dBm due to SBS nonlinear phenomena. The anti-Stokes and the BP Rayleigh reflection peak powers are increased by only about 5 dB and 11 dB, respectively. This shows that BS gain is so much higher than the gains of anti-Stokes and the Rayleigh scattering. This is attributed to the fact that anti-Stokes signal was generated at a shorter wavelength region, which has a higher energy. Therefore, it has a less probability of occurrence than the Stokes signal (Agrawal, 2003). The Brillouin threshold power is defined as the Brillouin pump power at which Brillouin Stokes power suddenly increases. As shown in figure 3.3, the threshold power is estimated at around 9.9 dBm since the BS power is growing up abruptly with a remarkable value at this pump power. One method to reduce the Brillouin threshold power is to modify the waveguide structures of the optical fibres (Kuzin *et al*., 1985; Eichler *et al*., 1997 and Harrison *et al*., 1999) so that high pump intensity is distributed along the full length of fibre. The SBS effect in a closed loop configuration also is expected to have a lower threshold value. The detail study on this will be presented in Chapters 4 and 5.

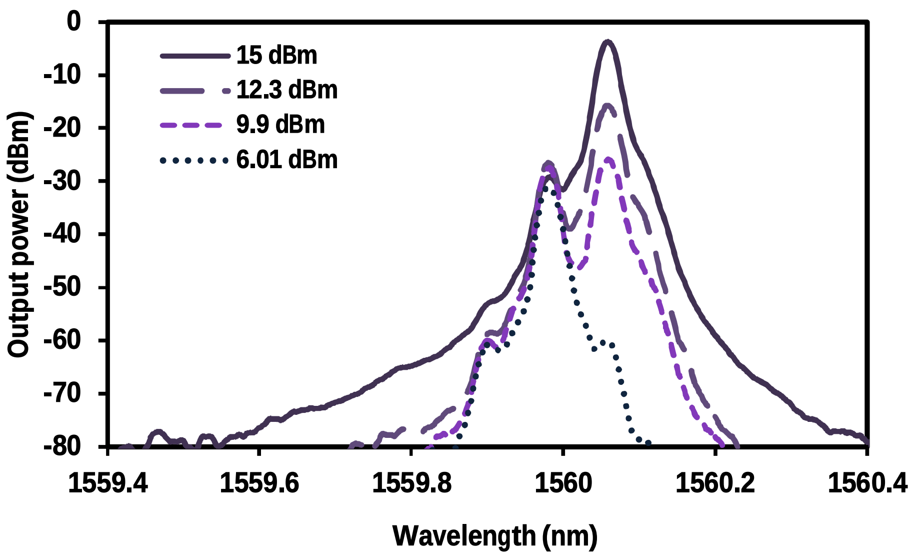

Figure 3. 3: The evolution of the BS spectra with the BP power.

3.3 Numerical evaluation of Brillouin threshold power in PCF

Brillouin scattering has been implemented in a wide range of applications as a narrowband fibre laser source (Shirazi, *et al.*, 2008), narrow band filtering (Trach *et al.*, 1989), and Brillouin fibre amplifier (BFA) (Ravet *et al.*, 2008). Since the Brillouin frequency shift is dependent on the material composition, the temperature and pressure of the medium, the Brillouin scattering can also be applied in various optical fibre sensors (Culverhouse *et al.*, 1989). In a development of distributed Brillouin sensors (DSB), the Brillouin shift is measured along the fibre length based on frequency (or time) domain modulation of the input pump wave (Ravet *et al.*, 2006). One of the main characteristics of the nonlinear Brillouin scattering effect in optical fibres is its threshold power condition for the occurrence of the SBS. The threshold power is normally defined as the input pump power, P_{th}, at which the output Stokes is some fraction (r), used as threshold criterion, of P_{th} (Kovalev *et al.*, 2007). This threshold input pump power value is strongly depended on the providing Brillouin gain medium or fibre length which plays an important role in SBS generation for lasers and sensors applications. For sensors application, a uniform resolution measurement over the entire sensing length cannot be achieved in case of strong pump depletion (Ravet *et al.*, 2008). Consequently, a precise and comprehensive theoretically measurement of the threshold input pump power with considering the pump depletion as well as fibre length variation is required.

PCFs are a class of micro-structured fibre which possesses a solid core surrounded by a cladding region that is defined by a fine array of air holes that extend along the full fibre length. PCFs are typically made of a single material, usually pure silica, and guide light through a modified form of total internal reflection since the volume average index in the core region of the fibre is greater than that of the surrounding micro-structured cladding

(Russel, 2003). Since the average refractive index of the cladding due to presence of air holes lowers the average refractive index from that of a pure fused silica and hence a modified total internal reflection could explain light guidance in such fibers. One of the most promising applications of PCFs is in the developmentof nonlinear optical devices for fibre-optic communication systems. Fibre fabrication technology has advanced significantly in recent years and has resulted in the production of high quality PCFs with low loss, ultrahigh nonlinearity, and controllable dispersion. In this section, the Brillouin scattering process in a piece of PCF is theoretically studied for possible use in a development of a Brillouin fibre laser. In this work, the Stokes emission is considered to be initiated by spontaneous Brillouin scattering, SpBS, and the 1% criterion is used for the threshold definition (Kovalev *et al.*, 2007). The theoretical result is also experimentally verified.

3.3.1 Theoretical principle of SBS generation

If the input pump intensity is sufficient, SBS in optical fibres will convert a pump field with frequency ω_p to a scattered counter-propagating probe field with frequency ω_s (Stokes waves), through an electrostrictive process. Indeed, Brillouin scattering arises from the nonlinear interaction of launched light with propagating density waves or acoustic phonons. Since momentum and energy can be conserved during these scattering events, the SBS effect is remarkable (Singh *et al.*, 2007). The interaction between the three fields of input pump signal, Brillouin scattered wave, and acoustic wave (phonon) along a single mode fibre of length can be represented by a set of differential equations as follows (Agrawal, 2001):

$$\frac{dI_S}{dz} = -g_B I_P I_S + \alpha_S I_S \tag{3.1}$$

$$\frac{dI_P}{dz} = -\frac{\omega_P}{\omega_S} g_B I_P I_S - \alpha_P I_P \tag{3.2}$$

where g_B is the Brillouin gain coefficient, and I_P and I_S are the pump and Stokes wave, respectively. α_p and α_s are the absorption coefficients at pump and Stokes frequency are denoted by ω_P and ω_S respectively and z is the position along the length of the fibre. Equation (3.1) is obtained using the fibre losses due to Stokes wave determined by fibre loss coefficient at Stokes frequency and counter propagating nature of this wave. The feedback process responsible for Brillouin scattering is controlled by these two coupled equations, (3.1) and (3.2).

If we assumed that $\omega_p \approx \omega_s$ and $\alpha_p \approx \alpha_s \equiv \alpha$ to describe the SBS effect based on the fact that the Brillouin shift is relatively small, equations (3.1) and (3.2) can be rewritten as (Smith, 1972);

$$\frac{dI_S}{dz} = -g_B I_P I_S + \alpha I_S \tag{3.3}$$

$$\frac{dI_P}{dz} = -g_B I_P I_S - \alpha I_P \tag{3.4}$$

The first terms of equation (3.3) and (3.4) represent the Brillion gain and the pump power depletion, respectively. It has to be considered that the transverse dependence of the wave across-section has been ignored. In case the Stokes power is much smaller than the pump power, one can assume that the pump power is not depleted and therefore the first term of equation (3.4) can be neglected (Smith, 1972). Thus, a more familiar closed-form expression of the SBS threshold power can be obtained as follow (Smith, 1972):

$$P_{th} \approx 21 \frac{A_{eff}}{g_B^{(0)} L_{eff}} \tag{3.5}$$

where $L_{eff} = (1 - \exp(-\alpha L))/\alpha$ is the effective length of interaction.

Equation (3.5) is one of the approaches to define SBS threshold in optical fibres (Bayvel *et al.*, 1990 and Tang, 1966). It is based on the condition in which the reflected Stokes optical power at the beginning of the fibre ($z = 0$) equals the input pump power $(P_{reflected} = P_{in})$ in the absence of pump depletion. Practically the SBS threshold power is identified as the amount of input power producing a reflected power that is equal to a fraction, r, of the pump ($P_{reflected} = r \times P_{in}$). This fraction factor or threshold criterion can vary between $\approx 10^{-4}$ and $\approx 10^{-1}$ according to various literatures (Kovalev *et al.*, 2007 and Jenkins *et al.*, 2007). Actually, for accurate determination of the threshold condition, the influence of pump power depletion term should be considered. Thus, considering pump depletion factor for a proper threshold definition, the simulation of the Brillouin scattering process in an optical fibre is revised by returning to Equations (3.3) and (3.4). It should be noted that the boundary conditions, which are known as the launched pump and Stokes intensities, are specified at the opposite ends of the fibre and small enough as initial spontaneous Brillouin scattering at the fibre end. This makes the equations slightly more complicated to be solved without writing a special code. Equations (3.3) and (3.4) are solved using the above mentioned boundary conditions. The algorithm adopted is based on the fourth order Runge-Kutta algorithm with 10-3 accuracy and shooting method to meet the complicated boundary condition.

3.3.2 Comparison of numerical and experimental results

The Brillouin scattering generation in a piece of PCF can be explained as schematically illustrated in Figure 3.4. The backward signal composed of Rayleigh and spontaneous Brillouin scattering (P_S) is generated when the BP is injected into the fibre. The SBS threshold in PCF is experimentally measured by using the setup of Figure 3.1. In the experiment, a tunable laser source (TLS) is used as a narrow linewidth laser with a maximum peak power of approximately 5 dBm at a fixed operating wavelength of 1550 nm. The pump wavelength is amplified by Erbium doped fibre amplifier (EDFA) to achieve a maximum power of around 21 dBm before it is launched into the PCF through ports 1 and 2 of the optical circulator. The reflected signal is observed and measured through port 3 of the OC using the optical spectrum analyzer (OSA) with a resolution of 0.01 nm.

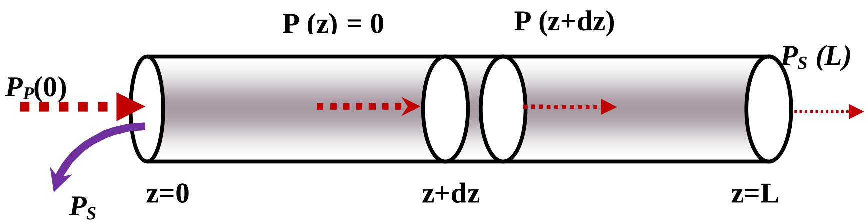

Figure 3. 4: Schematic diagram to explain the Brillouin scattering process.

The PCF used as the gain medium has a triangular core with an average diameter of 2.1 µm and cladding diameter of 128 µm. The scanning electron micrograph (SEM) image of the fibre is shown in Figure 3.5. It has a triangular core with average diameter of 2.1± 0.3 µm, cladding diameter of 128 ± 5 µm, and an effective core area A_{eff} of 6.1 µm^2. The average air hole diameter of the fibre is 0.8 μm with 1.5 μm pitch. The PCF is made from pure silica with 17.4 wt% of Ge-doped core region. The Ge-doped core functions to increase the nonlinear refractive index of the core, creates a smaller mode field diameter and reduces the confinement loss. This effect can reduce acoustic loss and avoid the broadening of Brillouin spectrum linewidth. The PCF is spliced to an intermediate fibre and then a single mode fibre (SMF) with a splice loss of 0.35 dB at each ends. The PCF is 100 m long with and an attenuation coefficient of less than 9 dB/km or $\alpha\ (km^{-1}) = \alpha\ (dB/km) \times (\ln(10)/10) = 2.07\ km^{-1}$.

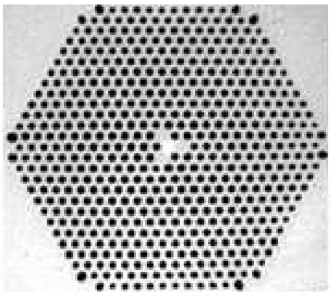

Figure 3. 5: SEM image of the PCF used in this study.

To explore the numerical results for a given length of the single mode fibre, L, we first assume that a pump wave with intensity of $I_p(0)$ is launched into the fibre, which initiates the Brillouin scattering in the fibre core (Singh *et al.*, 2007). The Brillouin gain coefficient, g_B, is measured to be 1.93×10^{-11}m/W at room temperature (Nicklès, M et al., 1997). Based on these parameters, we iteratively solve the equations over a range of values of the launched pump power $I_P(0)$ to determine the reflected Stokes intensity and its conversion efficiency.

Figure 3.6 depicts the experimental and the numerically simulated results of the transmitted pump and backscattered Stokes power as a function of the incident BP power.

In reality, the experimental value of the backscattered power is the sum of the Rayleigh and Brillouin scatterings. Below the line of 20 dB of *Pp*(0), which represents the criterion of 1% input pump power, Rayleigh scattering is dominant whereas in the neighborhood above this line, Brillouin scattering is the main contributor to the backscattering wave output. The threshold determination by 1% criterion as illustrated in Figure 3.6 shows that Rayleigh scattering does not play a significant role in dictating the threshold value. Rayleigh scattering has been disregarded in the simulation of the Brillouin scattering power resulting in the difference between the numerical and experimental results for the BP power of less than 15 dBm. Ideally, the SBS threshold is likely to be higher still considering other sources of loss in the experimental configuration. Nevertheless, the result shows a good agreement between the experimental outcome and the numerical prediction.

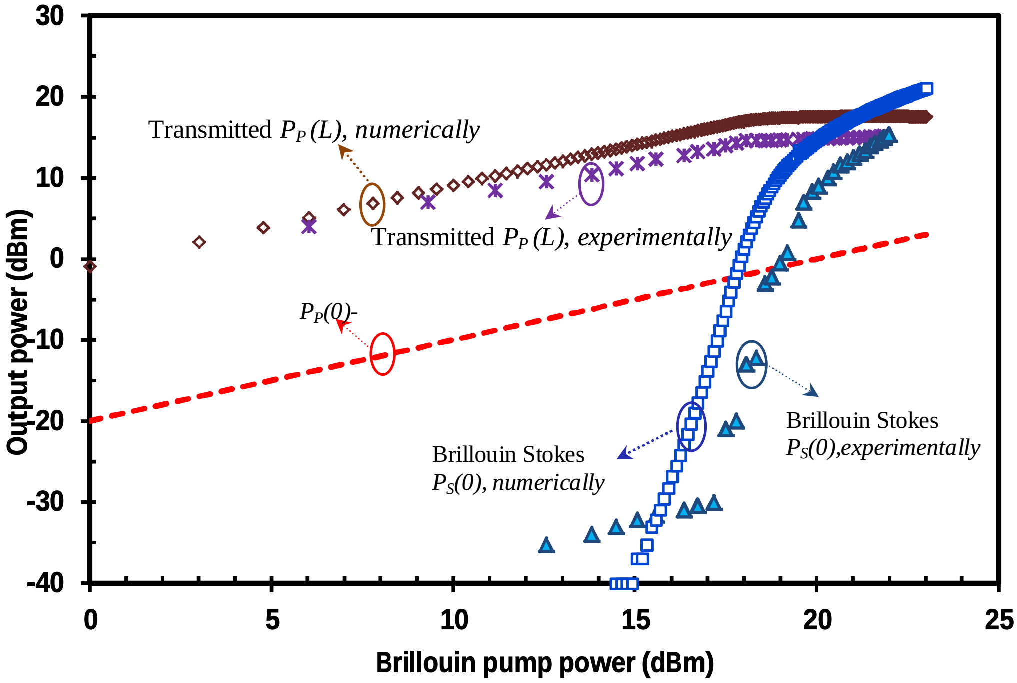

Figure 3. 6: Plot of the transmitted pump and backscattered Stokes power obtained by the theoretical and experimental results against the input pump power.

3.3.3 Threshold pump power evaluation

Spontaneous Brillouin scattering or Stokes wave is generated as the BP is launched into a PCF due to thermal fluctuations, which modulates the refractive index. The BP also interacts with the Stokes wave in a Brillouin gain medium to initiates SBS. To fulfill the threshold condition for the SBS generation, the single-pass gain obtained by the Brillouin gain medium, $G=g_B I_P(0)L_{eff}$, must exceed the Brillouin gain threshold, G_{th}, which is provided by the input pump at threshold power. The Brillouin gain threshold is estimated at a constant value of 21 by Smith's definition. Later, Bayvel has suggested that the value should be 19 for the modern single mode fibres (Bayvel *et al.*, 1989). The threshold pump power for SBS generation is strongly depended on the specifications of the fibre such as the fibre length used as the Brillouin gain medium, fibre's linear loss and the Brillouin gain coefficient. It is worth noting that the Brillouin Stokes, which arises from spontaneous Stokes intensity initiates at z = L. The intensity is speculated to be 10^{-9} times of the input pump power in this simulation.

In this study, the calculation is done to determine the optimum PCF length for the SBS generation, which depends on the linear loss and Brillouin gain coefficient characteristics of the fibre. The calculated results are used to further investigate the theoretical pump depletion and the Stokes power saturation regions as well as the optimum input pump power. The transmitted pump and Stokes powers are calculated against the input pump power variation for different PCF lengths using the Equations (3.3) and (3.4). The result is depicted in Figure 3.7. In this calculation, the input pump power is varied from 0 mW to 300 mW while the PCF length is varied from 10 m to 400 m. The amount of transmitted pump power at the end of the PCF is dependent on the absorbed light by the fibre and the light converted to backscattered Stokes waves. In the case where pump depletion is not considered, the transmitted power should rise linearly as the input pump power increases. However, as shown in Figure 3.7 (a), the transmitted pump power only increases linearly with input pump power before the depletion region. This initial level of the depletion region is dependent on fibre length. The residual pump power, which is not absorbed along the fibre, is converted to the backscattering Stokes through the electrostrictive process which results in the SBS as shown in Figure 3.7(b).

(a)

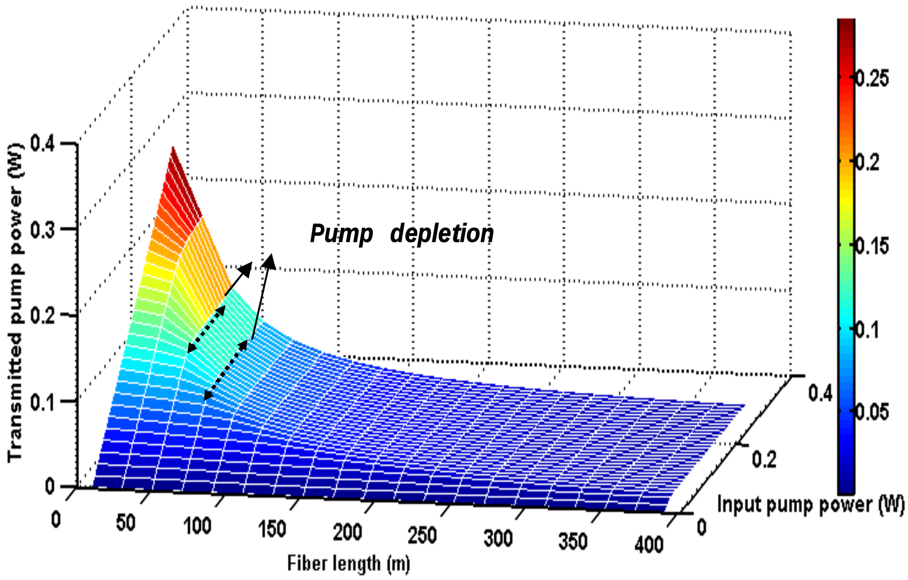

(b)

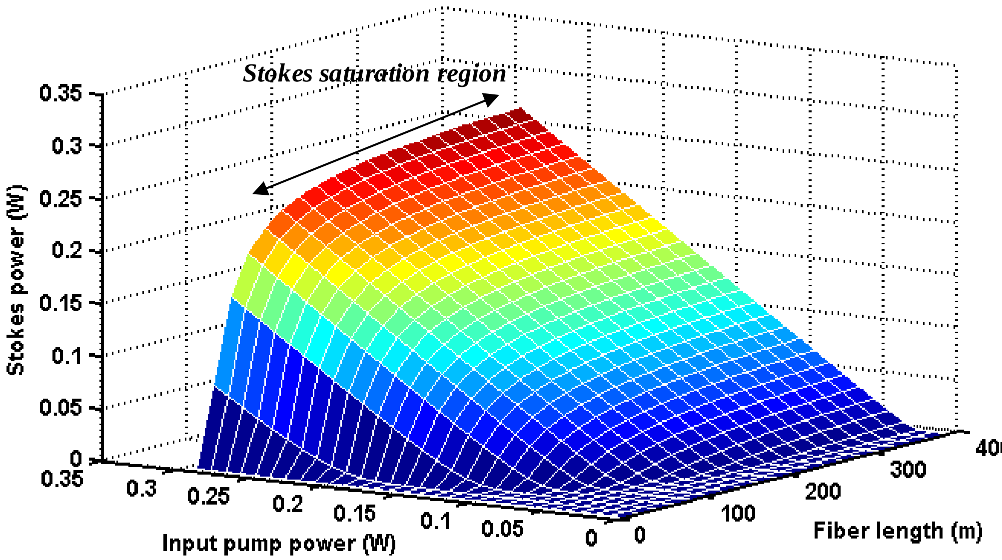

Figure 3. 7: Plots of (a) transmitted pump and (b) backscattered Brillouin Stokes power against input pump power for different fibre length.

The optimized length for the SBS generation can be determined from Figure 3.7(a) by observing the pump depletion. The transmitted pump power is also observed to be smaller with a longer fibre. This is attributed to the fact that the longer length allows the pump to interact more with the gain medium to produce a higher gain. This contributes to a more efficient Brillouin Stokes conversion, which decreases the transmitted pump power. For a shorter length of fibre especially in a region of less than 50m, the SBS threshold requirements cannot be fulfilled and the pump power cannot be efficiently converted to the Stokes even though the incident pump power is set at the maximum value. It is also seen that the Stokes power increases with input pump power especially at a longer PCF region. The Stokes power also increases with the increment of fibre length especially at high input signal power before it saturates at a certain power value as shown in Figure 3.7(b).

To assess the threshold power based on various criterion, the earlier results on the transmitted pump and the backscattered Stokes powers is transformed into another useful form defined as conversion efficiency percentage, is defined as: $(I_S(0)/I_P(0) \times 100)$. Figure 3.8 shows the conversion efficiency against both input pump power and the PCF length. Smith's definition of Equation (3.5) is obtained based on the condition that the reflected Stokes optical power is equal to the input pump power, which is equivalent to 100% conversion efficiency. One can also define the SBS power threshold to be the input power where the reflected power is equal to some fraction of the pump. Figure 3.8 shows that the conversion efficiency begins to grow sharply at around 1% against input pump power. Then, the threshold power of the PCF is defined as an input pump power which is able to provide 1% conversion efficiency at each fibre length (1% criterion). The PCF used has Brillouin gain coefficient of 1.93×10^{-11} m/W.

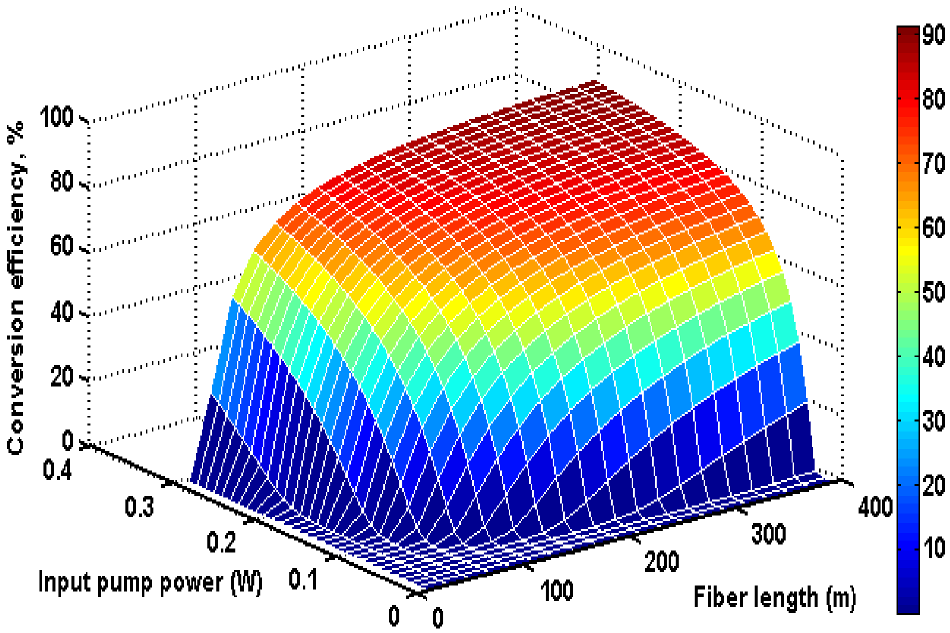

Figure 3. 8: Plot of conversion efficiency percentage against input pump power for different length of fibre.

Figure 3.9 shows the threshold pump power versus fibre length for both 1% and 100% criterions, which indicates that the threshold pump power is dependent on the fibre length. As shown in the figure, both threshold pump powers indicate a similar trend whereby the threshold power decreases with the increase in fibre length. If the fibre length is divided into two sections; less and more than 100 m, a sharp decrease of threshold pump power can be clearly seen for the length of less than 100 m. Therefore, the optimum length is considered to be around 100 m for achieving the highest Brillouin gain.

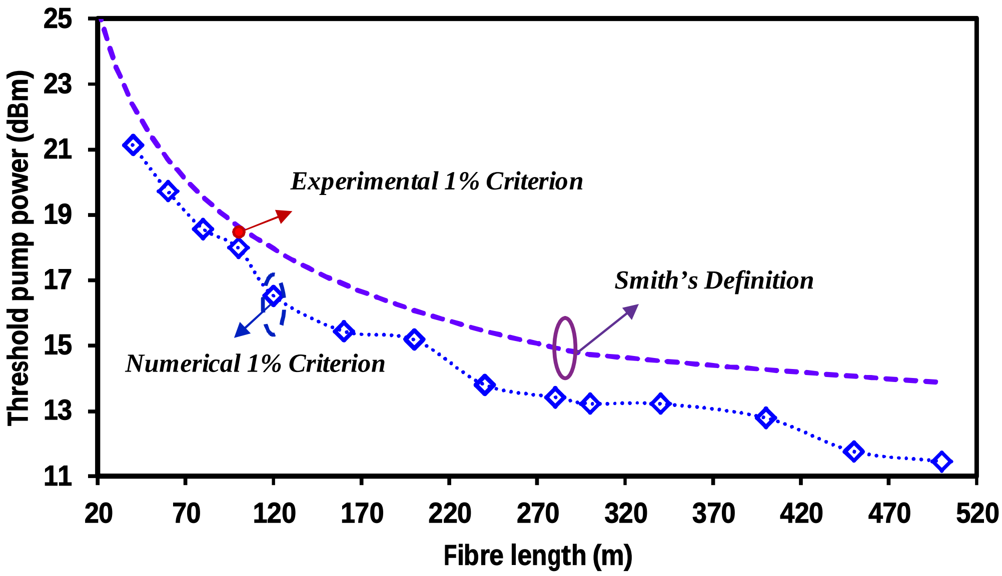

Figure 3. 9: Plot of the threshold pump power versus fibre length using 1% and 100% (Smith's definition) criterions.

The threshold pump power is also experimentally measured for 100 m long PCF. The measurement for other lengths is not carried out due to unavailability of the fibre. The experimental value is 18.5 dBm, which is in good agreement with numerical estimated value of 18.0 (1% criterion) as shown in Figure 3.9. The calculated threshold pump power based on Smith's estimation is basically higher than both the simulation and experimental results. This can be attributed to two facts that firstly, the pump depletion has not been considered in the Smith's calculation and secondly, the threshold condition is defined as the input pump power for which this power equals the backscattered Stokes power at z = 0 based on Smith's definition ($I_p = I_S$). In reality, these conditions are not experimentally observable since pump depletion inevitably occurs and consequently the backscattered Stokes power is less than the input pump power. As it can be observed in Figure 3.8, the threshold power decreases with the PCF length until a convergence is reached. Depending on the values of A_{eff} and g_B, the optimum length changes due to the changes in pump power requirement. This trend also shows that beyond the optimum length, the dependency of threshold power on the fibre length significantly reduces.

The threshold gain, G_{th} can be calculated from equation (3.5). Foremost, G_{th} is commonly taken to be a constant of nearly 21, independent of any effective SBS characterizing parameters. But, in practice, the constant value varies with the length and type of fibre. In this work, G_{th} for the PCF is simulated against the fibre length and the plot of threshold Brillouin gain as a function of PCF length is shown in Fig. 3.10. As discussed earlier, the threshold power depends on fibre parameters and thus, G_{th} is also treated similarly. Thus, it is evident that G_{th} is not a constant as commonly assumed in the literature. The use of higher values of g_B and smaller values of effective area provide the threshold power requirement with a shorter fibre length. Therefore, the actual value of G_{th} is fluctuating between 14 and 18 depending on the fibre length. Since P_{th} is nearly constant around 14 dBm as shown in Figure 3.9 for the length of 240 to 400 m and according to this relation of $G_{th}= g_B P_{th} (L_{eff}/A_{eff})$, the fraction of (L_{eff}/A_{eff}) is considered to play the main role of evaluating G_{th}. Therefore, the higher value of G_{th} is anticipated for longer length as long as threshold pump power doesn't vary. The SBS effect may also be obtained in other highly nonlinear fibres such as Bismuth-based Erbium-doped fibre (Bi-EDF). The next section investigates the amplification and nonlinear characteristics of this fibre.

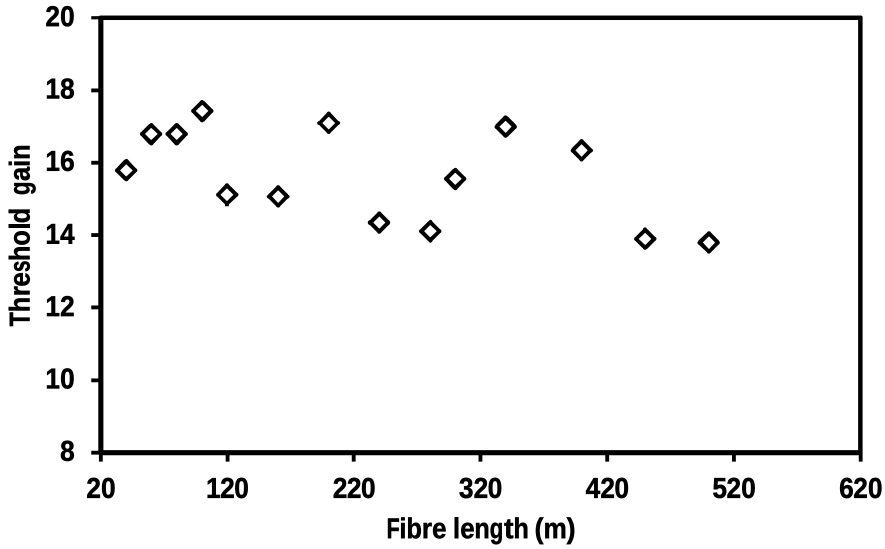

Figure 3. 10: Plot of G_{th} against fibre length corresponding to the calculated threshold powers.

3.4 Bismuth based erbium doped fibre (Bi-EDF) characteristics

Brillouin fibre laser (BFL) can be generated using a piece of nonlinear fibre and Brillouin pump in ring or linear cavity structures. In this application, it is desirable to have a medium that has a large Brillouin gain coefficient g_B to lower the power requirements and also to shorten the length of fibre devices. Erbium gain can also be used to assist BFL generation to compensate for cavity loss especially for multi-wavelength operation. This type of hybrid laser is called Brillouin Erbium fibre laser (BEFL), which uses a Brillouin gain to initiate the laser and Erbium gain to assist in multi-wavelength generation (Cowle*et.al.*, 2007). BEFLs have the capacity of generating optical combs with line spacing nearly 10 GHz at room temperature due to the Brillouin Stokes-shifted frequency from the launched BP (Zhan *et al.,* 2005). Such comb with higher number of lines in comparison with the conventional multi-wavelength laser has a possible application as laser sources for DWDM systems.

Recently, a bismuth-based erbium-doped fibre (Bi-EDF) has been extensively studied for use in compact amplifiers with short-gain medium lengths. It has inherently differentiated performance over conventional silica-based glass as host material for Erbium-doped fibre amplifier (EDFA). This fibre incorporates lanthanum (La) ions to decrease the concentration quenching of the erbium ions in the fibre (Harun *et al*., 2009), which allows the erbium ion concentration to be increased to more than 3000 ppm. A fibre with such a high erbium dopant concentration is expected to have enormous potential in realizing a compact erbium-doped fibre amplifiers (EDFAs) and EDFA based devices. The Bi-EDF has also a very high fibre nonlinearity, which can be used for realizing a compact BFL. In addition, this fibre is also fusion splice-able to ordinary silica fibre using a special method. Compared to silica-based EDFA, the higher refractive index of Bismuth-based glass (Yang *et al.,* 2003) provides a broader amplification bandwidth up to extended L-band region which is desirable for WDM network systems. The high refractive index resulted in a relatively shorter lifetime at $^4I_{13/2}$ level in Bi-EDF compared to silica EDF (Si-EDF).

Figure3.11 depicts the measured and calculated emission cross-section using the modified McCumber's relation defined as in Equation (3.6) and also the Si-EDF emission cross-section as a comparison (Desurvire *et al.,* 1994 and Harun *et al.,* 2009). Based on the modified McCumber's relation the absorption cross section function is given by;

$$\sigma_a(\nu) = \frac{\sigma_e(\nu)}{\eta^{peak}} \exp(\left\{ \frac{h(\nu - \nu^{peak})}{k_B T} \right\} \tag{3.6}$$

where

$$\eta^{peak} = \frac{\sigma_e^{peak}}{\sigma_a^{peak}} \tag{3.7}$$

, k_B is Boltzmann constant and T is temperature. The absorption cross-section was calculated using emission cross-sections, σ_e provided by Asahi Glass Co, and it can be seen in the figure that the calculated emission cross-section agrees well with the experimental data. This optical emission peaks at 1.53 μm, which is obtained due to the population inversion between energy level $^4I_{13/2}$ and $^4I_{15/2}$.

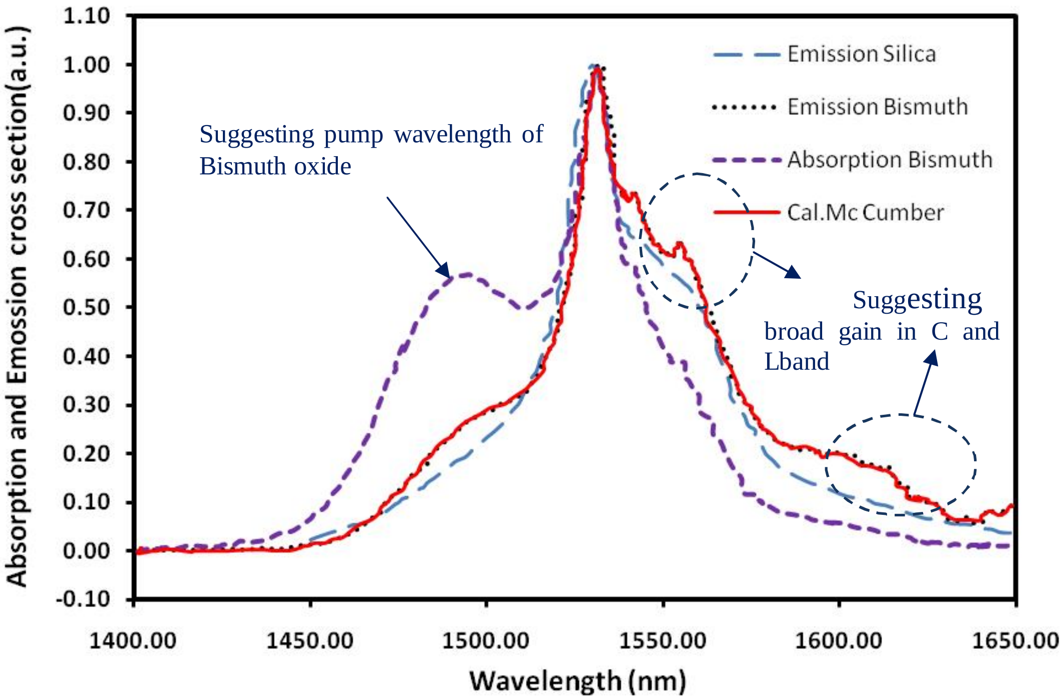

Figure 3. 11: Absorption and emission cross-section of Bi-EDF and Si-EDF. (The Bismuth absorption cross-section is obtained from Asahi Glass Co.). The calculated Bismuth emission curve coincides very well with the measured curve (Harun *et al.*, 2009)

From Figure 3.11, it can be also observed that the Bi-EDF has wider emission spectra as compared to Si-EDF, especially at the longer wavelengths of 1620 nm because of its larger emission cross-section. The Si-EDF has a bandwidth of only 40 nm while the Bi-EDF bandwidth is almost double at 80 nm for the same emission intensity. The widening of the emission spectra is attributed to the Stark level of the Er^{3+} ions in the Bi-EDF, which is separated to a larger degree due to the larger ligand field as reported earlier (Harun *et al.*, 2009). As shown in Figure 3.11, despite the Bi-EDF having a higher absorption cross-section of 7.58×10^{-25} m^2 at the 1530 nm peak as compared to the Si-EDF absorption cross-section (which is only 4.39×10^{-26} m^2), the peak full-width half maximum (FWHM) of the Bi-EDF is narrower than the FWHM of the Si-EDF. This is due to the larger inhomogeneous energy level degeneracy that the ligand field of the Bismuth host glass induced as a result of site to site variations, also known as the Stark effect (Desurvire *et al.*, 1994), causing the widened optical transitions. Other elements such as potassium oxide also have similar glass basicity expander effects (Tanabe *et al.*, 1992) and are used in the fabrication of Bi-EDF to obtain a broader amplification region. It is worth noting that the higher value of absorption of Bismuth oxide in wavelength 1480 nm suggests that it is preferable to use the pump wavelength of1480 nm. Thus, this fibre is a promising candidate for compact amplifier applications with broadband transmission capability.

Theoretical analysis and modeling of the amplification characteristics of Bi-EDF

The general theory light amplification in optical fibres is based on simple rate equations which describe the fractional light amplification as it propagates along a certain distance in an active medium (Desurvire, 1989 and Becker *et al.*, 1997). This theory explains the interaction of the atom (absorption or emission) when an electromagnetic field is launched in a fibre by using fundamental properties of the atom in a special environment as the energy level ion population density, pump intensity and rate equations. The energy level diagram of the erbium is shown in Figure 3.12. The ground level has a structure of ^{4}I, which splits into 9/2, 11/2, 13/2, and 15/2 due to the ligand field interaction between the non-central electrostatic fields, electron spin and its orbital angular momentum (Naito *et al.*, 2004). The absorption bands of 980 nm and 1480 nm depicted in the figure according to transitions from the ground level $^4I_{15/2}$ to the top of the $^4I_{13/2}$ and $^4I_{11/2}$ levels, respectively. The emission of excited Er^{+3} ion includes radiative and nonradiative emission. The radiative emission defines by the energy gap between the energy levels ranging from 10^3 to $10^4 cm^{-1}$. The electron is excited by the pump from ground state ($^4I_{15/2}$)to excited state ($^4I_{11/2}$) and then non-radioactively transits to the meta-stable energy level ($^4I_{13/2}$). After that, it transits from the meta-stable level to the ground state with emission of 1550nm photons.

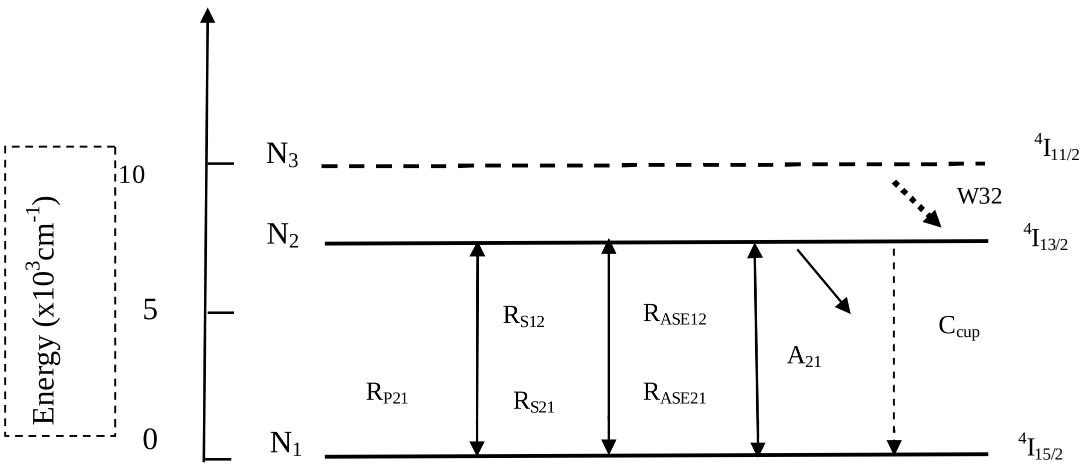

Figure 3. 12**:** Simplified energy-level diagrams and various transition processes of Er^{3+} ions in silica.

Rate equations are given by atomic energy levels to explain the effect of absorption, stimulated emission and spontaneous emission. Assume that the population densities of Er^{3+} ions at the ground level of $^4I_{15/2}$, meta-stable level (the so-called $^4I_{13/2}$ level) and the $^4I_{11/2}$pump level are N_1, N_2 and N_3, respectively. The denoted name of the meta-stable explains that the lifetimes of the transitions from this level to the ground level are very long compared to the lifetimes of the levels that led to this level. Therefore, the steady- state rate equations for the Bi-EDFA system can be written as (Hayashi *et al.*, 2006b):

$$\frac{dN_1}{dt} = (A_{21} + R_{S21} + R_{P21} + R_{ASE21})N_2 - (R_{S12} + R_{P12} + R_{ASE12})N_1 + CN_2^2 \qquad (3.8)$$

$$\frac{dN_2}{dt} = -(A_{21} + R_{S21} + R_{P21} + R_{ASE21})N_2 + (R_{12} + R_{P12} + R_{ASE12})N_1 - 2CN_2^2 + W_{32}N_3 \qquad (3.9)$$

$$\frac{dN_3}{dt} = -W_{32}N_3 + CN_2^2 \qquad (3.10)$$

So, the total population density N is expressed as:

$$N = N_1 + N_2 + N_3 \qquad (3.11)$$

HereA_{21} is the spontaneous emission probability of the 1.55 μm band calculated by the Fuchtbauer–Ladenburg formula (Bames*et al.,* 1991), and W_{32} is the non-radiative decay rate from the $^4I_{11/2}$ level that calculated by the measured lifetime. C is the corporative upconversion coefficient evaluated by Snoek's method (Snokes *et al.*, 1995).We neglect the non-radiative decay rate of the $^4I_{13/2}$level and the spontaneous emission from the $^4I_{11/2}$ level because A_{21} and $W_{32}$are dominant in those levels.

Equations (3.8) - (3.11) can be solved by considering the steady state regime where the populations are time independent, $dN_i/dt=0$ (i=0,1 ,…5). The average Er^{+3} ion concentration in the core is denoted as ρ and is quantified by (Desurvire *et al.,* 1994):

$$\rho = \frac{2}{b^2}\int_0^\infty n(r)rdr \qquad (3.12)$$

where b is the doping radius and n(r) is the Er^{+3}ions concentration profile. R represents the radiative decay rate of the signal, pump and ASE provided from the interaction of the electromagnetic field with the ions or the transition rate is expressed as follows:

$$R_{S21} = (\frac{\sigma_S^E}{A_{eff} h\upsilon_S})P_S \qquad (3.13)$$

$$R_{S12} = (\frac{\sigma_S^A}{A_{eff} h\upsilon_S})P_S \qquad (3.14)$$

$$R_{P21} = (\frac{\sigma_P^E}{A_{eff} h\upsilon_P})(P_p^+ + P_P^-) \qquad (3.15)$$

$$R_{P12} = (\frac{\sigma_P^A}{A_{eff} h\upsilon_P})(P_p^+ + P_P^-) \qquad (3.16)$$

$$R_{ASE\,21} = (\frac{\sigma_P^E}{A_{eff} h\upsilon_S})(P_{ASE}^+ + P_{ASE}^-) \qquad (3.17)$$

$$R_{ASE12} = (\frac{\sigma_P^A}{A_{eff} h\upsilon_S})(P_{ASE}^+ + P_{ASE}^-) \qquad (3.18)$$

where h, A_{eff} are the plank constant and effective area, respectively. $P_P^{\pm}$ And $P_{ASE}^{\pm}$ are the forward and backward propagating pump power and ASE powers while P_S , σ_P^E and σ_P^A are the signal power, emission and absorption cross sections at the pump wavelength, respectively. σ_P^E and σ_P^A are the functions of the input signals estimated from (Harun *et al.*, 2009). We assume that all the Er^{3+}ions excited to the $^4I_{9/2}$ levels by the cooperative up-conversion process relax to the $^4I_{11/2}$ immediately.

The evolution of the pump power, ASE powers and signal power along the Bi-EDF fibre (z) is given as (Desurvire *et al.*, 1994);

$$\frac{dP_S}{dz} = \Gamma(\lambda_s)(\sigma_S^e N_2 - \sigma_S^a N_1) \times P_S - \alpha_S P_S \qquad (3.19)$$

$$\frac{dP_P^{\pm}}{dz} = \Gamma(\lambda_P)(\sigma_P^e N_2 - \sigma_P^a N_1) \times P_P^{\pm} - \alpha_P P_P^{\pm} \qquad (3.20)$$

$$\frac{dP_{ASE}^{\pm}(\lambda_{ASE})}{dz} = \Gamma(\lambda_{ASE})(\sigma_{\lambda}^{e}N_2 - \sigma_{\lambda}^{a}N_1) \times P_{ASE}^{\pm}$$
$$+ \Gamma(\lambda_{ASE})h\nu\Delta\nu\sigma_{\lambda}^{e}N_3 - \alpha_{ASE}P_{ASE}^{\pm} \qquad (3.21)$$

Where Γ is the overlap factor of every wavelength (Hayashi *et al.*, 2006a) and α is the fibre background loss measured (Desurvire *et al.*, 1994). The subscripts s and ASE mean the signal and the ASE, respectively. In the ASE equation, $\Delta\nu$ represents the effective ASE bandwidth that is the resolution of the measuring device such as an optical spectrum analyzer. The overlapping factors between each radiation and the fibre fundamental mode, $\Gamma(\lambda)$ can be expressed as (Desurvire *et al.*, 1994):

$$\Gamma(\lambda) = 1 - e^{-\frac{2b^2}{w_0^2}} \qquad (3.22)$$

$$w_0 = a\left(0.761 + \frac{1.237}{V^{1.5}} + \frac{1.429}{V^6}\right) \qquad (3.23)$$

where w_0 is the mode field radius defined by Equation (3.23), a is the core radius, b is the thulium ion-dopant radius and V is the normalized frequency.

The pump, signal power, population densities and ASE rate equations described in the previous section are required to be solved numerically. There is a basic difficulty in numerical solution of the rate equations of P_s, P_p and P_{ASE} as the evaluation of boundary condition. Regardless of the pumping configuration, the P_{ASE} distribution along the fibre is not known priori. Although only the forward pumping is considered in single pass structure, but the backward ASE power has to be applied for double pass pumping structure. While P^{+}_{ASE} power is zero at the input of EDFA, corresponding P^{-}_{ASE} power is maximum at this point. Thus, in order to perform the numerical method of the equation starting at first length of fibre, assumption has to be considered for unknown P^{-}_{ASE} power. Indeed, the shooting method and relaxation method are two methods to solve the boundary conditions equations (Desurvire *et al.*, 1994).On the other hand, relaxation method provides the iterative adjustment to the solution. In this method, an initial set of boundary value is chosen for the first integration. Then the system is integrated again, for example in the reserve direction, incorporating correct boundary values.

The gain of the Bi-EDFA is calculated by numerically solving Equations (3.8) - (3.21) of the previous section. The parameters used in the calculations 3×10^{8} m/s for the light speed c in vacuum, 6.626×10^{-34} m^2kg/s for the Planck's constant h, 2.7×10^{-6} m for the radius of the optical fibre and $8.5\times10^{-24}$for the C. The pump and input signal powers are fixed 150mWand 10^{-3}mW, respectively; and the fibre background loss is 0.6 dB/m. All of equation used for pump, signal and pump power are first order differential equations. We have used P_P (z=0) = P_P, P_S(z=0) = P_S and P_{ASE} (z=0) = 0asthe boundary conditions on pump power, signal power and ASE spectral at input signal wavelength. The amplification in the EDF can be described by calculating the optical powers in slices, Δz, along the propagation direction as shown in Figure 3.13. To get accurate result a relaxation method is used by dividing fibre to many small slices of 10cm long.

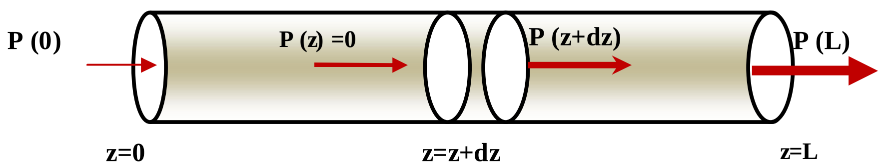

Figure 3. 13: Schematic model of light amplification along the fibre.

Noise figure is generated by spontaneous emission and therefore is closely related to ASE which can be calculated using the following equation;

$$NF = 1/G + P_{ASE} / (G \times h \times \nu \times \Delta\nu) \qquad (3.24)$$

where P_{ASE} is the ASE power, h is Planck's constant, ν is the frequency of the signal and $\Delta\nu$ is the resolution of the measuring device such as an optical spectrum analyzer (Desurvire*et al.*, 1994).

Experimental measurement

The experimental setup of the forward pumped Bi-EDFA is illustrated in Figure 3.14. It consists of a Wavelength Selective Coupler (WSC), two optical isolators, one Variable Optical Attenuator (VOA) and a piece of Bi-EDF. Both optical isolators are used to avoid the reflection and ensure unidirectional operation in the amplifier. The 1480nm laser diode is used to pump the Bi-EDF. WSC is used to combine the pump light with 1550nm signal. AVOA is incorporated immediately after the TLS to control the input signal power into the optical amplifier. The gain and noise figure of this amplifier is investigated using an OSA in conjunction with TLS.

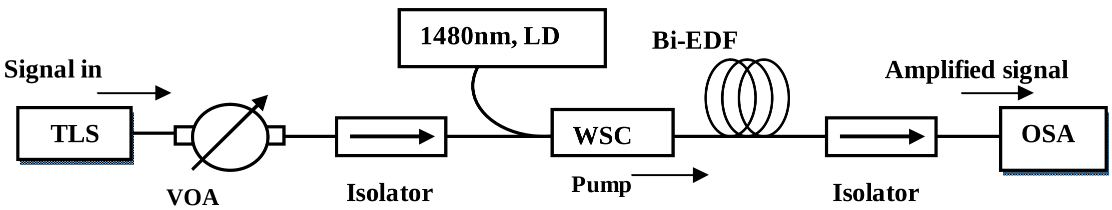

Figure 3. 14: Experimental set-up for the forward pumped Bi-EDFA.

Theoretical and experimental results on the amplification characteristics of Bi-EDF

Figure 3.15 shows the calculated gain as a function of Bi-EDF's length at various input signal wavelength. In this calculation, the erbium ion concentration and pump power are set at 7.6×10^{25} ions/m^3 and 150 mW, respectively. As shown in the figure, the maximum gains of 26 dB, 20 dB and 15 dB are obtained for 1530, 1575 and 1615 nm at Bi-EDF's length of 1.0 m, 1.0 m and 1.5 m respectively. At a longer Bi-EDF length, the gain of the Bi-EDFA shifts to the longer wavelength region (towards L-band) as depicted in Figure 3.15. This is attributed to the quasi two level system effects in the Bi-EDFA, which the C-band photons are absorbed to emit at a longer wavelength. Figure 3.16 compares the experimental gain and noise figure characteristics of the Bi-EDFA with the theoretical values at the pump power of 150 mW and the Bi-EDF's length of 49 cm. The input signal power is fixed at -30 dBm. The gains are observed in both C- and L-band regions with the higher gain are obtained at the C-band region ranging from 1530 to 1560 nm. It is shown that the calculated value is in good agreement with the experimental measured one, verifying the feasibility of our theoretical model.

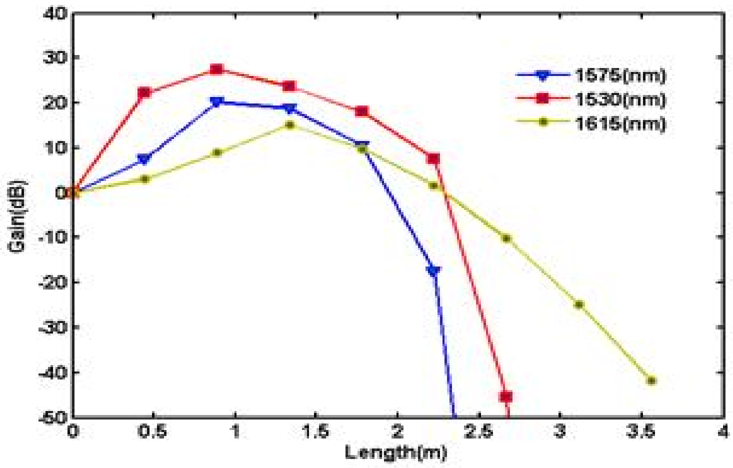

Figure 3. 15**:** Variation of gain as a function of Bi-EDF's length for three different input signal wavelengths.

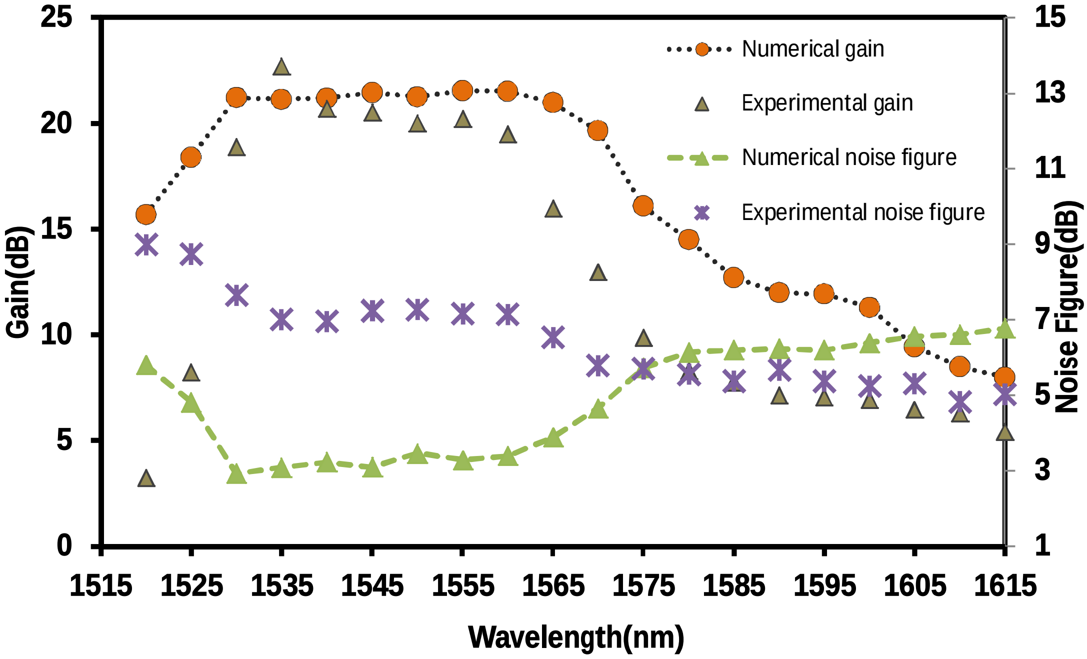

Figure 3. 16**:** Comparison of calculated gain and noise figure with experimental results for the Bi-EDFA with 49cm long Bi-EDF.

As shown in Figure 3.16, the theoretical and experimental gains of the Bi-EDFA are obtained within 20 to 23dB at C-band region. The theoretical gain is flat within 35nm bandwidth from 1530nm to 1565 nm. The slightly lower gain for the experimental results especially at longer wavelengths is expected due to the effect of multiple reflections from both the fiber splice points whereby the signal is reflected back into the Bi-EDF due to the large refractive index difference. This causes the increased cavity loss and spurious laser generation which suppresses the gain of the Bi-EDFA. As shown in Figure 3.16, the Bi-EDFA gain bandwidth covers until the extended L-band region and is also much wider than that of the standard Si-EDFA. This is attributed to the suppression of Excited State Absorption (ESA) effect by the incorporation of La ions in the Bi-EDFA. The suppression of ESA reduces the dissipation of pump energy and increases the population inversion especially at extended L-band region. The experimental noise figure is obtained at approximately 7 dB within the C-band region as shown in Figure 3.16. The high erbium ion doping concentration and high insertion loss of the Bi-EDF incur a high noise figure for the Bi-EDFA. The theoretical noise figure is lower since the insertion loss of the Bi-EDF was ignored during simulation.

Figure 3.17 shows the theoretical gain spectrum of the Bi-EDF with variation of Bi-EDF length from 0 to 1m. The input signal and pump powers are set at -30dBm and 150mW, respectively. As shown in Figure 3.17, the gain of the Bi-EDFA is remarkable in C band with a shorter length of Bi-EDF and as the length increases the gain increment is more pronounced in L band region. The optimum length for the Bi-EDFA to operate in C-band is around 0.5 to 0.8m.

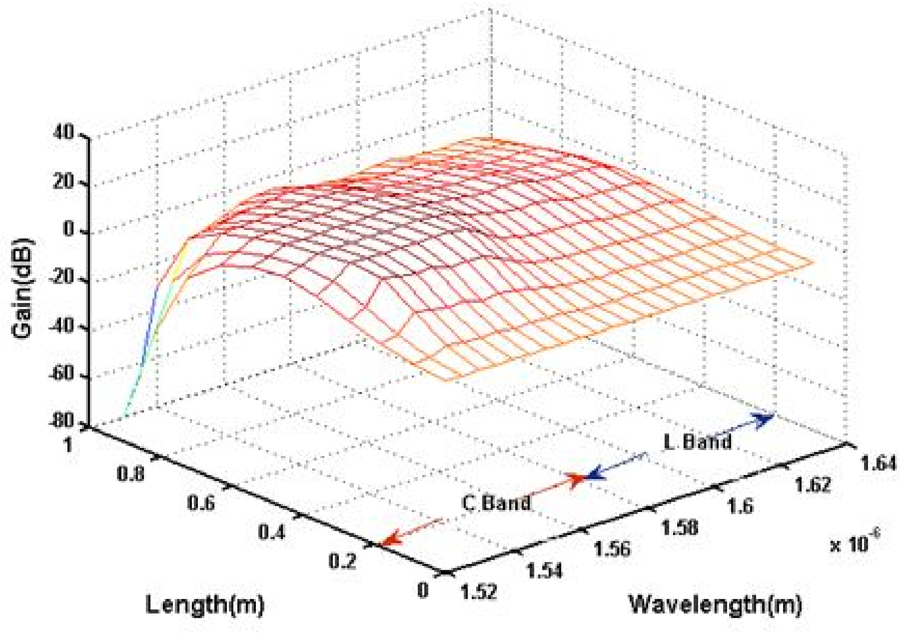

Figure 3. 17**:** Theoretical gain versus input signal wavelength and Bi-EDF's length for the Bi-EDFA.

The amplification characteristic of the Bi-EDF is very important in this study since the Erbium gain will be used to assist in multi-wavelength generation, which will be presented in the next chapter. Another interesting feature of this fibre is its nonlinear specifications as generating SBS and FWM effects. In order to explore SBS, we have to use the main configuration of generating SBS effect as shown in Figure 3.1. It is worth noting that we couldn’t achieve any considerable results with incorporating Bi-EDF in this configuration but it was obtained by utilizing a closed loop laser configuration which will be discussed in detail on the next chapters. The next section demonstrates a FWM effect in both PCF and Bi-EDF.

3.5 FWM effects in nonlinear fibres

One of the biggest challenges in optical communication systems, with increasing transmission rates and improved system capability, is to overcome the nonlinear effects in optical fibres. This effect is much more harmful in optical fibre communication systems. Four-wave mixing seems to be the most harmful in the case of dense wavelength division multiplexing (DWDM) systems (Eiselt, 1999) that use low dispersion fibre or narrow channel spacing. However, it can be useful in some applications such as wavelength conversion and switching (Sharping, et al., 2002). The conventional silica fibres are widely used as a standard nonlinear medium for these devices. However, the nonlinearity of these fibres is intrinsically low and long fibre length is required to obtain a sufficient nonlinear phase shift. Recently, the interest of the effect of FWM in highly nonlinear fibres is increasing for various applications including a multi-wavelength laser generation. In this section, a FWM effect in both PCF and Bi-EDF are investigated using two injecting lasers.

In general, the phenomena of FWM and parametric amplification are due to the third-order nonlinear polarization effect from an interaction between the intense pump lights of frequencies ω_1, ω_2, ω_3, ω_4 and the nonlinear medium. The interaction can generate waves at new frequencies while the net energy and momentum are conserved. In the case of degenerate FWM, in which $\omega_1 = \omega_2 = \omega_3 = \omega_4$, two frequencies of ω_S and ω_P, signal and pump waves, generate two new frequencies when phase matching requirements are met as shown in Figure 3.18. Indeed, FWM efficiency strongly depends on optical channel spacing and fibre dispersion. These conditions can be fulfilled if two or more signals are launched in a low dispersion media and optical channel spacing.

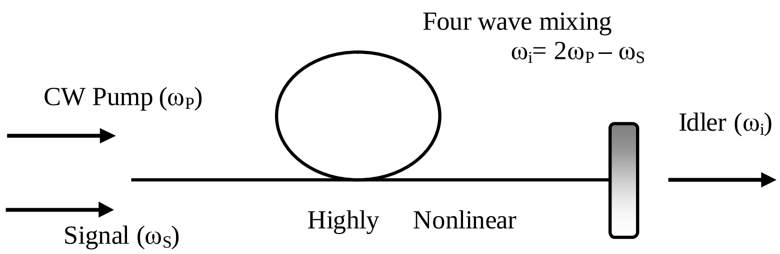

Figure 3. 18: Schematic of FWM-based providing new side band signals.

FWM effect in PCF

In this section we have studied FWM effect based on 100 m long PCF to measure the optical nonlinear and dispersion parameters which are the main factors related to FWM effect. Figure 3.19 shows the experimental set-up for the simultaneous measurement of nonlinear and dispersion characteristics in the PCF via partially degenerated FWM. Two input pump waves from two TLSs (TLS1 and TLS2) are combined by a 3 dB coupler. The combined waves are amplified by an EDFA before it is launched into the PCF, which is also a polarization maintaining fibre. Since the FWM efficiency depends on the light‘s polarizations, two polarization controllers (PCs) are incorporated to adjust the polarization at the input to obtain maximum FWM efficiency. When the pump wave and signal wave propagate in the fibre, FWM is generated as an optical side-band by the third order optical nonlinearity. The FWM products are measured with OSA at the output.

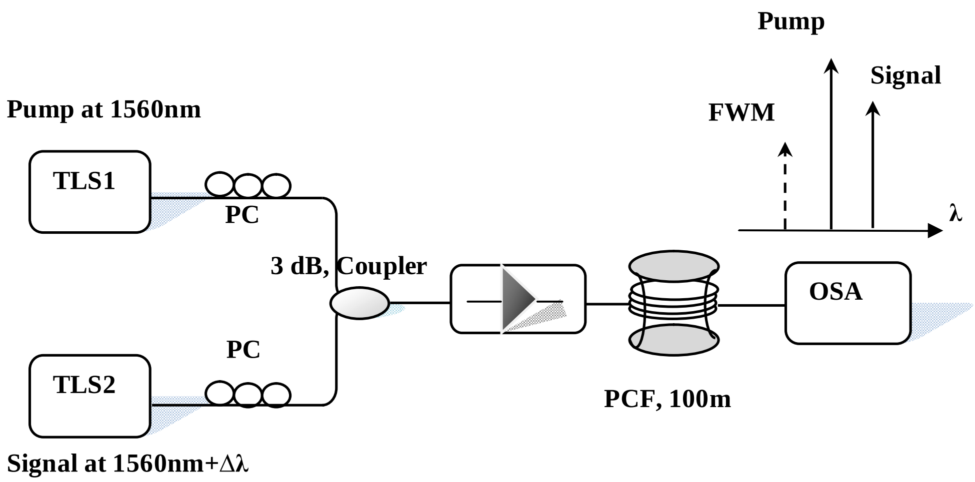

Figure 3.19: Experimental setup for providing new side band signals based on FWM effect.

Figure 3.20 illustrates the optical spectrum at the output of the 100 m long PCF when the channel spacing is fixed at 1and 0.5nm. In this experiment the TLS1 is considered as a pump with a fixed wavelength of 1560 nm. The TLS acts as a signal source with a variable wavelength. As shown in the figure, an optical side-band is observed at the output spectrum even in quite short-length of PCF for both signal source wavelengths of 1560.5 and 1561nm, which a closer wavelength generates a relatively higher power side-band. This shows that the pump power of 14 dBm and the gain medium of 100m are sufficient for providing and exploring the nonlinear FWM effect. FWM of degenerated pump wave and signal wave appears at the frequency of $2\omega_P$-ω_S, which is 1nm from the pump as shown in Figure 3.20. Two peaks also are generated on the right side of the pump wavelength due to the FWM as well. Because FWM effect can happen mutually even we change the definition of the pump and signal waves names. These peaks are produced in the equal spacing with the left side generated peaks that this is the specifications of FWM effect.

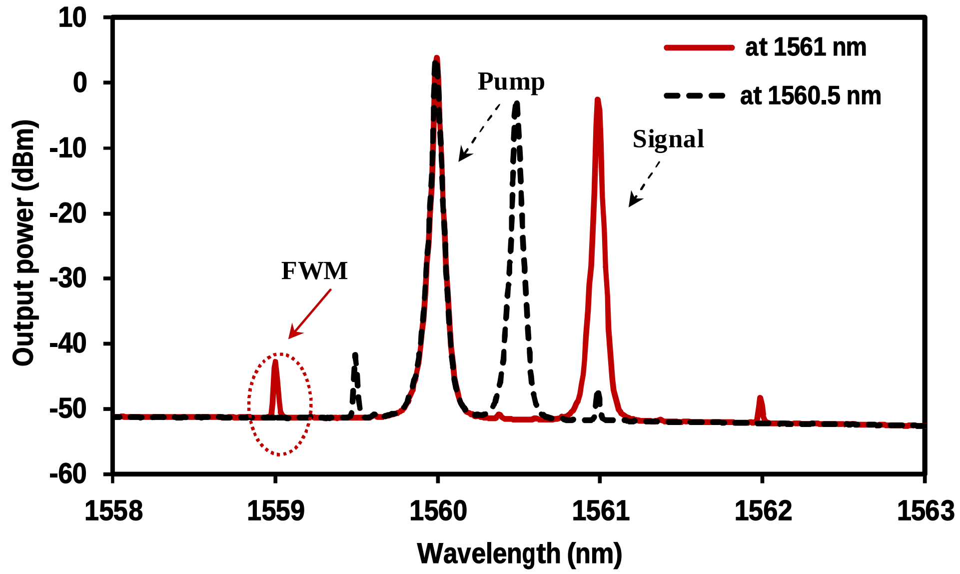

Figure 3. 20: FWM spectrum by 100 long PCF with the wavelength detuning is Δλ=1 and 0.5 nm.

The stability of the side-band generations is playing a vital role in practical applications. Figure 3.21 shows the spectral evolutions of the FWM side-band in terms of time. In the experiment, the output spectral is repeatedly scanned for every 20 min. The side-band power is observed to very stable with power fluctuations of less than 0.5 dB for more than 4 hours. To indicate that this short length of PCF can assess the practical implication even in L-band, we have tried to amplify the input signals in L-band region and then launch them to the fibre. Figure 3.22 shows the output of FWM effect by 100 m long PCF provided by injected signals with the wavelength detuning of Δλ=1, 0.5, and 0.3 nm from 1600 nm wavelength of pump wave. It is seen that the similar effect is also observed in L-band region. These results show that the proposed configuration is suitable for the studying of FWM and related nonlinear parameters as chromatic dispersion and nonlinear coefficient.

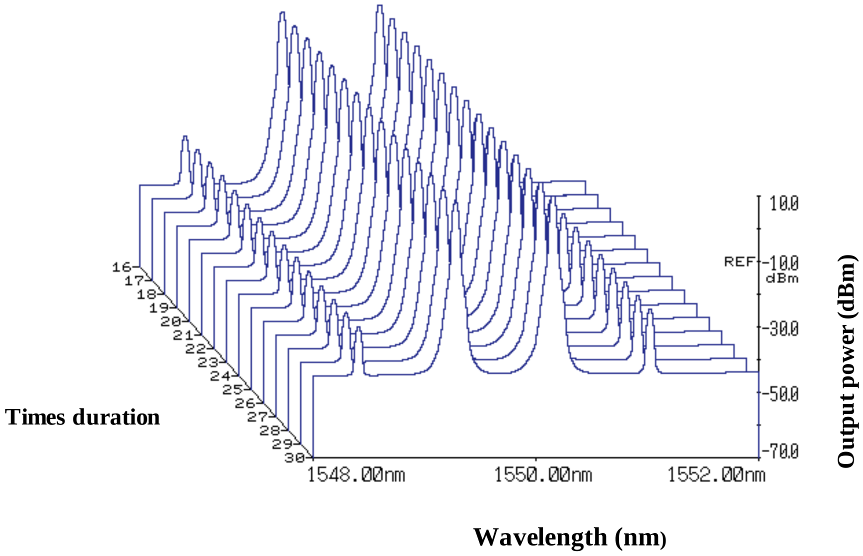

Figure 3. 21: Spectral evolutions of the FWM effect structure output against time. (The laser spectra scanned over every 20 minutes).

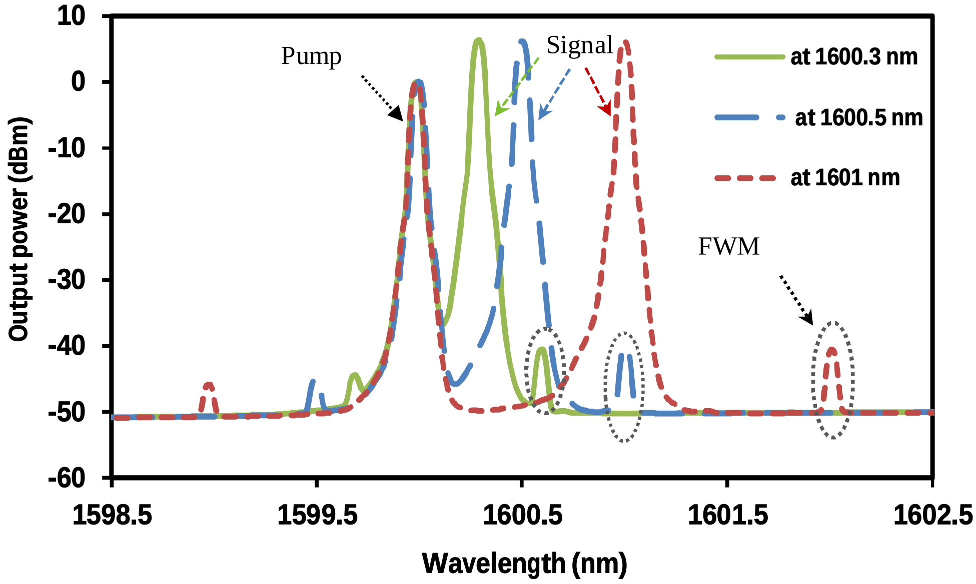

Figure 3. 22: FWM spectrum by 100 long PCF with the wavelength detuning is $\Delta\lambda$=1, 0.5, and 0.3 nm in L-band region.

3.6 Simultaneous measurement of nonlinearity and dispersion parameters of PCF using the FWM effect

In this section, the FWM effect is used to simultaneous measure the nonlinearity and dispersion parameters of PCF. FWM efficiency in PCF is experimentally measured and the result is used to estimate the nonlinearity and dispersion parameters theoretically. In the situation where pump continuous-wave is partially degenerated, power of launched signal is P_S and the spacing is Δf, the FWM sideband power is given by (Bogoni *et al.,* 2003)

$$P_{FWM} = \frac{\eta}{9} d^2 \gamma^2 P_P^2 P_S \exp(-\alpha L) L_{eff}^2 \qquad (3.25)$$

Where η is the FWM efficiency, d is the degeneracy factor (d = 3 and 6 in case of two and three channels, respectively), γ is the nonlinearity parameter, α is the fibre attenuation coefficient, L and L_{eff} are the length and the effective length of the fibre respectively. This equation is the master formula, which has been widely used in recent years to evaluate the FWM induced crosstalk in WDM systems.

Nonlinearity parameter is defined as follows (Agrawal, 1986):

$$\gamma = {}^{2\pi n_2}\!/_{\lambda A_{eff}} \qquad (3.26)$$

where A_{eff} is the effective core area, λ is the vacuum wavelength, and n_2 is the nonlinear-index coefficient which is defined based on the nonlinear susceptibility $\chi^{(3)}$ by

$$n_2 = \frac{48\pi^2}{cn^2} \chi^{(3)} \qquad (3.27)$$

where n is denoted the refractive index of the fibre core and c is the vacuum speed of light. Effective length, L_{eff}, of the fibre with linear loss of α is defined as

$$L_{eff} = \frac{1}{\alpha}(1-\exp(-\alpha L)) \qquad (3.28)$$

The FWM efficiency η can be expressed as

$$\eta = \frac{\alpha^2}{\alpha^2+\Delta\beta^2}[1+\frac{4.\exp(-\alpha L).\sin^2(\Delta\beta.L/2)}{(1-\exp(-\alpha L))^2}] \qquad (3.29)$$

The phase mismatch *Δβ* which depends on the fibre chromatic dispersion and channel frequency spacing is then given by (Hasegawa *et al*., 2008)

$$\Delta\beta = \frac{2\pi\lambda^2}{c}D\Delta f^2 \qquad (3.30)$$

where D is the chromatic dispersion parameter and Δf is the detuned spacing between signal and pump wavelength. Since $\Delta\beta$ is not a function of signal powers, it is also known as linear phase-matching factor (Song *et al*., 1999). The dispersion parameter can be expressed as;

$$D = -\frac{2\pi\lambda^2}{c}\beta_2 \qquad (3.31)$$

whereβ_2 is the group velocity dispersion (GVD) parameter (Hasegawa *et al*., 2008).From Equation (3.25), the maximum FWM signal power can be used to determine the nonlinear coefficient γ by carefully measuring input pump and signal powers, PCF length and fibre loss. To assess the practical evaluation of this theoretical analysis, we estimate the dispersion of incorporated PCF as a simple example. Since λ_s is closed enough to λ_p, FWM efficiency η is estimated to be around 1. Therefore, the nonlinear coefficient of the PCF is calculated to be about 43(WKm)$^{-1}$ at 1560nm according to equation (3.25). The averaged zero dispersion wavelengths is estimated to be around 1560nm due to the maximum FWM intensity that was observed in this wavelength region.

The measured FWM signal intensity against wavelength is analyzed to extract the fibre dispersion characteristic by tuning signal laser wavelength while the pump laser wavelength is fixed. Figure 3.23 shows the measured FWM spectra when the pump wavelength is fixed at 1560 nm and the signal wavelength is changed from 1560.5 nm to 1565 nm. The FWM is observed in anti-stokes side to the signal wave. With detuning the signal wavelength, the FWM efficiency also changes because of the phase mismatching. Figure 3.24 indicates the relation between the channels spacing Δf and the FWM power conversion efficiency. The theoretical results are obtained by solving and fitting Equations (3.25), (3.30) and (3.31) as a function of the spacing detuning. The theoretical fitting is found to be in a good agreement to the experimental results as shown in Figure 3.24. In order to demonstrate the vital role of nonlinear coefficient in the FWM power conversion efficiency, the theoretical data is also investigated for higher values of γ; 60 and 100 $(Wkm)^{-1}$ for comparison purpose. This comparison shows that the FWM power conversion efficiency increases with the fibre nonlinearity and this trend is not linear.

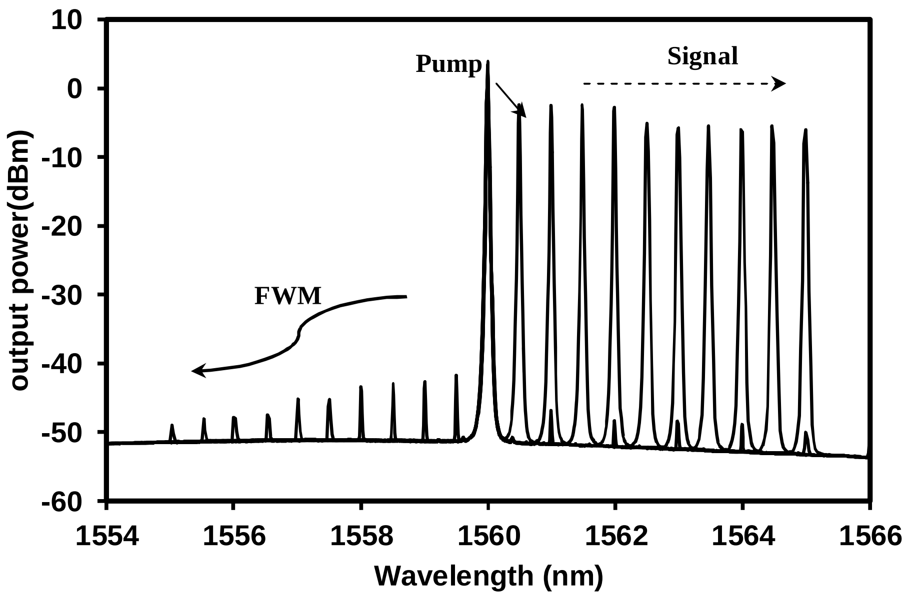

Figure 3. 23: Wavelength detuning FWM spectra in PCF. The pump wavelength is fixed at 1560nm.

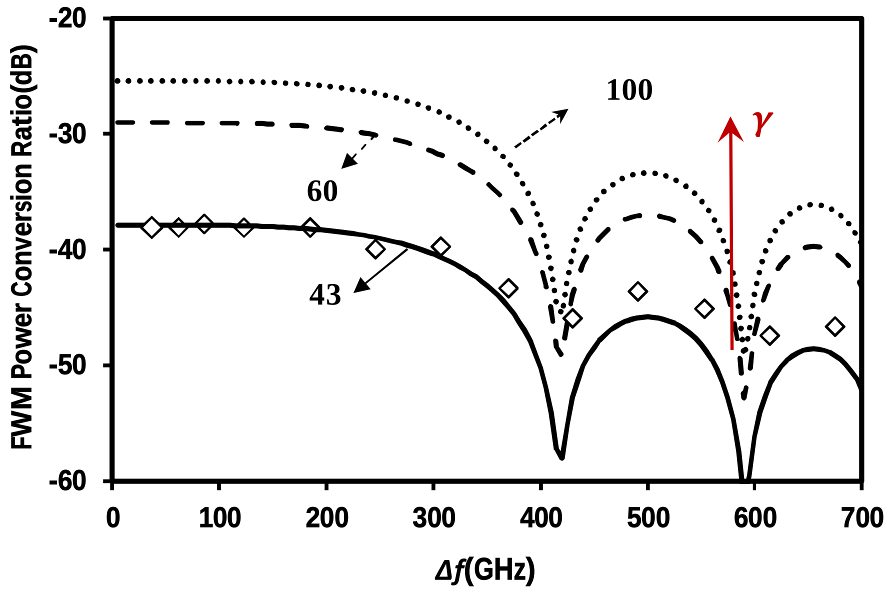

Figure 3. 24: FWM power conversion efficiency vs signal and pump frequency spacing in GHz scale. The solid and dash curves are the theoretical results from Equations (5-1), (5-5) and (5-6) and points curve is the results obtained from experimental setup.

The analysis of FWM signal power minima, from the curve of FWM conversion efficiency ratio against channel spacing, is then used for calculating the dispersion characteristic of the optical fibre. Figure 3.25 shows the FWM curve at three different lengths of PCF, which clearly indicates that first minima fringe of P_{FWM} occurs at different channel spacing Δf. It also observed that the FWM power conversion ratio decreases with the increment of the channel spacing. These results prove that FWM can be restricted somewhat by increasing the channel spacing. To measure fibre dispersion, it is necessary to find the channel spacing for which P_{FWM} reaches its first minimum and calculate the chromatic dispersion using the following equation;

$$D = \frac{c}{\lambda^2 . \Delta f^2 . L} \tag{3.32}$$

where λ is the operating signal wavelength. Based on Equation (3.29), the minimum of the P_{FWM} is obtained when $\Delta\beta .\ L/2 = k.\ \pi$, where k is integer due to the phase mismatch between the signals that propagate inside the fibre. As shown in Figure 3.25, the first minimum of the FWM power conversion efficiency is obtained at 430 GHz spacing for the PCF with 100m length. Assuming c = 3 x 10^8 m/s and λ = 1560 nm, the chromatic dispersion of the PCF is calculated to be around 6.05ps/nm.km. The numbers of fringes depend on the FWM mismatch factor or k integer, which increases with the fibre length for the case of same phase mismatching. Therefore, the number of fringes is observed to be higher at 300m compared with 100m by 3 times as shown in Figure 3.25.

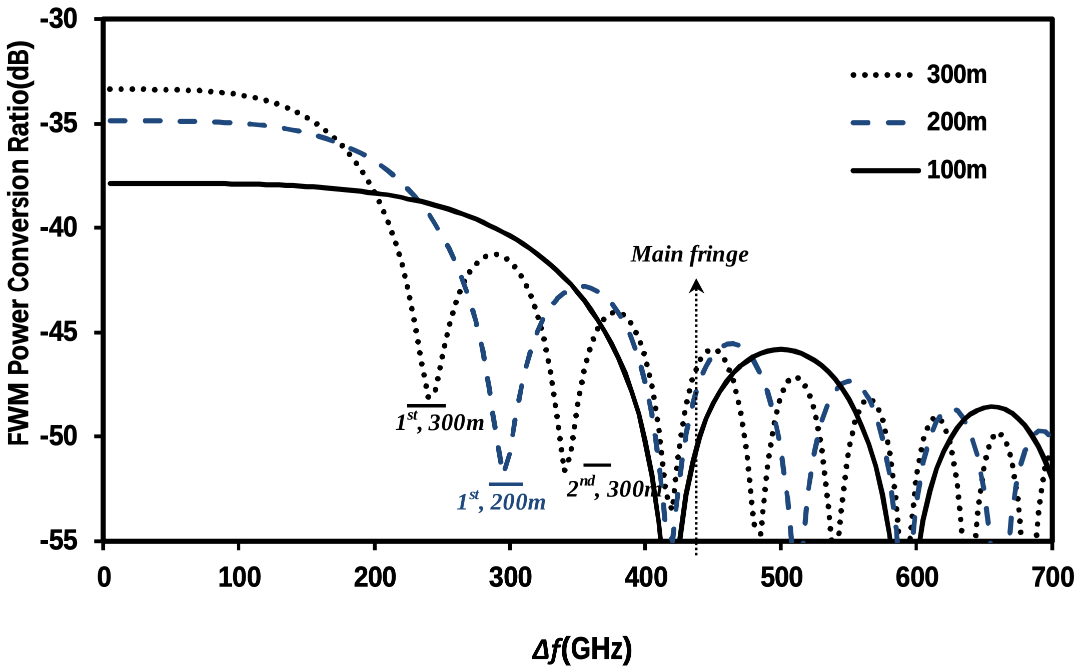

Figure 3. 25: FWM power conversion efficiency against the frequency spacing detuning at various PCF lengths.

Evaluation of the Kerr nonlinearity Figure-of-merit

If two beams of continuous light wave with a particular frequency difference are injected into a fibre, a beat signal will be generated. When the beat signal propagates along the fibre, its spectrum will broaden due to the GVD and self-phase modulation (SPM) (Agrawal, 1998). To evaluate the nonlinear performance of the PCF, a figure-of-merits (FOMs) is derived based on the required input signal power to achieve a certain nonlinear phase shift. The Kerr nonlinearity FOM is given by (Agrawal, 1998);

Figure 3.26 shows the nonlinear phase shift calculated against the input optical power. As shown in the figure, the nonlinear phase shift is linearly increased with the input signal power. The slope of the linear curve determines twice of the FOM, which evaluates the nonlinear performance of this fibre. As shown in Figure 3.26, the FOM for the 100 long PCF is observed to be around 0.737 (W^{-1}) which is comparable to the nonlinearity performance of another PCF mentioned in Ref. (Song *et al.*, 1999). It is probably attributed to its special structure based on air and silica by making an efficient refractive index.

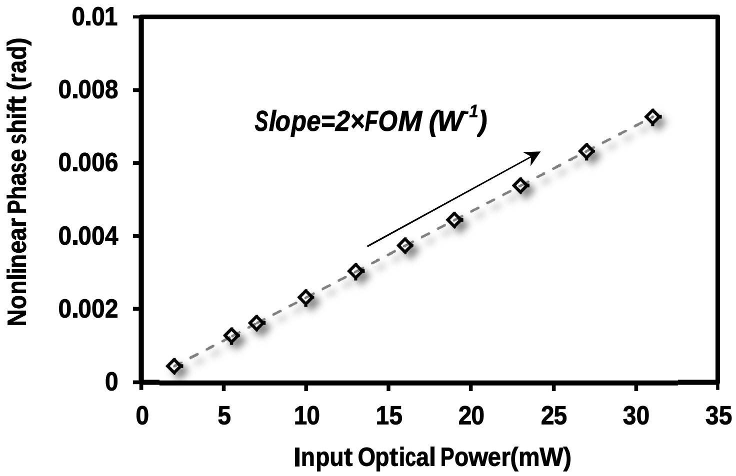

Figure 3. 26**:** Nonlinear phase shift calculated as a function of the input optical power.

3.7 Investigation of FWM effect in Bi-EDF

In this section, the FWM effect in Bi-EDF with two different lengths is investigated by injecting two signals, which the experimental set-up is almost similar to Figure 3.19

expected for the 1480 nm pump. The Bi-EDF is pumped by 120 mW to compensate for absorption loss as well as to provide gain for the FWM pumps. Two different lengths of 49 and 215 cm Bi-EDF are used as a nonlinear gain medium to realize the FWM sideband. This Bi-EDF has a nonlinear coefficient of ~60 $(W\cdot km)^{-1}$ which other special features have been mentioned in previous chapters. Figure 3.28 shows optical spectra obtained when two signals with different spacing are launched into a piece of 49 cm long Bi-EDF. In this experiment, the spectral spacing of the three wavelengths was changed by tuning TLS2. As shown in the figure, only dual-wavelength output is observed in the output. This shows that this fibre is not able to provide any idler signal probably due to insufficient interaction length.

These investigations show that FWM signal cannot be achieved in the open-loop configuration of Figure 3.27 with 49 cm long Bi-EDF. To enhance its FWM efficiency and operating in the C-band region, the 49 cm Bi-EDF is used in closed loop such as in linear and ring cavities as explained in the following chapters. Figure 3.28 shows the output spectrum obtained when two signals with 1.0 nm spacing are launched into a longer piece of 215 cm long Bi-EDF. The Bi-EDF provides amplification in L-band with this length and therefore the pump wavelength operates in L-band region. By incorporating a longer length of fibre, the product γPL is larger and somehow 215 cm of Bi-EDF is sufficient to generate FWM sideband signals as shown in Figure 3.28. γ is the nonlinear coefficient of the fibre, P is the optical power passing through the fibre and L isthe effective length of the used fibre.

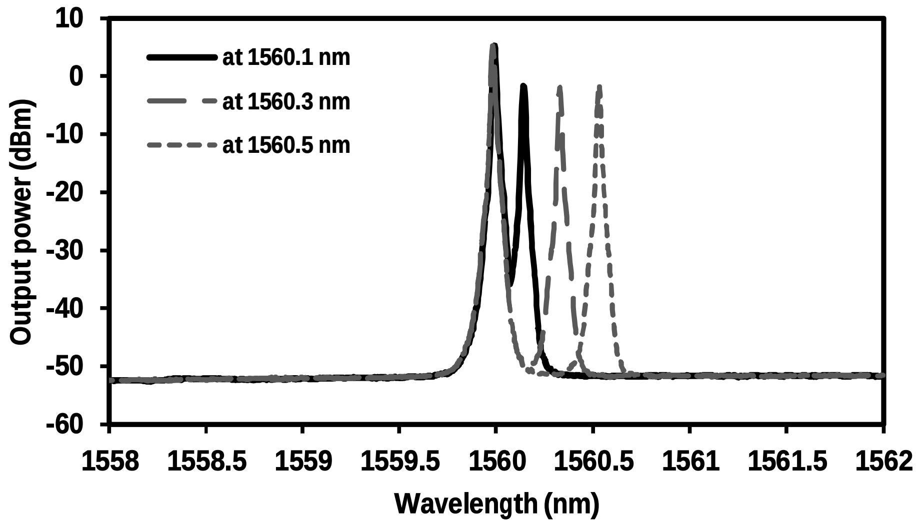

Figure 3. 27: Optical spectra obtained from the different spacing-tunable dual-wavelength source using 49 cm long Bi-EDFA.

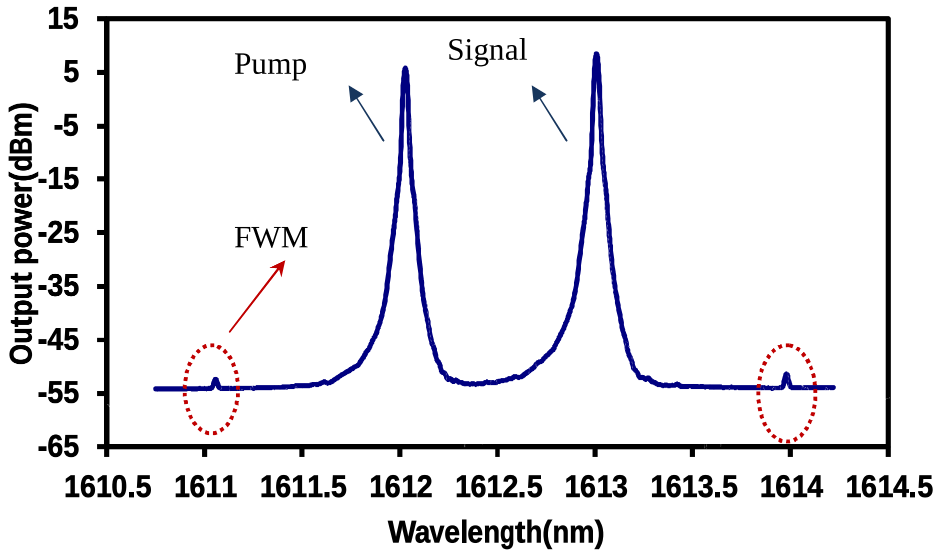

Figure 3. 28: Optical spectra obtained from the different spacing-tunable dual-wavelength source using 215 cm long Bi-EDFA with the inset graph of stability of this achieved FWM.

In the next chapter, performances of nonlinear fibre lasers are investigated using two different gain media of PCF and Bi-EDF. Various configurations of Brillouin fibre lasers will be proposed and demonstrated for both single- and dual-wavelength operations. FWM-based fibre laser will also be demonstrated for multi-wavelength operation.

CHAPTER FOUR: COMPACT NONLINEAR FIBRE LASER CONFIGURATIONS EMPLOYING PHOTONIC CRYSTAL FIBRE AND BISMUTH BASED ERBIUM DOPED FIBRE

4.1 Introduction

In the previous section, both Stimulated Brillouin Scattering (SBS) and Four-Wave Mixing (FWM) effects are observed in Photonic Crystal Fibre (PCF) and Bismuth-based Erbium-doped fibre (Bi-EDF). Brillouin fibre lasers (BFLs) can be generated by the SBS and has many potential applications in instrument testing and sensing, as well in an optical source for dense wavelength division multiplexing (DWDM) systems (Yang *et al.,* 2005). Provided that SBS induced Brillouin amplification overcompensates the cavity loss, Brillouin Stokes waves oscillates and it generates BFLs. Furthermore, the Brillouin threshold reduces when operating in a closed loop such as ring and linear cavities. The BFL device is desirable to use a gain medium with a large Brillouin gain coefficient such as PCF and Bi-EDF to lower the power requirements and to shorten the length of the device (Inoue, 1995; McIntosh *et al.,* 1997 and Lee *et al.,* 2005 (a)). The use of Erbium gain in BFL's cavity such as in Brillouin erbium fibre laser (BEFL) would also reduce the power requirement and enhances the efficiency of the Stokes generation process in the laser. On the other hand, the FWM effect can also be used to construct nonlinear fibre laser.FWM-based fibre laser has many applications in multi-wavelength generation as well as a wavelength convertor.

In this chapter, a conventional BFL set-up is introduced. Various new architectures for BFL have been proposed using either PCF or Bi-EDF as the gain medium to reduce the threshold power of the SBS effect as well as to increase the efficiency of the BFL. A compact laser is also demonstrated using a 49 cm long Bi-EDF as the gain medium. Dual wavelength laser is then demonstrated using PCF. FWM-based laser is demonstrated at the end of this chapter using a Bi-EDF as a gain medium.

4.2 A conventional Brillouin Fibre Laser

This section demonstrated a BFL generation using a piece of PCF as the gain medium in a ring configuration. The configuration of the conventional ring BFL is illustrated in Figure 4.1, which consists of an optical circulator, a 3dB coupler and a piece of PCF. The Brillouin pump (BP) is an external cavity Tunable Laser Source (TLS) with a line-width of approximately 20MHz, which is amplified by an Erbium-doped fibre amplifier (EDFA) to provide sufficient power for this study. The BP wavelength is fixed at 1560 nm in this experiment. The BP is launched through the optical circulator to generate a backward propagating SBS, which oscillates inside the resonator to generate the laser at wavelength downshifted by 0.08 nm from the BP wavelength. The clockwise oscillating laser is extracted from the resonator via the 3dB coupler to route into the Optical Spectrum Analyzer (OSA) via optical circulator. In this BFL, only single-wavelength of the Brillouin Stokes line is obtained because the Brillouin Stokes cannot act as subsequent BP to create higher order Brillouin Stokes signals. The output of the BFL is characterized using an OSA with a resolution of 0.015 nm. The experiments are carried out for three different lengths of PCF; 100m, 50m and 20m.

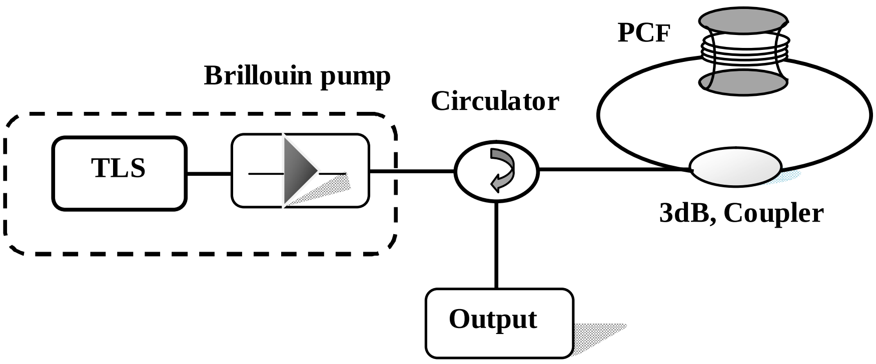

Figure 4. 1**:** Experimental configurations of the PCF-based BFL conventional ring cavity.

Figure 4.2 demonstrates the output spectrum of the BFL at different lengths of PCF while the BP power is fixed at 15.7 dBm. The line spacing is obtained at approximately 0.08 nm in the wavelength domain, as measured by the OSA. The 3dB spectral bandwidth of the BFL is measured to be less than 0.02 nm, limited by the OSA resolution. The peak power of the laser is obtained as 0.9 dBm and -3.6 dBm at 50 m and 100 m, respectively. The peak power of 100 m long PCF is less than 50 m long PCF due to more absorption by longer length. However, as shown in Figure 4.2, side mode suppression ratios (SMSRs) of the BFL are obtained at 26.4 dB and 22.2 dB with 100 m and 50 m long PCF respectively due to the Brillouin gain by longer length of PCF. Although the longer PCF in the BFL resonator increases the cavity's loss, it provides a better nonlinearity characteristic to achieve an efficient SBS using a micro-structured cladding region with air holes to guide light in a pure silica core. No lasing is observed with the 20 m long PCF due to the insufficient fibre length is not enough to generate an adequate Brillouin gain to compensate for the cavity loss.

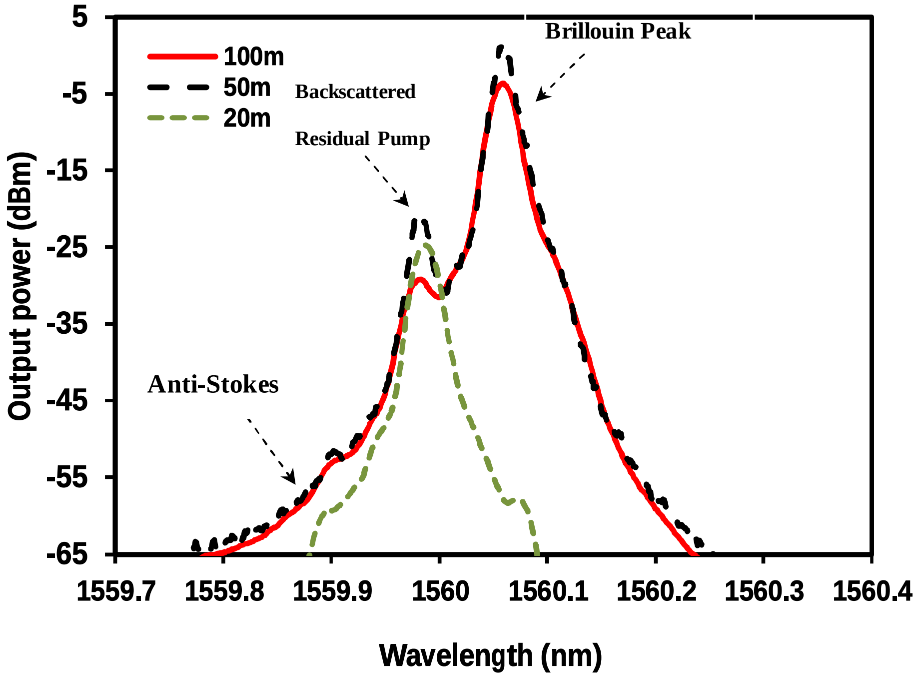

Figure 4. 2: Output spectra of the ring BFL with different long PCF.

Figure 4.3 shows the measured peak power of the BFL against the input BP power. As shown in the figure, the peak power increases with the BP power. The threshold power is the BP power at the point where the resonator starts to generate laser via SBS. It is defined as the input BP power at which a sudden jump of the BFL's peak power is observed (as was discussed in detail on section 3.2). Below this threshold power, only spontaneous scattering emission is oscillating in the resonator. The SBS thresholds are obtained at about 8.1and 9.9dBm with the use of 100 and 50 m PCF respectively. As shown in Figure 4.3, the BFL power increment with BP power starts to saturate at around 13 dBm due to the power transfer to the higher order Stokes meanwhile for the 20 m PCF the threshold requirements are not met by this pump power using the conventional configuration. With 20 m long PCF, no abrupt change from spontaneous scattering to the stimulated scattering is observed as shown in Figure4.3 due to insufficient interaction length. The output of the BFL is observed to be stable at room temperature with only minor fluctuations observed coinciding with large temperature variances. Therefore, the threshold power of the BFL reduces with increasing PCF length.

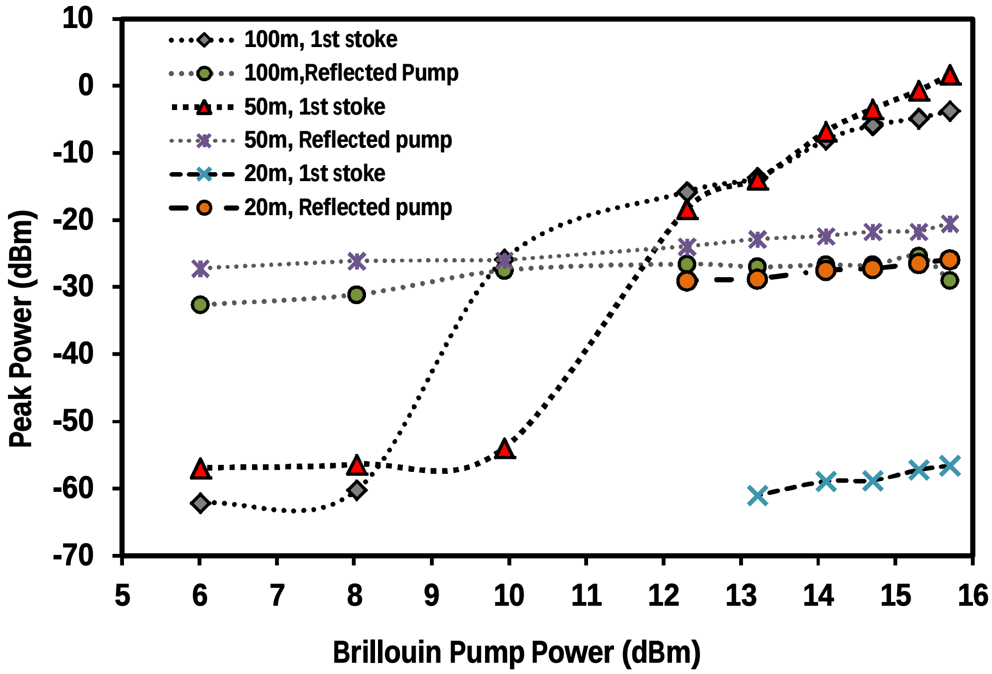

Figure 4. 3: Brillouin Stokes power as a function of BP power at different gain medium.

4.3 Measurement of Brillouin frequency shift

Brillouin scattering happens when an intense light interacts with the medium to generate Stokes in the backward direction at a frequency, which is downshifted by the characteristic of the acoustic frequency (Agrawal, 2003).The typical Brillouin frequency shifts for liquids and gases media are of the order of 1–10 GHz and for silica fibres, it is of the order of nearly10–20 GHz. Since, the frequency shift is reasonably small, a high resolution device is normally required to directly measure the shift. Therefore, a heterodyne method is proposed to measure the frequency shift by using a configuration as depicted in Figure 4.4. The configuration consists of a Brillouin pump, an Erbium-doped fibre amplifier (EDFA), a ring cavity Brillouin gain block and a frequency shift measurement setup. The gain block consists of a piece of PCF and a 3 dB coupler, in which the Brillouin gain oscillates in an anti-clockwise direction to generate a BFL. The gain block is constructed with a ring cavity to provide sufficient Brillouin laser due to the high threshold power of the 100 m long PCF in the open loop configuration. The BP light operating at 1555 nm is split into the reference and probe signals, by using a 10 dB coupler. The probe signal from the 10 % part is optically amplified by an EDFA to provide a sufficient output power of 14 dBm for this study. Since the peak power of the beating signals of TLS and Brillouin laser is nearly same, the 90% is separated and 10% is amplified to reach that one. This amplified signal is launched into the PCF through an optical circulator, which is also used to couple out the backward propagating light from the ring cavity, including a BFL operating at wavelength downshifted by 0.08 nm from the BP wavelength, into the photodiode. The output Brillouin signal is combined with the reference or BP signal by a 3 dB coupler for the Brillouin shift measurement. The combined optical signal is converted into an electrical signal by a phodiode which is connected to an RF spectrum analyzer. The threshold power of SBS effect in this PCF is more than 19 dBm as mentioned in section 3.2; however, the power of injected signal is about 14 dBm and thus the ring BFL setup is used in this study. The ring laser is capable to reduce the threshold power for SBS generation. The experiment is repeated by changing the gain medium of the BFL to a piece of 25 km long standard SMF instead of the PCF.

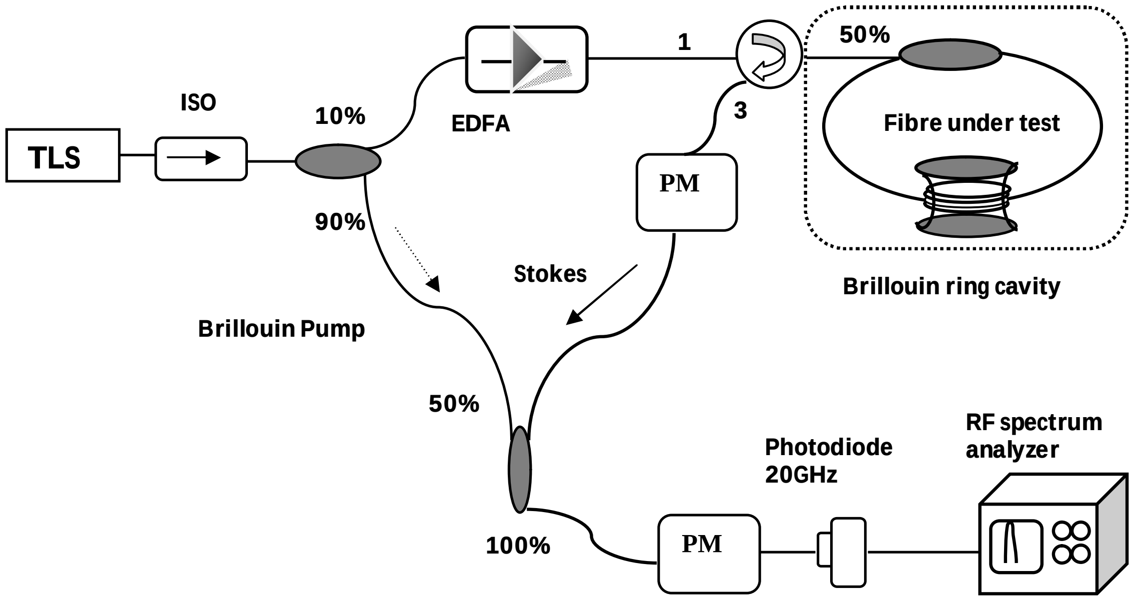

Figure 4. 4: The experimental setup utilizing the heterodyne technique for Brillouin frequency shift measurement in PCF by using a BFL.

The Brillouin Stokes laser is generated from interactions between the optical mode and acoustic modes in the fibre core. Thermally excited acoustic waves (acoustic phonons) produce a periodic modulation of the refractive index. Brillouin scattering occurs when the light is diffracted backward on this moving grating, giving rise to frequency shifted Stokes and anti-Stokes components. This process can be stimulated when the interferences of the laser light and the Stokes wave reinforce the acoustic wave through electrostriction. Since the scattered light undergoes a Doppler frequency shift, the Brillouin shift depends on the acoustic velocity and is given by (Alahbabi *et al.*, 2005):

$$\upsilon_B = \frac{2nV_a}{\lambda} \tag{4.1}$$

where V_a is the acoustic velocity within the fibre, n is the refractive index and λ is the vacuum wavelength of the incident lightwave. The strong attenuation of sound waves in silica determines the shape of the Brillouin gain spectrum. Actually, the exponential decay of the acoustic waves results in a gain presenting a Lorenzian spectral profile (Heiman, 1979):

$$g_B(\upsilon) = g_0 \frac{(\Delta\upsilon_B/2)^2}{(\upsilon-\upsilon_B)^2+(\Delta\upsilon_B/2)^2} \qquad (4.2)$$

where Δv_B is the full-width at half maximum (FWHM). The Brillouin gain spectrum peaks at the Brillouin frequency shift v_B (or the frequency difference between the two beams), and the peak value is given by the Brillouin gain coefficient:

$$g_B(\upsilon) = g_0 = \frac{2\pi n^7 p_{12}^2}{c\lambda_p^2\rho_0 V_a \upsilon_B} \qquad (4.3)$$

where p_{12} is the longitudinal elasto-optic coefficient, ρ_0 is the density, λ_p is the pump wavelength and *c* is the vacuum velocity of light (Agrawal, 1989).

Figure 4.5 compares the Brillouin gain spectrum obtained by both PCF and SMF. The peak spectrum denotes the Brillouin frequency shift in the fibre provided by the beating signal between backward propagating Stokes and the reference BP. To ensure the accuracy of the measurement, the powers of both signals are fixed at nearly similar level during the measurement. As shown in Figures 4.5 (a) and (b), the frequency shift of Brillouin scattering provided by PCF is nearly 9.75 GHz whereas it is around 10.83 GHz by employing SMF. This change is probably attributable to the higher amount of Ge_2O_3 is doped in the PCF than the SMF.

The Brillouin scattering is widely used in fibre distributed sensing, since this process is sensitive to temperature and strain linearly (Nikles, *et al.*, 1996).

(a)

(b)

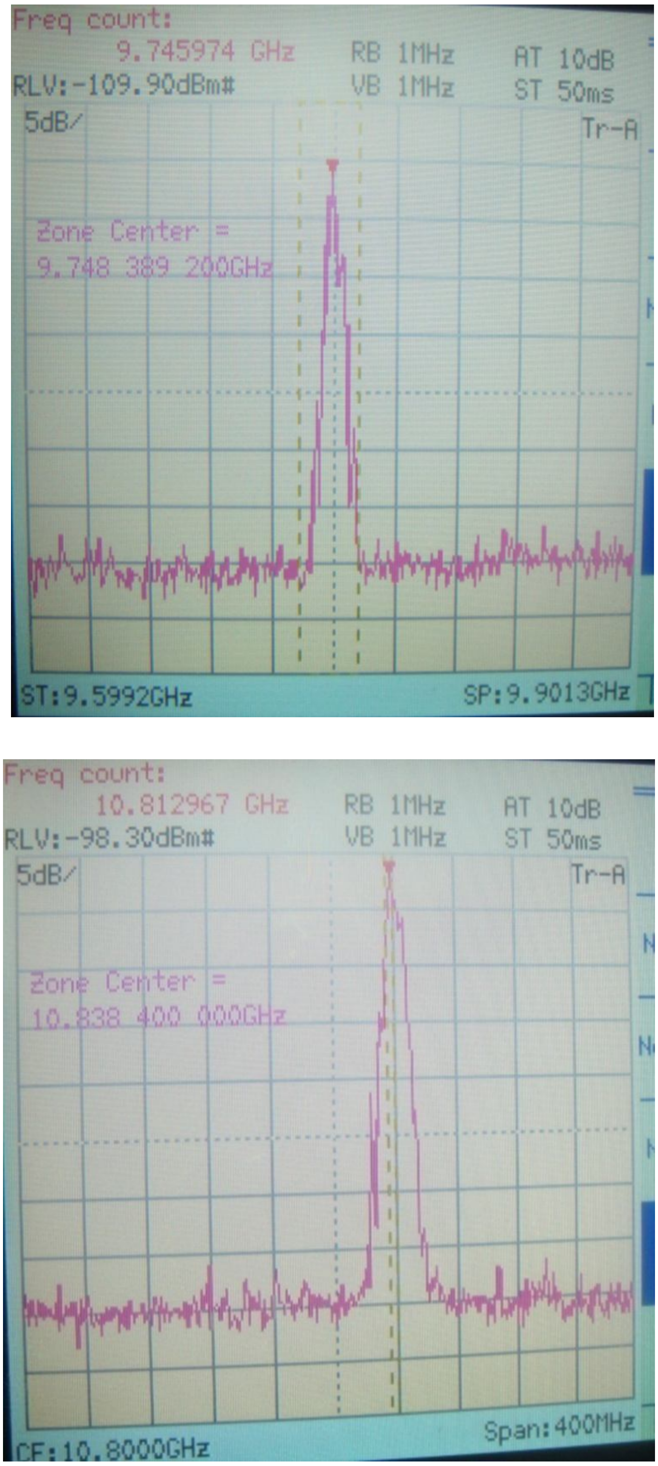

Figure 4. 5: The Brillouin gain spectrum measured by RF spectrum analyzer for (a) 100 m PCF and (b) 25 km SMF.

4.4 A new configuration of ring Brillouin Fibre Laser

In this section, a new ring BFL is demonstrated using components that are similar to the conventional BFL except for an optical isolator, which is incorporated to provide unidirectio nal backward propagating. Figure 4.6 shows the proposed configuration, which consists of an optical circulator, an output coupler, an isolator and a 100 m long PCF as Brillouin gain medium. However, in this configuration, the coupler is placed inside the resonator to extract only the counter-clockwise output BFL and route into the OSA. An external cavity TLS with an output power of approximately 5 dBm is amplified by an EDFA to achieve a maximum BP power of 15 dBm. As shown in the Figure 4.6, the BP with a linewidth of 15 MHz is launched into the PCF from port 1 passing through port 2 of the optical circulator in a clockwise direction to generate a Brillouin Stokes. The backward-propagating Stokes oscillates inside the ring cavity in the counter clockwise direction to generate the Brillouin laser, which is coupled out using the 10 dB coupler. The optical circulator also acts as an isolator to protect the BP from any backward reflection and also to force the unidirectional operation of the laser in the ring cavity.

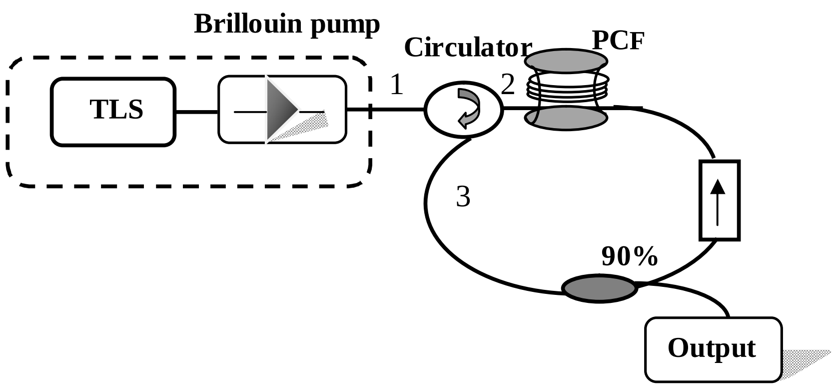

Figure 4. 6**:** New configuration of the PCF-based BFL modified ring cavity.

Figure 4.7 compares the output spectrum of the proposed new BFL with the conventional BFL of Figure 4.1. Both BFLs lase at the wavelength of 1560.1 nm, which is 0.08 nm shifted from the BP wavelength. The new BFL has a SMSR of around 31.5 dB, which is nearly 6.3 dB higher compared to the conventional BFL as shown in Figure 4.7. This is attributed to the PCF, which receives more BP power in the proposed ring cavity rather than the conventional one. The higher BP power generates a higher back-propagating Brillouin Stokes power as well as a higher Brillouin gain to improve the lasing process. Therefore the BFL output is higher in the proposed new BFL as compared to the conventional BFL.

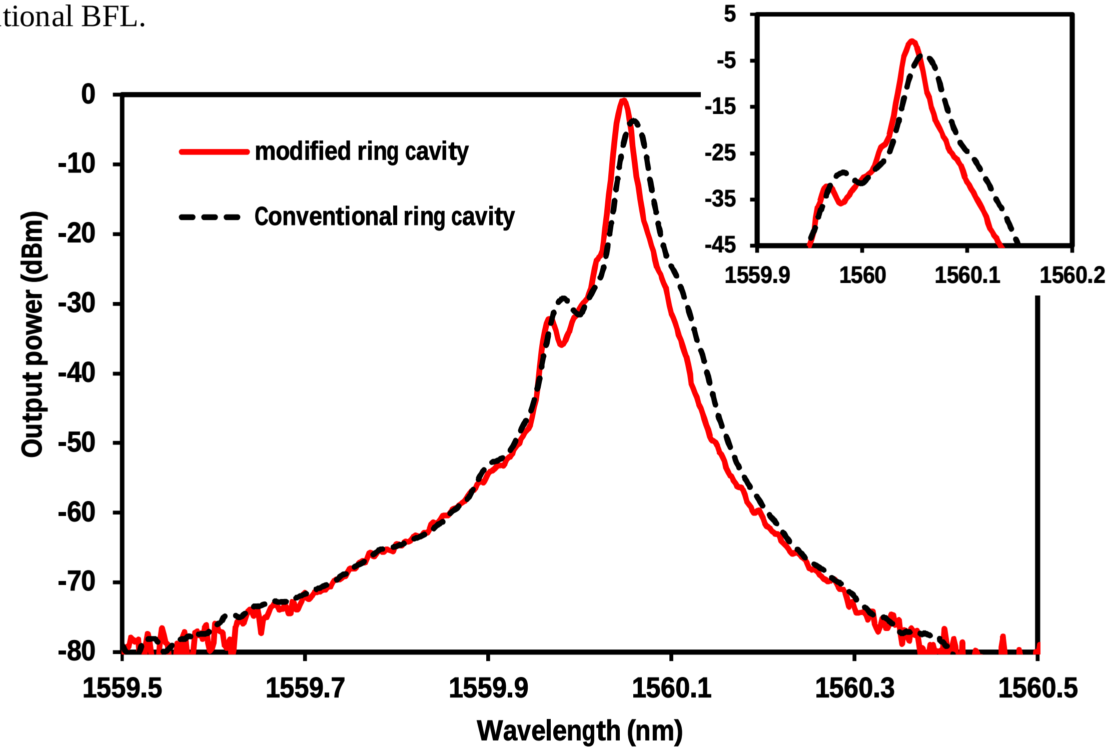

Figure 4. 7: A Comparison of the BFRL output spectrum of the modified and conventional configurations.

Figure 4.8 illustrates the measured peak power for the Stokes against the launched BP powers. As shown in this figure, the peak power gradually increases with the launched BP power before it increases sharply when the spontaneous Brillouin scattering is able to generate Stokes via SBS. The laser thresholds for the conventional and the proposed new BFL are obtained at around 12.7 and 10.4 dBm, respectively. The threshold power is defined as the BP power where the resonator starts to generate laser or Stokes via SBS and abrupt changes happening as discussed in the previous chapter of section 3.2. Below this threshold power, only spontaneous scattering emission oscillates in the resonator, which provides no Brillouin gain to overcome the cavity loss. Besides having a better SMSR, the proposed BFL has also a smaller threshold power compared to that of the conventional BFL as shown in Figure 4.8. This is most probably due to the cavity loss which is lower in the proposed configuration.

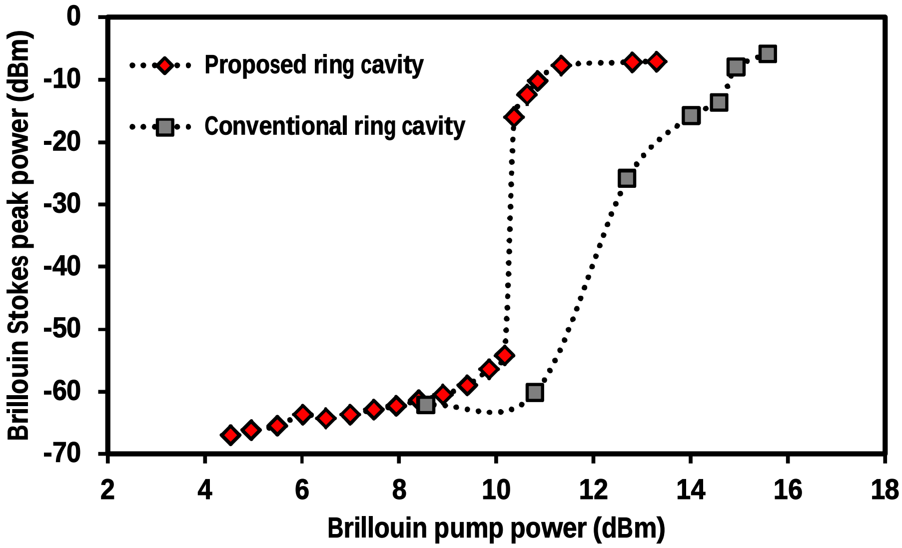

Figure 4. 8**:** Brillouin Stokes power as a function of BP power for both new and conventional BFLs.

4.5 Brillouin Stokes generation with a Bismuth-based EDF (Bi-EDF)

As discussed in Chapter 3, the Bi-EDF is an effective gain medium for realizing the compact optical amplifier. Another striking feature of the Bi-EDF is its ultrahigh nonlinear coefficient, which is 100 times larger than that of silica-based highly nonlinear fibre (HNLF) (Guan *et al.*, 2003). Therefore, it can offer strong nonlinear effect in a relatively very short length (~0.5 m) of fibre for realizing a compact BFL or BEFL. To date, many works have been reported on compact BFLs using a reduced length of nonlinear fibre (Sugimoto *et al.*, 2004). In an earlier study, a compact BEFL has been demonstrated using a 215-cm-long Bi-EDF as the gain medium (Harun*et al.*, 2008). In this section, a BEFL is demonstrated using a further reduced length of Bi-EDF (49 cm) as the gain medium. Although the maximum peak power obtained is just approximately -4 dBm, the BFL has a very narrow linewidth and low relative intensity noise (RIN).

Figure 4.9 illustrates the architecture of the proposed BEFL, which consists of an optical circulator, output coupler and Bi-EDF in a ring configuration. The Brillouin gain medium is provided by a piece of 49-cm-long Bi-EDF. The Bi-EDF is pumped by a 1480-nm laser diode to provide amplification in C-band region from 1525 to 1570 nm so that it can amplify the SBS Stokes. The circulator used in this ring cavity laser system also act as an isolator to direct the propagation of Brillouin–Stokes into a counterclockwise direction. The measured results were extracted from the laser system by using a 90/10 coupler where 10% power is used for monitoring and measurement purpose while the 90% power is circulated back into the laser cavity. The 1480-nm pump is injected into the Bi-EDF via the 1480/1550-nm wavelength selective coupler (WSC).

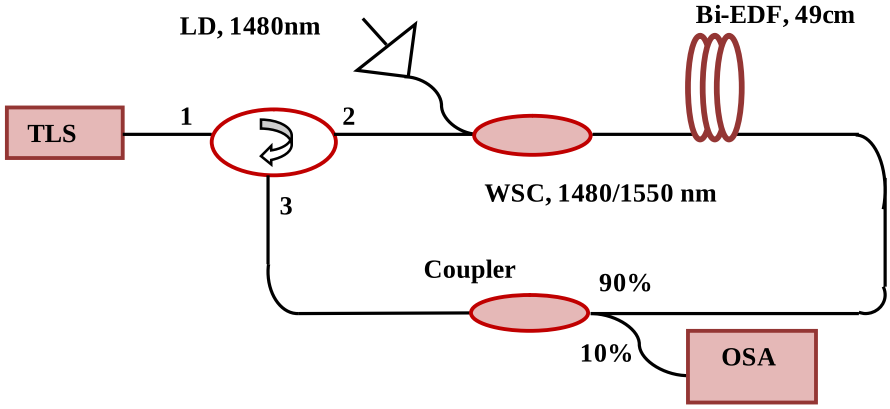

Figure 4. 9: Configuration of ring cavity based Bi-EDF.

Figure 4.10 shows the output spectrum of the BEFL at various 1480-nm pump powers. In the experiment, the BP power and wavelength is fixed at 6 dBm and 1559.40 nm, respectively. As shown in the figure, the BEFL operates at 1559.49 nm, which is 0.09 nm shifted from the BP wavelength at the maximum 1480-nm pump power of 144 mW. The 0.09-nm difference between the wavelengths of the BEFL and BP is the Brillouin frequency shift of the Bi-EDF. The operating wavelength of the BEFL is determined by the Bi-EDF gain and cavity loss in the ring, and therefore, the BP wavelength should be adjusted to match the peaks of the free-running Bi-EDF laser. The inset of Figure 4.10 illustrates a free running Bi-EDF laser (without the BP) spectrum of the BEFL system which shows multiple peaks at 1559-nm region. The multiple peaks are obtained due to the mode competition in the Bi-EDF, which has an inhomogeneous broadening gain characteristic. Due to the small Brillouin gain, the wavelength of operation of the BEFL must be close to the peak of Bi-EDF free-running laser. Therefore, the BP signal is launched at this wavelength region to make use of the Bi-EDF gain. The 3-dB bandwidth of the BEFL is measured to be approximately 0.02 nm limited by the OSA resolution.

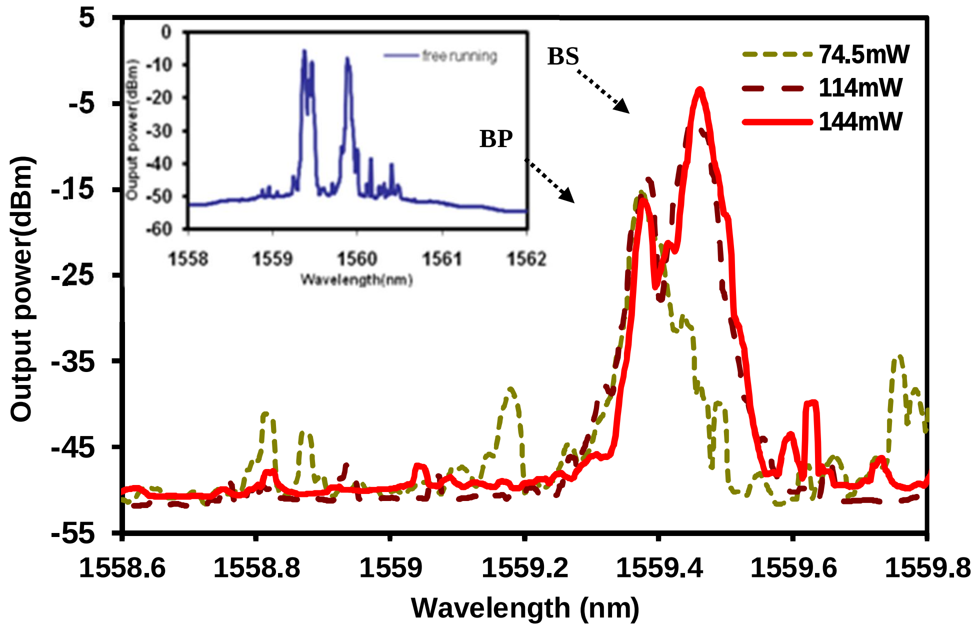

Figure 4. 10: Brillouin spectra at 1559.4 nm and free-running spectrum of Bi-EDFA.

At the maximum 1480-nm pump power, the SMSR is obtained at approximately 14 dB. In this work, the SMSR is defined as the power difference between the BEFL's peak and the second highest peak, which is the residual backscattered BP signal. The SMSR decreases with the reduction of the 1480-nm pump power as shown in Figure 4.10.Figure 4.11 depicts the output spectrum of the BEFL at various BP wavelengths. In this experiment, the BP and 1480-nm pump power are fixed at 6 dBm and 144 mW, respectively. As shown in the figure, the BP can be tuned from 1558.8 nm to 1560.0 nm and the maximum power of the generated BEFL is approximately -4 dBm.

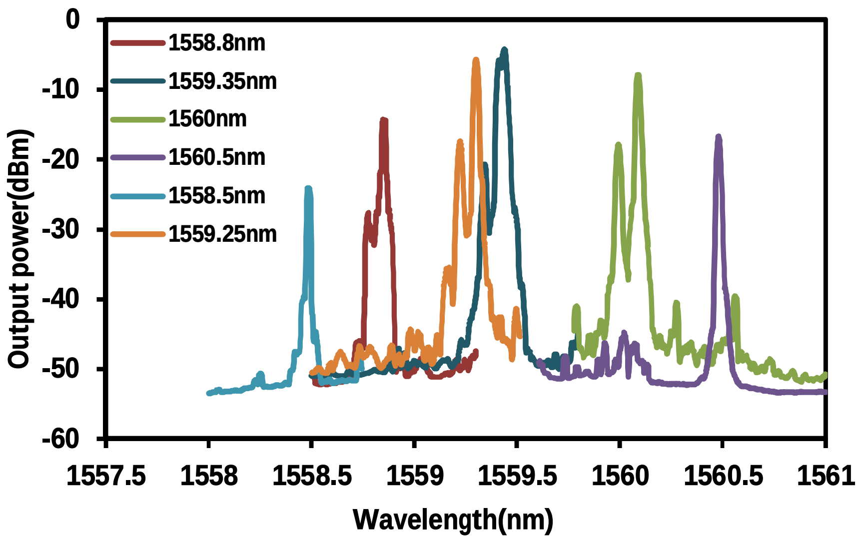

Figure 4. 11: Brillouin spectra based on different wavelengths at 1480 nm and 144mW pump power.

As the BP scans across the spectrum, different spectral shape results from SBS interaction with some peaks more distinct than other at different locations of the spectrum. This is attributed to the amplification characteristic of the Bi-EDF as well as the cavity loss, which determine the optimum operating wavelength of the BEFL. The tuning range is smaller compared to our previous work (Harun *et al.*,2008a) due to the use of a shorter gain medium (Bi-EDF), which resulted in a smaller Brillouin gain. The increase of BP power is expected to increase the tuning range. The proposed BEFL operates at 1560 nm as opposed to 1613 nm in the previous report (Harun *et al.*, 2008a). This is attributed to the peak wavelengths of the Bi-EDF lasers, which depends on the length of the Bi-EDF used as well as the emission characteristics of the erbium ion. The operating wavelength can be slightly tuned within the width of the free-running Bi-EDF laser by varying the BP wavelength. The further reduction of the Bi-EDF section will reduce the erbium gain and prevents the BEFL generation due to the emission cross section of the Bi-EDF peaks at 1530 nm. The single wavelength BEFL is expected to have a very narrow linewidth as well as low RIN and frequency noises, which makes it suitable for sensing application.

Figure 4.12 shows the Stokes power against the 1480-nm pump power. As shown in the figure, the 1480-nm pump power threshold is approximately within 80 to 90 mW. Below this pump power, the amplifier gain is very low and cannot sufficiently compensate for the loss inside the laser cavity, and thus, no Stokes is observed. After the threshold power, the Stokes power is observed to linearly increase with the 1480-nm pump power. Compared with the earlier report which uses 215-cm Bi-EDF to generate BEFL (Harun*et al.*,2008), this BFL has a lower threshold power. This is attributed to a lower cavity loss in this setup, which is obtained by removing an optical isolator and optimization of the output coupler by allowing more power to oscillate in the ring cavity. Figure 4.13 shows the curve of Stokes power against BP power. The BP power threshold is approximately within 0 to 2 dBm. Below this pump power, the Brillouin gain is very small and cannot support the SBS process in the cavity. The use of optical circulator in the ring cavity allows the unidirectional operation of the BEFL. This suppresses the four-wave mixing process in the cavity and therefore no anti-Stokes is observed. These results shows that that a single wavelength BEFL can be achieved using only a 49-cm Bi-EDF as a gain medium.

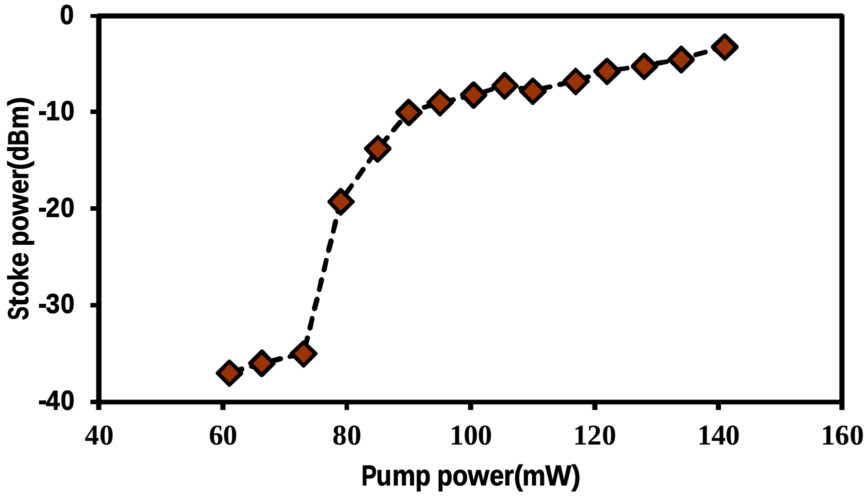

Figure 4. 12: Brillioun Stokes (BS) peak power against 1480 nm pump power in the BEFL system at fixed BP power of 6 dBm.

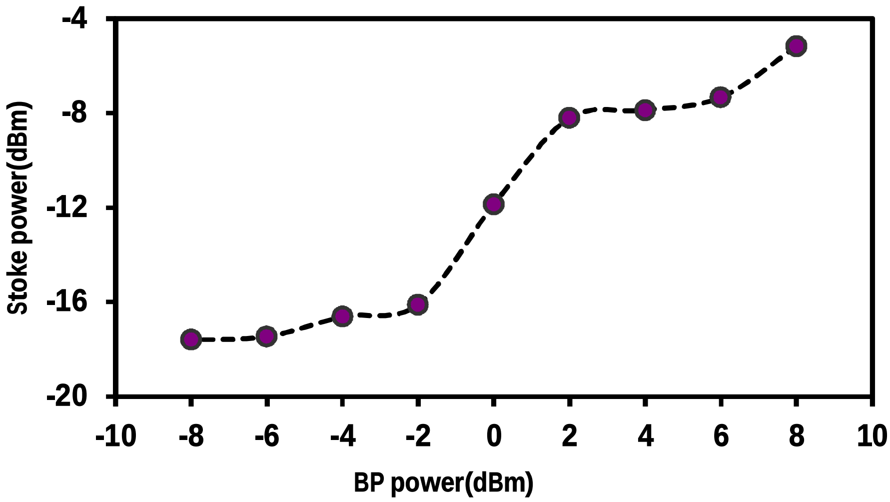

Figure 4. 13: Output spectra of the BFL Bi-EDF based on different power of Brillouin pump with pump wavelength 1480 nm at fixed output power of 144 mW.

4.6 Various configurations of BEFL

In the previous section, a BEFL with a SMSR of about 14 dB was demonstrated using only a piece of 49 cm long Bi-EDF as a gain medium in a ring configuration. In this section, the BEFL with the same length of (Bi-EDF) is optimized to achieve a better SMSR. Two different configurations; ring and linear are used to generate BEFL and their performances are compared in this work. Figures 4.14 (a) and (b) show the proposed ring and linear BEFL, respectively. The ring BEFL is configured to be almost similar to the previous configuration of Figure 4.9 except for the incorporation of an optical isolator and a polarization controller (PC) in the new configuration. The Bi-EDF is pumped by a 1480nm laser diode via a WSC at pump power of 144mW to provide amplification in C-band region so that it can amplify the generated SBS Stokes in both configurations. In the ring configuration, a circulator is used to direct the propagation of Brillouin–Stokes into an counterclockwise direction while an isolator is incorporated in the ring to block the backward propagating ASE and thus improves the SBS nonlinear phenomenon in the forward direction. In the linear set up, an optical circulator and a broadband FBG that operating in the C band region are used as reflector at the end of the cavity to provide oscillation for the SBS Stokes. In both cavities, the output BEFL is extracted from the laser system by using 90/10 coupler where 10% power is used for monitoring and measurement purpose while the 90% power is circulated back into the laser cavity. PC has been used to control the polarization and the birefringence inside the cavity for both configurations. An external laser source from TLS is used as a BP, which is injected into the cavity via a circulator for the ring configuration and via a 20 dB coupler in the loop mirror for linear cavity configuration. For the ring cavity, the experiment is also repeated for the case of backward pumping (for Bi-EDF) which is obtained by shifting the WSC to a new location in between the Bi-EDF and optical circulator. In this case, the 1480 nm pump light is injected in an opposite direction of the oscillating Brillouin laser.

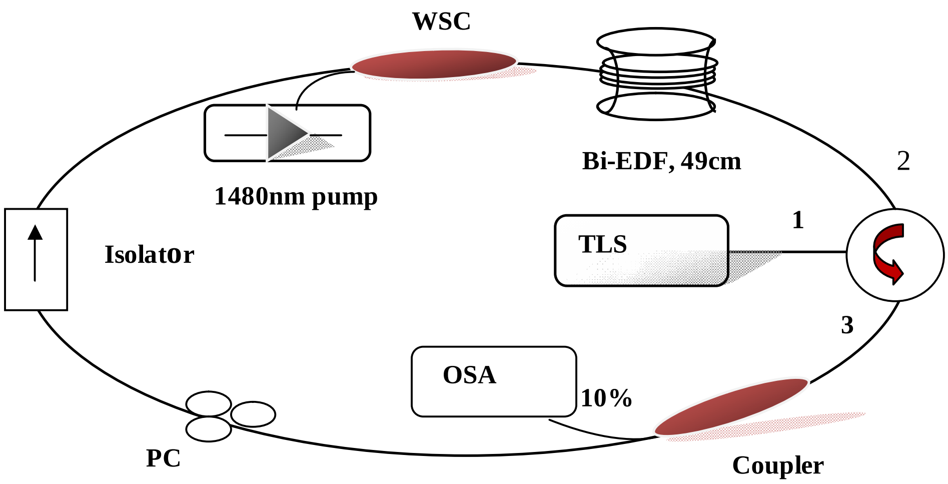

(a)

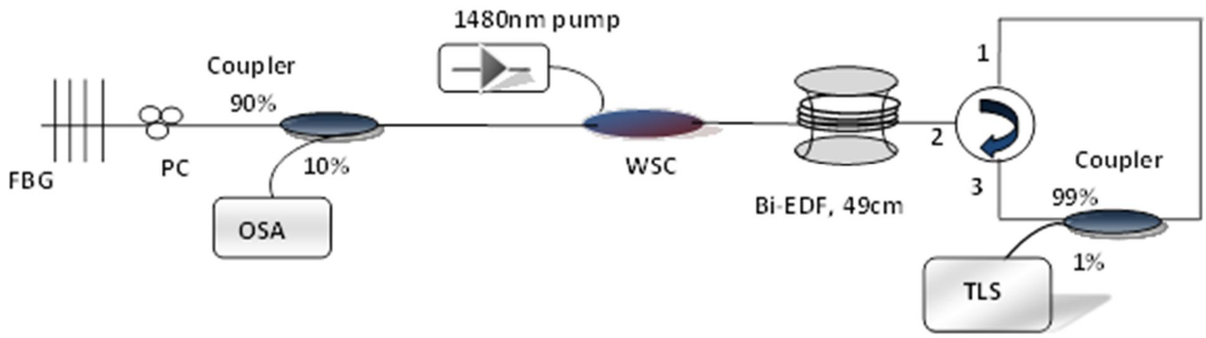

(b)

Figure 4. 14: Structures of proposed BEFL with a (a) ring and (b) linear configuration.

The BP signal is injected into the nonlinear Bi-EDF to generate a narrow linewidth spontaneous Brillouin scattering signal in the opposite direction of the BP propagation with the frequency downshifted by 10 GHz (0.08) from the BP wavelength. The Brillouin scattering signal is then amplified by the erbium gain from the 1480nm pumped Bi-EDF to oscillate in the ring or linear cavity. The laser oscillation is in the direction of clockwise for the ring configuration. Once threshold condition is fulfilled, the oscillated signal becomes

Brillouin laser Stokes via a SBS process with assistance from the Erbium gain. Figure4.15 compares the output of the proposed BEFL at various configurations. In the experiment, the BP wavelength is launched at the optimum wavelengths of 1562.5, 1563.0 and 1564.5nm for the forward ring, backward ring and linear configuration, respectively to make use of the linear gain of the Bi-EDF. Forward and backward ring represent the BEFLs with forward and backward 1480 nm pumped Bi-EDF respectively. The BP and 1480nm pump power are fixed at 6 dBm and 144mW, respectively. The optimum wavelengths were close to the peak of Bi-EDF free-running laser and are also dependent on the cavity loss. For the linear configuration, the optimum wavelength is the longest because the effective cavity loss is the lowest.

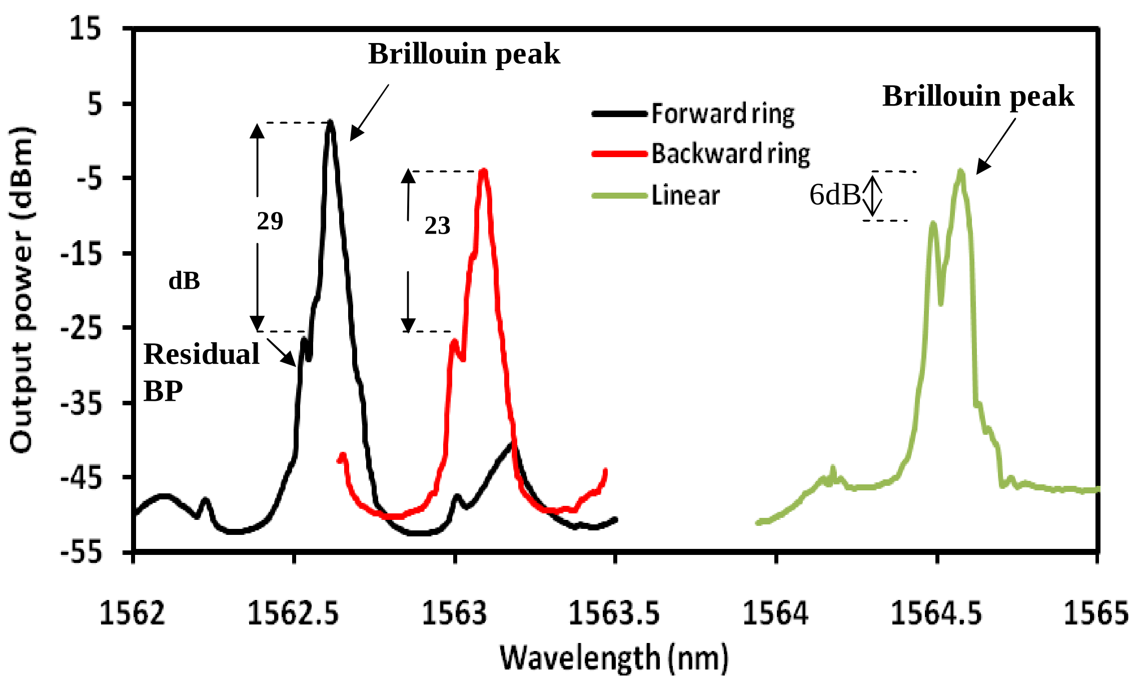

Figure 4. 15: Output spectrum of the BEFL at various configurations when the BP and 1480 nm pump power are fixed at 6dBm and 144mW, respectively.

The SMSR of the BEFL are obtained at around 29, 23 and 6dB for the forward ring, backward ring and linear configurations, respectively as shown in Figure 4.15. The forward ring shows the highest SMSR compared to both backward ring and linear cavity. The ring cavity shows a reasonably higher SMSR compared to the linear one. The bidirectional operation in the linear cavity encourages the mode competition and reduces SMSR. Compared to the previous ring cavity of Figure 4.9, the proposed forward ring BEFL provides a higher SMSR by 15dB due to the incorporation of the isolator and the PC. The isolator functions to ensure the unidirectional operation of the ring BEFL which in turn reduces the noise. The PC function to filter out the unnecessary modes in the cavity so as to improve the SMSR. Figure 4.16 shows the Stokes peak power characteristic against the BP power at various configurations. The threshold of the BEFL is easily identified by the sudden increase in the peak Stokes signal against the BP. After the threshold power is reached, the Stokes power is maintained since most of the BP is transferred to the Stokes wave. As shown in Figure 4.16, the SBS threshold power of the BEFL is -2 dBm, 0 dBm and 4 dBm for forward and backward ring and linear configuration, respectively.

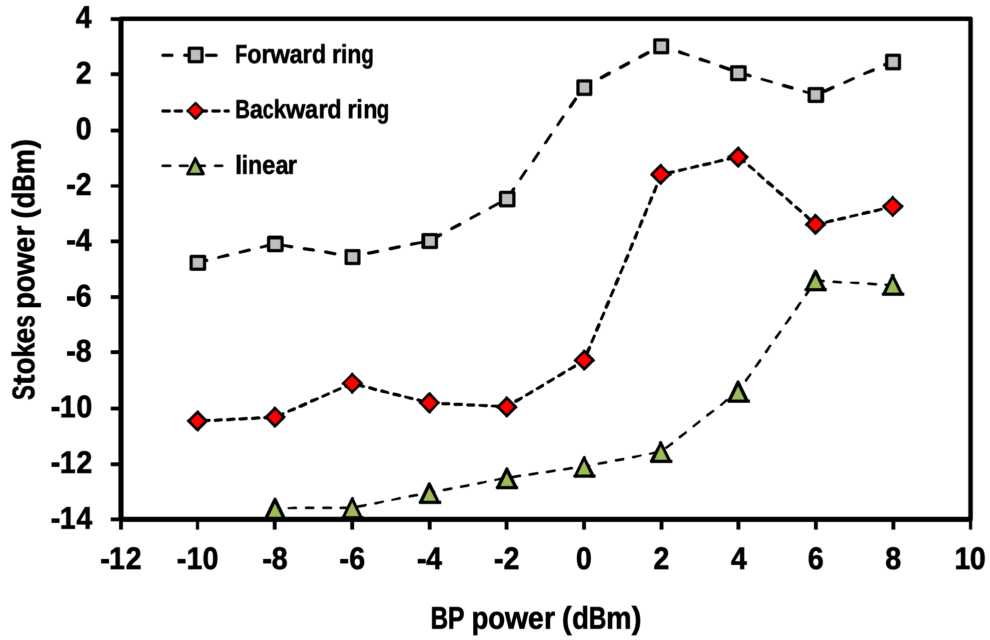

Figure 4. 16: SBS peak powers against input BP peak power for forward, backward and linear cavity configurations with pump wavelength 1480 nm at fixed output power of 144 mW.

Figure 4.17 shows the Stokes power against the 1480-nm pump power for all BEFLs configured with ring and linear configurations. As shown in the figure, the1480-nm pump power threshold is obtained at approximately within 90 to 100 mW for all configurations. Below this threshold pump power, the amplifier gain is very low and cannot sufficiently compensate for the loss inside the laser cavity, and thus, no Stokes is observed. After the threshold power, the Stokes power is observed to be increasing abruptly with the 1480-nm pump power to reach the saturation region. The ring configuration has a slightly lower threshold due to unidirectional operation of the laser obtained by incorporating an optical isolator as well as the optimization of the output coupler by allowing more power to oscillate in the laser cavity.

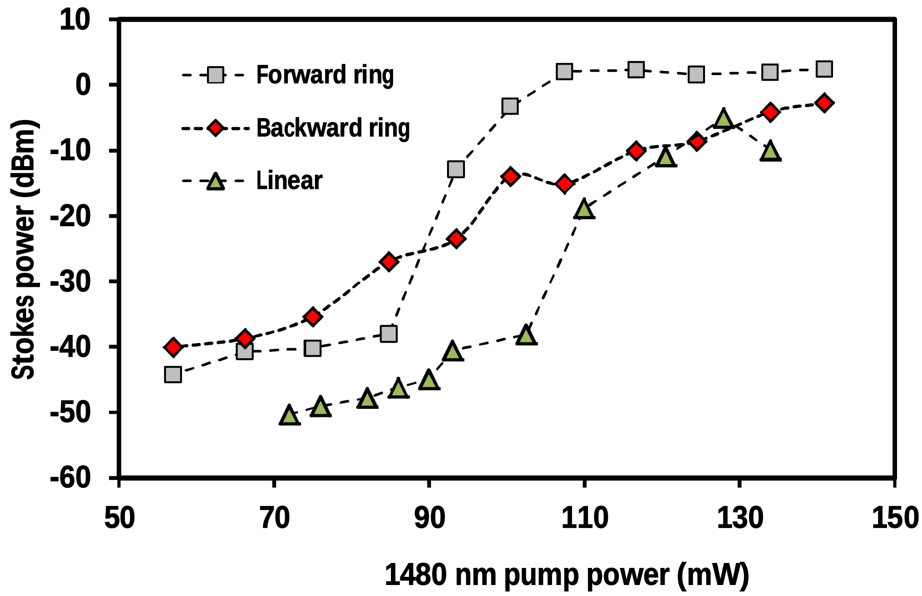

Figure 4. 17: Brillouin Stokes powers against the 1480nm pump power at the fixed BP power of 6 dBm.

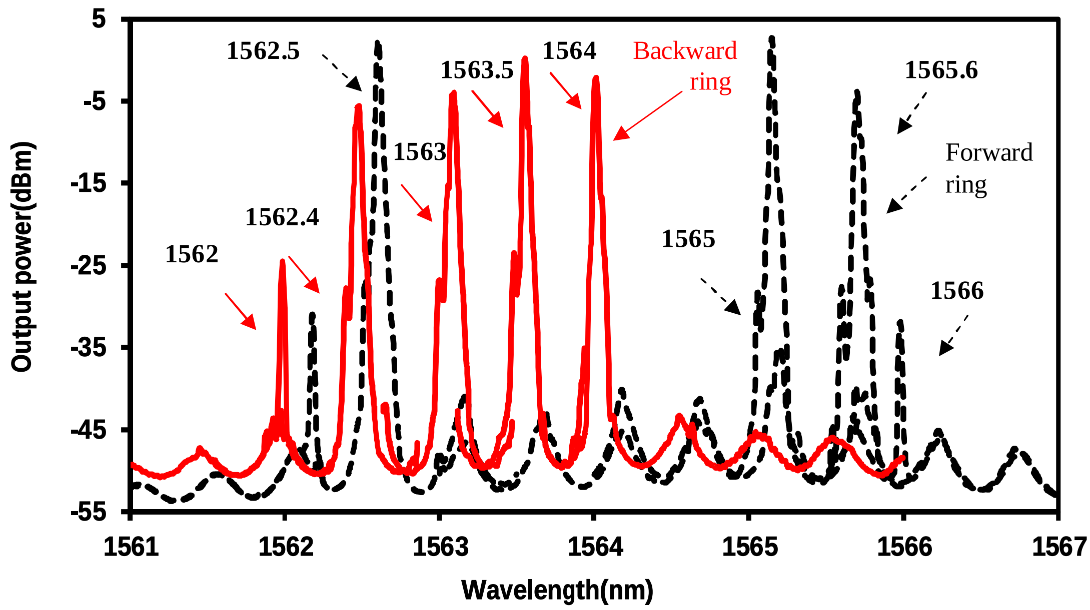

Figure 4. 18**:** Output spectra of the BEFL at various BP wavelengths when the BP and 1480nm pump power are at the fixed 6 dBm and 144 mW respectively. (Solid and dash lines denote the backward and forward ring configurations respectively).

Tuning range of the BEFL is also investigated for various configurations as shown in figure 4.18. This graph shows the output spectra of the ring BEFL at various BP wavelengths for both forward and backward pumping schemes. The tuning range is very limited in the linear configuration, which is probably due to the high loss at the broadband FBG and loop mirror components. Therefore the tuning range of the linear BEFL is not included in Figure 4.18. In this experiment, the BP and 1480nm pump power is fixed at 6 dBm and 144 mW, respectively. As can be seen in this figure, the tuning ranges are obtained within 1562.5nm to 1565.6 for the forward ring configuration and within 1562 to 1564 nm for the backward ring configuration. This is attributed to the injected BP power into the Bi-EDF, which is slightly lower in the backward ring configuration. The insertion loss of the WSC reduces the initial BP power and thus limits the tuning range.

4.7 Dual-wavelength BFL

Dual-wavelength fibre lasers have been of interest for recent years because of their potential applications in optical communications, fibre optical sensors and microwave photonics systems. In order to achieve narrow linewidth and single longitudinal mode output, various techniques have been proposed and demonstrated, includes introducing an ultra-narrow dual-transmission-peak band-pass filter in the laser cavity (Dai *et al.*, 2006 and Li *et al.*, 2008), cascading distributed feedback fibre lasers (Kim *et al.*, 2008) and utilizing the superimposed chirp FBGs (SCFBGs) in the photosensitive erbium–ytterbium co-doped fibre laser (Sun, *et al.*, 2007). Another way to achieve the dual-wavelength lasing is using a passive triple-ring cavity and a hybrid gain medium. But the parameters of the laser need to be properly adjusted to guarantee the dual wavelength operation (Pan, *et al.*, 2008). A multi-wavelength lasing can also be achieved using a SBS process in single-mode fibre (SMF) (Shahi, *et al.*, 2009 and Harun, *et al.*, 2005).

SBS has potential applications in sensors (Han, *et al*., 2005) and in the realization of very narrow linewidth BFLs to achieve dual- or multi-wavelength lasing, whereby the Stokes linewidthbecomes significantly narrower than the pump linewidth with reductions of up to a few hertz (Harun, *et al*., 2005).Moreover, a BFL can be designed to operate at any wavelength, provided that the required pump laser is available, thus showing a high potential for applications in metrology and spectroscopy. In section 4.4, PCF-based BFLs have been demonstrated for single-wavelength operation. In this section, the PCF-based BFL is experimentally investigated for dual-wavelength operation. The proposed laser uses a piece of 100 m PCF as a Brillouin gain medium and a broadband FBG operating in C-band region as a reflector in dual-pass architecture. This type of laser does not require a linear gain medium such as EDF to increase the effect. Therefore it can operate at any wavelength depending on the BP wavelength.

The experimental setup of the proposed dual-wavelength laser is depicted in Figure 4.19, in which a high-reflectivity broad band FBG is placed at the cavity end. The FBG has a 40nm bandwidth centered at 1545nm with a reflectivity of more than 99%.An external cavity of TLS is amplified by an EDFA to provide sufficient power for this study and acts as BP. The BP is launched into the PCF through an optical circulator to generate the Brillouin Stokes in the backward direction at wavelength downshifted by 0.08nm from the BP wavelength. The broad band FBG allows dual-pass of BP inside the gain medium to further enhance the Stokes power, which oscillates in the linear cavity to form BFL. The linear cavity is formed between the splice joint at port 2 of the circulator and the FBG due to spurious reflection as well as scattering effects. The residual BP and the Stokes lines oscillate in the linear cavity to increase the nonlinear gain in the resonator which in turn improves the dual-wavelength lasing process. The performance of dual-wavelength BFL is also investigated for single-pass architecture, which was obtained by removing the FBG for comparison purpose.

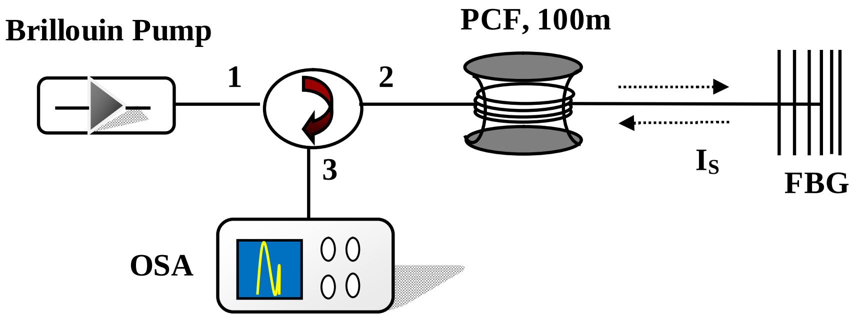

Figure 4. 19: The proposed dual-wavelength BFL architecture with FBG.

Figure 4.20 shows the output spectrum of the dual wavelength laser with and without the broadband FBG. In the experiment, the BP power and wavelength are fixed at 15.7 dBm and 1559.99 nm, respectively. Without the FBG, spectrum measured at the port 3 of the circulator shows a new wavelength at 1560.07 nm, which is shifted by 0.08 nm from the residual BP wavelength. The residual BP is obtained with the assistance of Rayleigh backscattering while the Brillouin Stokes is backscattered from the BP due to the nonlinear characteristic of the PCF. The peak power of the Brillouin Stokes wavelength measured by the OSA in single-pass architecture is -26.9 dBm, which is 22.3 dB lower compared to that of the back-scattered BP signal. This indicates that an amplitude-equilibrium dual-wavelength lasing cannot be achieved in the single-pass architecture.

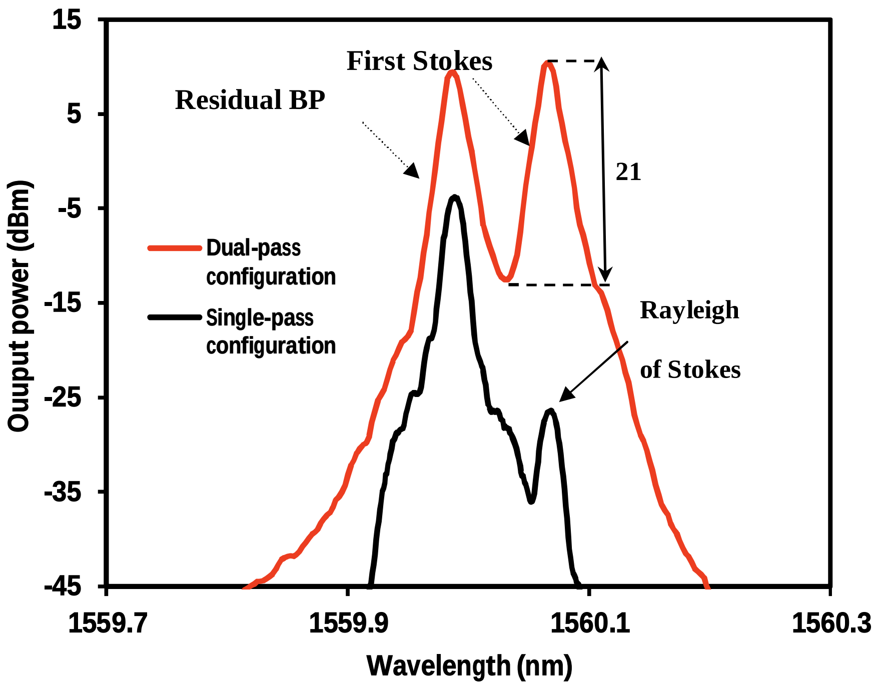

Figure 4. 20: Output spectra of the BFL in single-pass and dual-pass configurations.

In dual-pass architecture, the forward Brillouin Stokes and residual BP are reflected back by the FBG and oscillates in the linear configuration (due to spurious reflection or scattering at the input part of the system) to generate dual-wavelength output. Figure 4.20 shows two simultaneous lasing lines at 1559.09 nm and 1560.06 nm with a wavelength separation of 0.08 nm at a BP power of 15.7 dBm when the FBG is incorporated at the end of linear system. The optical signal to noise ratio of each line is over 21 dB. By applying the FBG, the amount of oscillating BP power in the PCF is increased and therefore more power is converted to the Stokes. The Stokes power is also improved due to the increased Brillouin gain in the dual-pass system. As shown in the spectrum of Figure 4. 20, the output peak powers at the two wavelengths of residual BP and Brillouin Stokes are 8.9 dBm and 9.8 dBm, respectively.

The impact of BP power on the peak power of Brillouin Stokes and the transmitted residual BP generated by the single-pass and dual-pass BFL is shown in Figure 4.21. The BP wavelength is set at around 1559.99 nm, while the BP power is varied from 12.2 dBm to 15.7 dBm. Below BP power of 12.2 dBm, the experiment is not continued as the SBS gain cannot sufficiently compensate for the loss inside the laser cavity and thus cannot support dual-wavelength generation. The peak power of generated Stokes is observed to increase as the BP increases and this can be attributed to the increase of the nonlinear Brillouin gain as the BP power arises. As shown in Figure4.21, Brillouin Stokes line of single-pass configuration cannot meet the threshold requirement. However, due to the stronger oscillation of the BP signal through nonlinear gain media, Brillouin Stokes of the dual-pass architecture can satisfy threshold power of about 14.5 dBm and reach to the saturation condition. Figure 4.22 also depicts the 14 times repeated scanning spectra of the two-wavelength lasing oscillations with a time interval of 10 minutes, which indicates the stability of the laser. The maximum peak wavelength shifts at the two wavelength were both less than 0.002 nm measured by the OSA. The maximum power fluctuations at the peak wavelength of 1559.99 nm and 1560.07 nm were below 0.5 dB, which indicate an excellent stability in the dual-wavelength oscillation. The small power fluctuation is mainly due to the fluctuation of the input BP signal and a small quantity of Rayleigh components in the two lines which are unstable. Perhaps more stable dual-wavelength lasing output can be achieved if we try to improve the stability of the input BP and restrain or reduce the Rayleigh scattering.

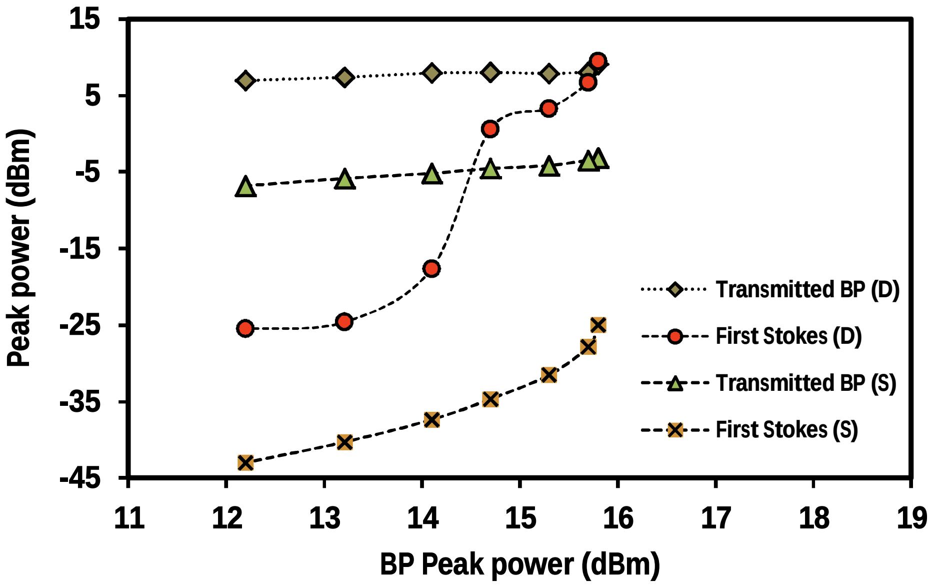

Figure 4. 21: Residual BP and Stokes wave powers plotted against BP power.

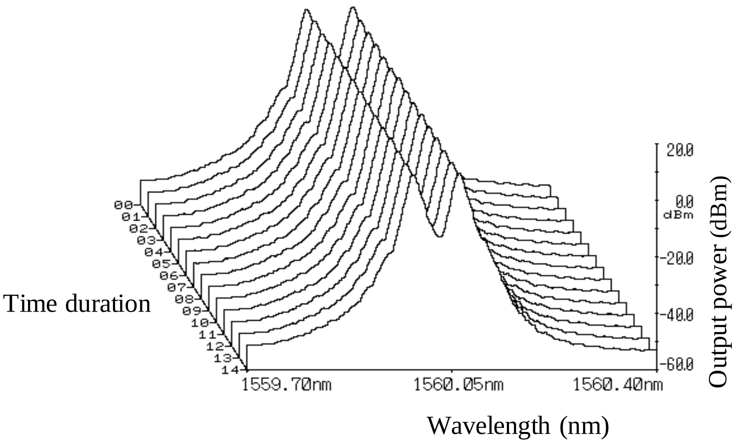

Figure 4. 22: the spectral evolutions of the proposed BFL against time, which is repeatedly scanned every 10 minutes.

By tuning the BP wavelength, the wavelength of the Brillouin-stokes line is also changed correspondingly. As such, tunable dual-wavelength lasing output with a certain wavelength spacing of 0.08 nm can be achieved by adjusting the input BP wavelength. Figure 4.23 shows the tunable dual-wavelength lasing spectra at the same BP power (~15.7dBm). As one can see from this figure, amplitude-equilibrium dual-wavelength lasing outputs could be obtained in a tunable wavelength range of at least 35 nm from 1530 nm to 1565 nm, with a difference between the two peaks being less than 4 dB. The tuning range is limited by the viability of broadband FBG and BP power. This is one of the remarkable advantages of Brillouin laser which can provide multi wavelength lasing in a broadband region of tuning wavelength as long as the BP with the fixed power in any wavelength is launched to the setup and the FBG's reflection region is used.

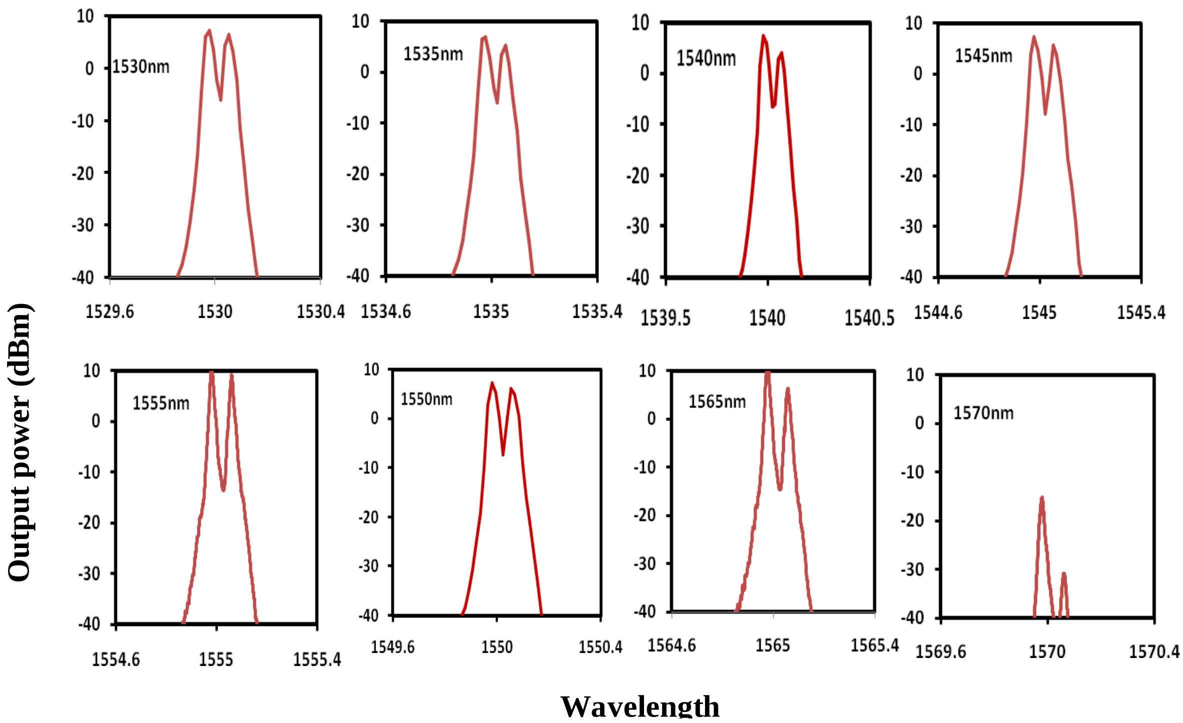

Figure 4. 23: Residual BP and Stokes wave powers plotted against the input signal BP power.

4.8 Four-wave mixing based Multi-wavelength Erbium fibre laser

Various approaches have been proposed by researchers for multi-wavelength laser generation. One of the approaches is based on Erbium-doped fibre laser (EDFL) that has attracted tremendous interest because of its many important applications in fibre optic test and measurement (Lee *et al.*, 2005 (b)), fibre communications (Teodoro *et al.*, 2005) and fibre sensing (Chremmos *et al.*, 2005) systems. These lasers exhibit wide tunable range, narrow line width and could be tuned at high speed allowing fast component characterization. Multi-wavelength lasers are also achievable by utilizing the hybrid integration of two gain media, the nonlinear gain in optical fibres and the linear gain from Erbium doped fibre as reported in many literatures and also earlier discussed in this chapter (Yamashida *et al.*, 1992). Recently, Bismuth-based erbium-doped fibres (Bi-EDFs) have been extensively explored for use in compact amplifiers with short gain medium lengths. A fibre with a high Erbium dopant concentration is expected to have enormous potentials in realizing compact EDFAs and EDFA-based devices as mentioned in chapter 3. In this section, a four-wave mixing (FWM) based multi-wavelength laser is proposed using a Bi-EDF as both linear and nonlinear gain media in conjunction with a broadband FBG.

FBGs are ideal wavelength-selective components for fibre lasers. Various types and arrangements of FBG have been used to achieve multi-wavelength fibre laser operation such as cascaded FBG cavities (Cowle *et al.*, 1996) and Hi-Bi fibre based FBG (Zhang *et al.*, 2005 and Sugimoto *et al.*, 2004). For instance, FBGs written in multimode or few-mode optical fibres have multiple resonance peaks in the transmission and reflection spectra and therefore they are normally used in multi-wavelength laser set-up. In this work, a broadband FBG operating in C-band is inserted in the laser cavity to remove the other wavelengths and improve the multi-wavelength output characteristic of the laser. This technique suppresses other potential modes to circulate in the laser cavity, thus the self-lasing modes are eliminated and hence rectifies the multi-wavelength line numbers limitations faced by the previously reported multi-wavelength EDFL architectures (Harun *et. al.*, 2009). Also, the proposed structure that consists of only 3 optical components in the resonator is simple, cost effective and devoid of the complexity normally associated with the enhancement of feedback mechanism found in the previous report.

Figure 4.24 shows two different cavity designs of the FWM-based multi-wavelength EDFL system. Figures 4.24 (a) and (b) depict the ring- and linear-cavity EDFL, respectively. The gain block used in both configurations is made up of 49 cm long Bi-EDF, which is pumped by a 1480 nm laser diode via WDM coupler. A 1480 nm pump laser has the maximum power of 160mW. The Bi-EDF used has an erbium concentration of 3250 wt.ppm with a cut-off wavelength of 1440 nm and a pump absorption rate of 130dB/m at 1480 nm. The ring resonator of Figure 4.24 (a) consists of the gain block, a circulator, a broadband FBG, a PC, an output coupler and an isolator. An isolator is used to ensure a unidirectional operation of the laser. The linear resonator of Figure 4.24 (b) incorporates a loop mirror and a broad band FBG as the reflectors using the same gain block as the previous setup. The FBG used in both setup allows only a certain laser modes to oscillate by suppressing other modes so that the stability and the number of output channels can be increased. A 10 dB coupler is used to tap the output while allowing 90% of the light to oscillate in the cavity. In both configurations, a PC has been used to control the polarization and the birefringence inside the cavity, which in turn control the number of lines generated, channel spacing and the peak power.

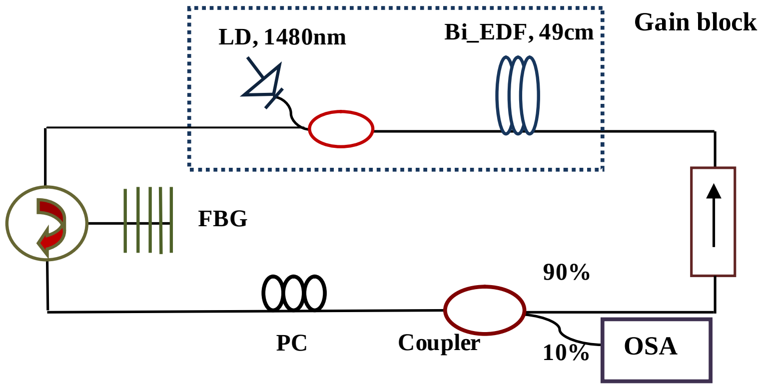

(a)

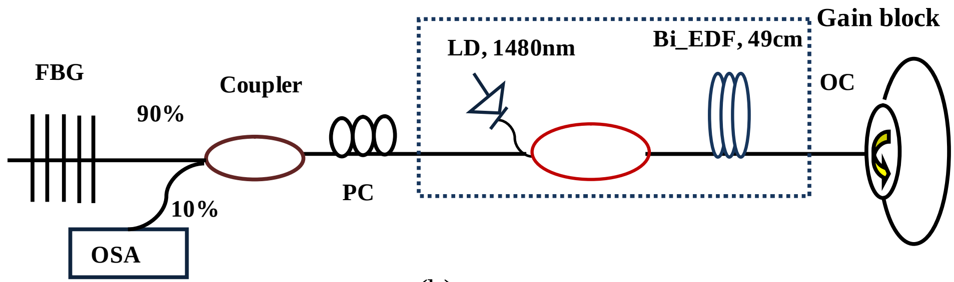

(b)

Figure 4. 24: (a) ring (b) linear-cavity design of MWEDFL to enhance FWM.

Figure 4.25 compares the output spectrum of the proposed EDFL for different cavity scheme with the same pump power fixed at 160mW. The operating wavelength of the EDFL is determined by the Bi-EDF gain spectrum which covers the C-band window from 1530 to 1560 nm as well as the cavity loss. The multi-wavelength comb is generated in the region where the difference between Bi-EDF's gain and cavity loss is the largest. The forward pumped Bi-EDF generates ASE at the FBG region which oscillates in the ring cavity to generate at least two oscillating lines with a constant spacing due to the longitudinal modes interference. The multi-wavelength laser generation with a constant spacing is assisted by the four-wave mixing process, which annihilates photons from these waves to create new photons at different frequencies. Compared to the loop mirrors that reflect all wavelengths back into the linear-cavity, the FBG filter only selectively reflects about 40 nm of wavelengths (1520–1560±2 nm) back into the cavity of the laser system. The wavelengths in the region where self-lasing occurs (>1560 nm) were not reflected by the FBG i.e. they are removed from the cavity. On the other hand, incorporating the FBG filter in place of the loop mirror in the ring-cavity design would make the self-lasing to be more efficient by removing the other wavelengths from the oscillation. As shown in Figure 4.25, the ring configuration provides a higher number of lines compared to that of the linear one. This is attributed to the unidirectional operation of the ring EDFL, which increases the population inversion in the Bi-EDF and thus support more oscillating lines.

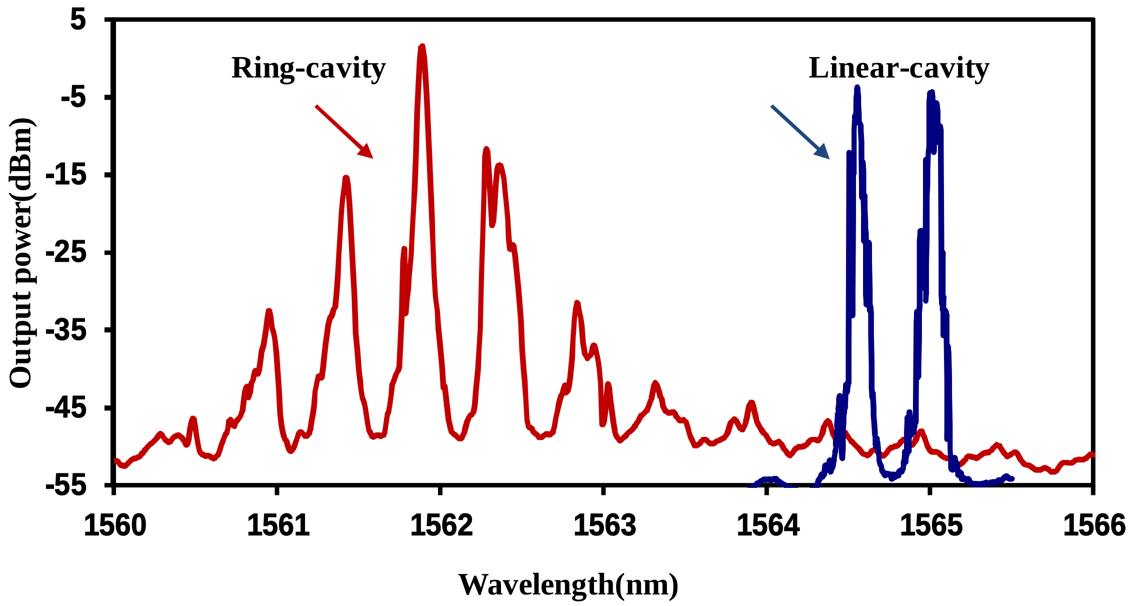

Figure 4. 25: Multi-wavelength FWM spectrum for Ring-cavity and linear-cavity MWEFL.

Figure 4.26 compares the output spectrum of the EDFL with and without the FBG for the ring configuration. In the configuration without FBG, both circulator and FBG are removed from the setup. As shown in the figure, the multi-wavelength operation is improved with the FBG. This is attributed to the FBG which suppresses other modes to provide a lower noise in the laser cavity and thus enhances a FWM interaction. The strongest line has a peak power of approximately 1.26 dBm as shown in Figure 4.26.

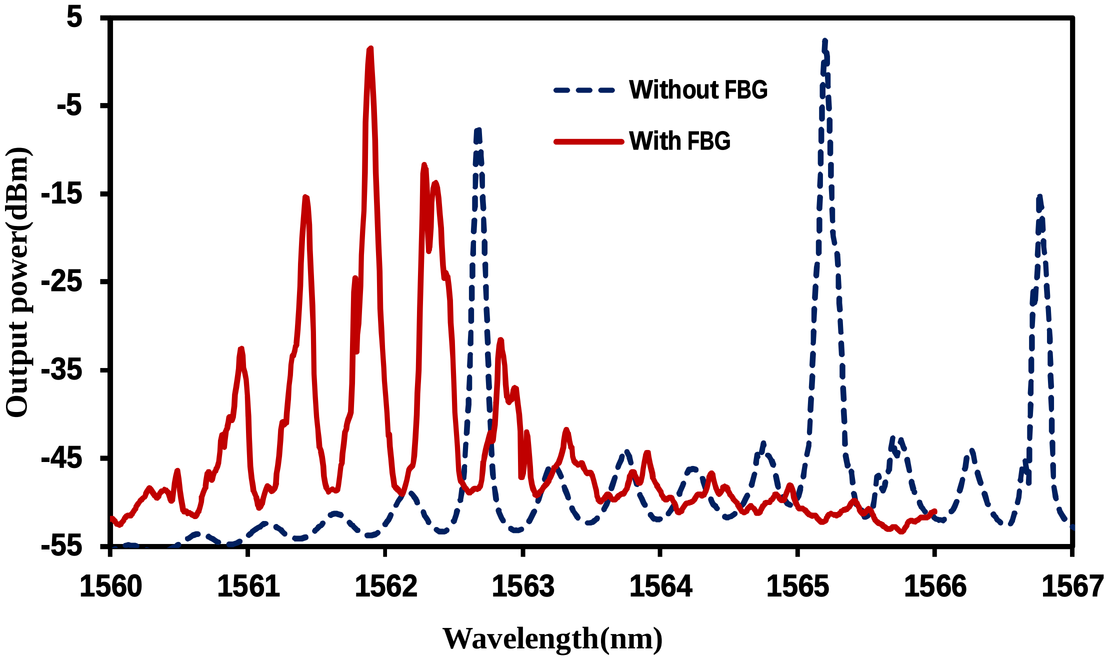

Figure 4. 26: Multi-wavelength FWM spectra with and without FBG by same pump power at 1480 nm.

The number of lines is limited by the availability of the 1480nm pump power, fibre nonlinearity, polarization filtering effect in the ring cavity laser and the length of the ring cavity laser. As shown in Figure 4.27, by optimizing the state of polarization in the ring cavity by a PC, a better comb spectrum can be obtained. This shows that the PC is capable of controlling the number of line generated, channel spacing and the peak power. The numbers of generated multi-wavelength increases up to 7 lines with nearly 0.3 nm fixed spacing in optimized condition.

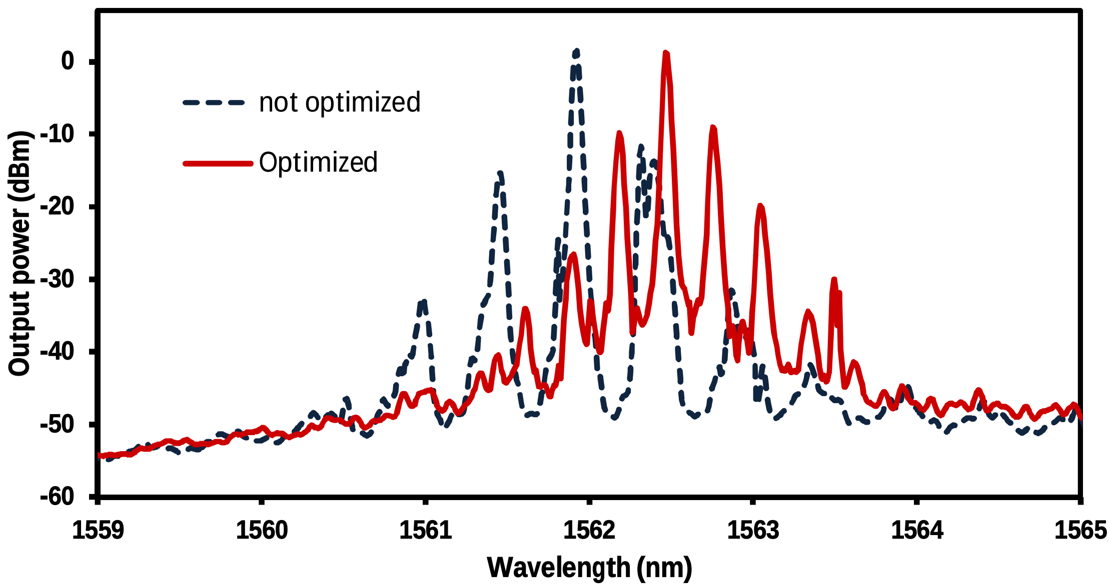

Figure 4. 27**:** Multi-wavelength FWM spectra with and without PC by 147mW pump power fixed at 1480 nm.

In the next chapter, advanced configurations of the multi-wavelength laser will be presented. The proposed lasers use nonlinear effects such as SBS and FWM for assisting multi-wavelength generation as well as high nonlinear fibres such as PCF and Bi-EDF to reduce the interaction length and produce a compact design for the lasers.

CHAPTER FIVE: ADVANCED CONFIGURATIONS FOR MULTIWAVELENGH NONLINEAR LASERS

5.1 Introduction

To date, Stimulated Brillouin Scattering (SBS) based multi-wavelength lasers have been investigated extensively (Shirazi, *et al.*, 2008 and Gross, *et al.*, 2010) due to their many advantages such as low threshold and narrow line-width. The multi-wavelength lasers have many potential applications such as in microwave photonics (Banchi, *et al.*, 2010), fibre sensors (Han, *et al.*, 2005) and high capacity wavelength division multiplexing (WDM) communication networks (Song, *et al.*, 2004) Normally, a hybrid Brillouin/Erbium (Harun *et. al.*, 2009a; Shahi, *et al.*, 2009; Zhan. *et al.*, 2006) or Brillouin/Raman fibre lasers (Liu, *et al.*, 2008a; Liu, *et al.*, 2008b) are used to achieve a multiple Stokes lines with a constant spacing and a high number of Stokes lines as reported in many literatures. For instance, the generation of 160 Brillouin Stokes has been experimentally demonstrated using a linear cavity self-seeded Brillouin/Erbium fibre laser (BEFL) (Zhan. *et al.*, 2006). Stable Brillouin/Raman fibre laser has also been demonstrated with 30 lasing lines by Liu *et al.*, (2008a). Another versatile alternative to generate multi wavelength laser is Four-Wave Mixing (FWM) effect which is able to create channels with a larger spacing than SBS effect. However, Four-wave mixing seems to be the most harmful in the case of dense wavelength division multiplexing (DWDM) systems (Eiselt, 1999) that use low dispersion fibre or equal channel spacing. Nevertheless, it can be useful in some applications such as multi wave length generation, wavelength conversion and switching.

In this chapter, various multi wavelength fibre lasers are proposed using nonlinear effect in conjunction with a piece of highly nonlinear fibre. SBS based multi-wavelength lasers are demonstrated using a Photonic Crystal Fibre (PCF) and a hybrid of PCF and Bismuth-based Erbium-doped Fibre (Bi-EDF). FWM-based multi-wavelength lasers are also proposed and demonstrated using a Bi-EDF as well as a hybrid of PCF and Bi-EDF. In the next section, a new configuration of multi-wavelength BFL is proposed using a dual-pass approach. This approach is used to reduce the cavity loss so that it can provide an efficient output. The proposed BFL can operate at any wavelength depending on the Brillouin pump (BP) wavelength.

5.2 Multi-wavelength Brillouin Fibre Laser with Dual-Pass Configuration

The proposed multi-wavelength BFL architecture is depicted in Figure 5.1, which consists of a short piece of PCF, a 3dB coupler and a high-reflectivity broad band FBG at the cavity end. The new configuration has two main sectors; a ring cavity as a Brillouin gain block which includes a piece of PCF and a 3 dB coupler, and a broad band FBG operating in C band region at the end of this linear structure to allow dual-pass Stokes lines oscillation in the ring resonator. This can improve the output powers of the cascading Stokes lines which in turn increases the number of Stokes obtained. The BP is an external cavity tunable laser source (TLS) with a line-width of approximately 20MHz, which is amplified by an Erbium-doped fibre amplifier (EDFA) to provide sufficient power for this study. The BP is launched into the PCF through a 3 dB coupler via optical circulator to generate the first order Brillouin Stokes in the clockwise direction at wavelength downshifted by 0.08nm from the BP wavelength. The Brillouin Stokes oscillates inside the ring resonator to generate Brillouin laser. When the laser power exceeds the threshold condition, it will then create the second order Stokes signal in the opposite direction. In the same way, the second order Stokes signal will create the third order Stokes signal. The process will continue until the next higher order Stokes signals power is too small to exceed the threshold condition and hence creation of subsequent Stokes order signal will diminish. The residual BP and even order Stokes lines propagating in the clockwise direction are reflected by the broadband FBG to double propagate inside the ring resonator in the opposite direction. This will increase the nonlinear gain in the resonator which in turn improves the multi-wavelength lasing process.

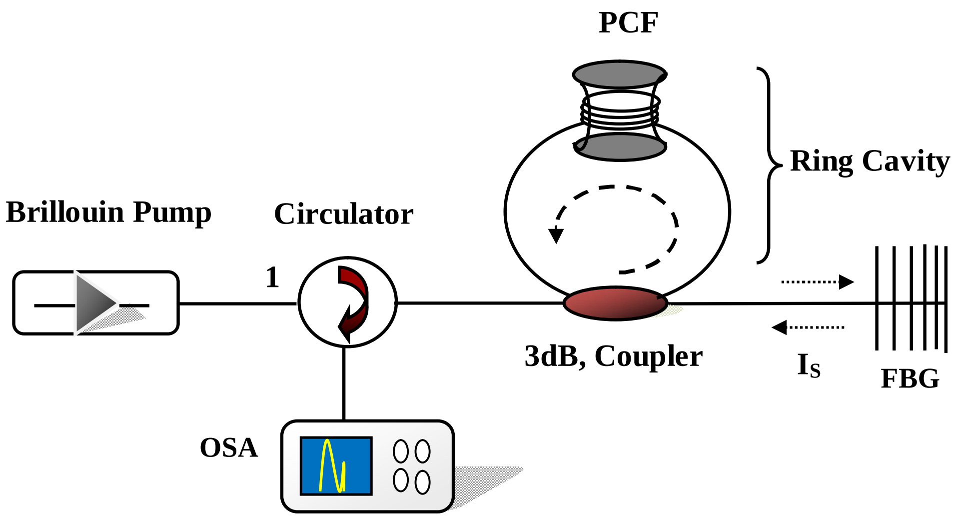

Figure 5. 1: The proposed multi-wavelength BFL architecture.

Figure 5.2 compares the output spectrum of the BFL in different configurations at the maximum BP power of 15.7 dBm. First of all, the output of the BFL in the presence of the ring cavity but without FBG was studied. With this configuration, only the first Brillouin Stokes is achieved at 1560 nm wavelength with side mode suppression ratio (SMSR) of 26 dB. However, by incorporating the broad band FBG as in the proposed configuration of Figure 5.1, seven Stokes waves and four anti-Stokes waves with nearly 13 dB signal to noise ratio (SNR) are obtained by 100 m PCF around the oscillated BP at 1559.98 nm, whereas we have only the first Stokes wave in the same configuration by incorporating 50 m PCF. This is attributed to that the 50 m long PCF is not sufficient to create multi-wavelength in this configuration. By incorporating the 100 m long PCF, four anti-Stokes waves also arises due to four-wave mixing (FWM) between co-propagating BP and BFL photons during the oscillation. The bi-directional operation of the laser also contributes to the anti-Stokes generation. The output spectrum of the BFL is also investigated in the absence of ring cavity where the ring cavity is replaced by the PCF. In this BFL, only the first Stokes is observed with 2.5 dB SMSR. These results show that the presence of ring cavity and FBG is very important for multi-wavelength generation. The presence of FBG at the end side allows the BP and SBS light beams to propagate twice into the ring cavity section and thus the cavity is able to make more Stokes lines.

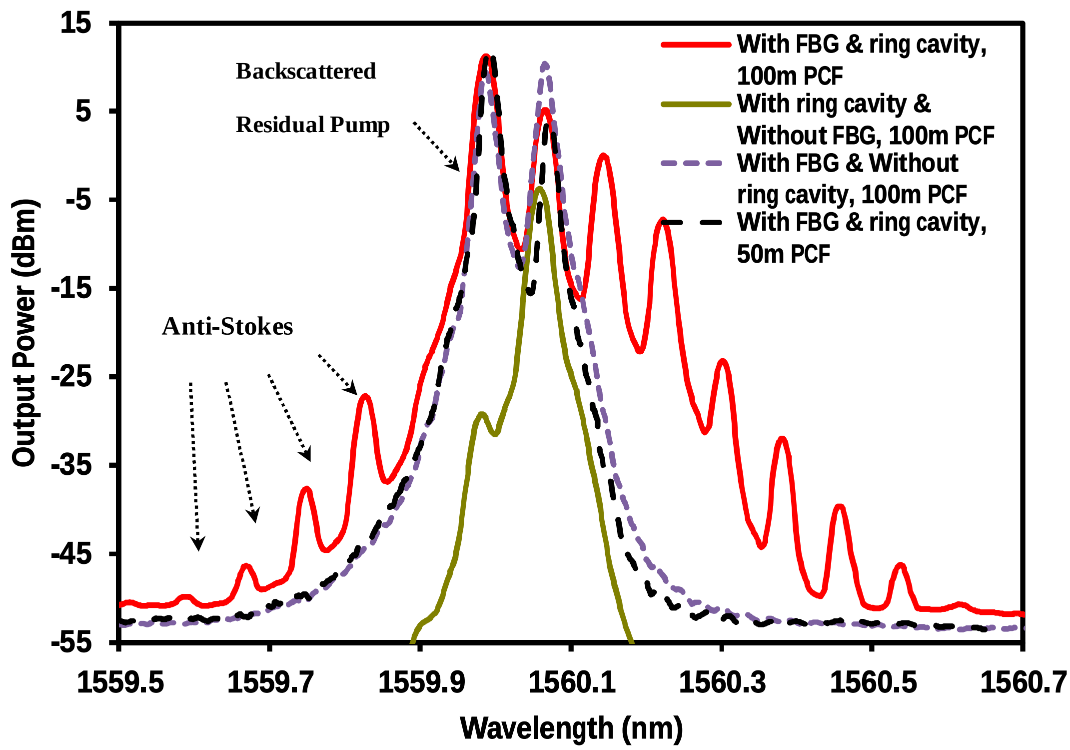

Figure 5. 2: Output spectra of the BFL with different configurations and PCF's lengths.

The impact of the BP power on the number of Stokes generated by the BFL is shown in Figure 5.3. The BP wavelength is set at around 1560 nm, while the BP power is varied from 6.1 dBm to 15.7dBm. Below BP power of 6dBm, the experiment is not continued as the SBS gain cannot sufficiently compensate for the loss inside the laser cavity and thus cannot support multi-wavelength generation. The number of generated Stokes is observed to increase as the BP increases and this can be attributed to the increase of the nonlinear Brillouin gain as the BP power rises. This situation provides sufficient signal power for higher order Stokes signals to pump the PCF and maintain the cascading process of the Stokes into multiple Stokes. However, the power of each subsequent Stokes line is typically lower than that of the previous Stokes line as each subsequent Stokes is generated with the energy of the previous Stokes, thus slightly reducing the Stokes line's power. As shown in Figure 5.4, the output of the BFL is stable at room temperature with only minor fluctuations observed coinciding with large temperature variances.

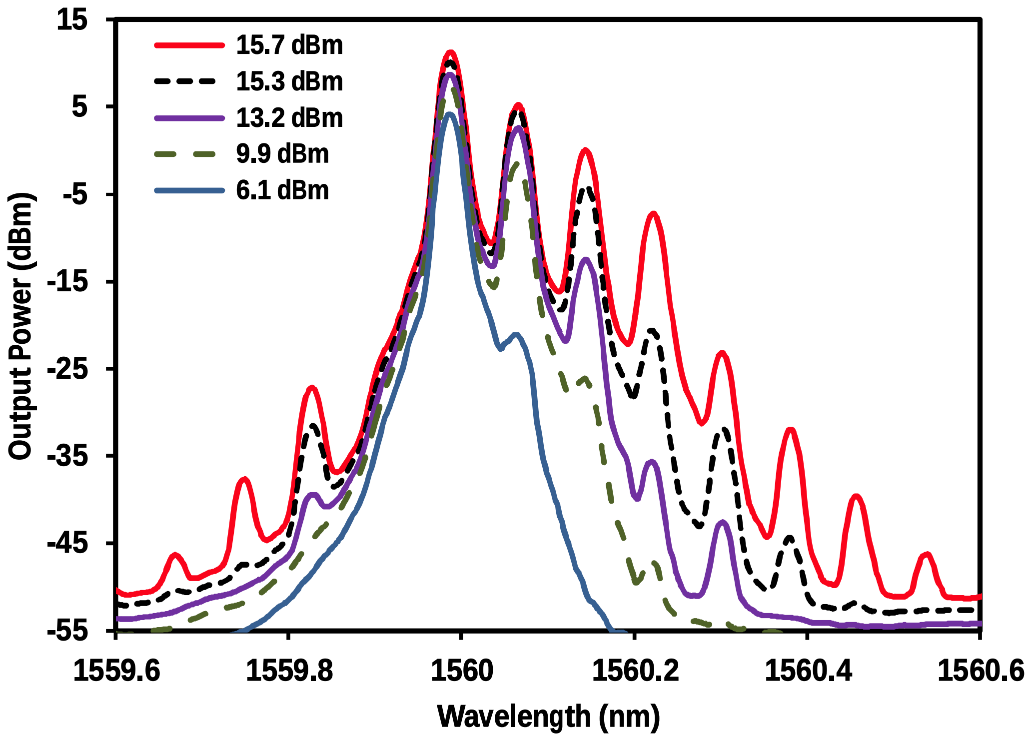

Figure 5. 3: The output spectrum of the proposed BFL at various input BP power.

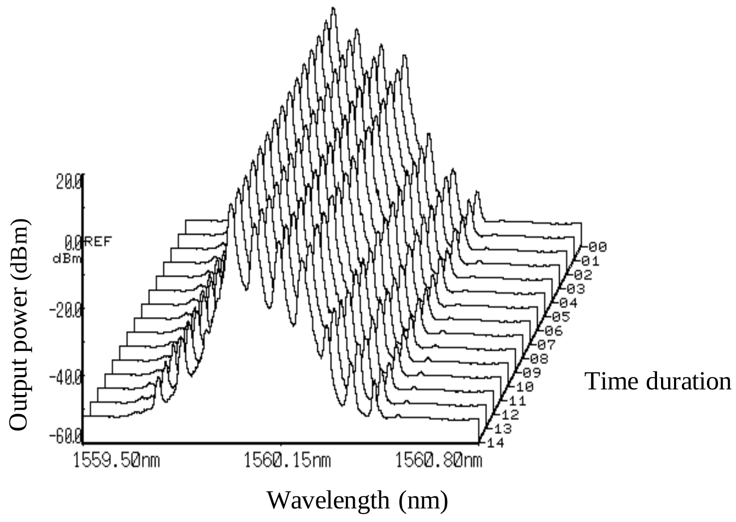

Figure 5. 4: the spectral evolutions of the proposed BFL against time, which is repeatedly scanned every 10 minutes.

Figure 5.5 demonstrates the output Brillouin Stokes power and the transmitted residual BP power against the input signal BP power. As shown in the figure, all the Stokes powers increase as the BP power increases. However, the Stokes lines begin to saturate as the BP power increases above the threshold power of the subsequent Stokes. For instance, the second Stokes line saturates as the threshold for the third Stokes is reached. This is due to the power transfer from the second Stokes to the third Stokes, which occurs when the BP power is approximately at 14.7 dBm. For the higher order Stokes, however, the threshold BP powers are obtained at almost the same level of 15.3 dBm. This is probably due to the FWM between the oscillating BP and Stokes signals which improves the conversion efficiency by providing amplification for the higher order Stokes generation.

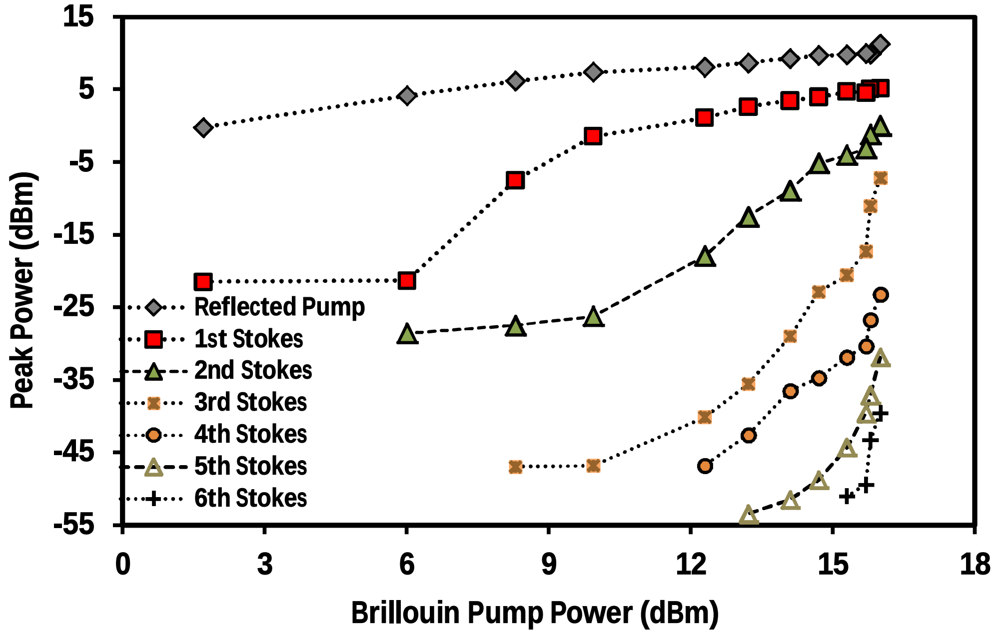

Figure 5. 5: Residual BP and Stokes wave powers plotted against BP power.

5.3 Double spacing multi-wavelength BFL

In this section, a double spacing multi-wavelength BFL is demonstrated using a short piece of PCF as a nonlinear Brillouin gain medium in conjunction with a figure-of-eight configuration. The proposed BFL can achieve stable multi-wavelength simultaneous lasing with 20 GHz or 0.16 nm line spacing, less threshold power and also capable to mitigate the limitation of tuning range. Compared to the previous BFLs and hybrid Brillouin lasers, the line spacing of the proposed BFL is twice as wide due to the removal of odd-order Stokes waves with the proposed figure-of-eight configuration and therefore it has more potential to be implemented in future WDM systems.

The configuration of the proposed figure-of-eight PCF-based multi wavelength BFL is shown in Figure 5.6. The BFL resonator consists of an optical circulator, two couplers, and a 100 m long PCF as the Brillouin gain medium. The PCF is used to significantly reduce the length of Brillouin gain medium. The BP is sent into a piece of PCF from port 1 through port 2 of the optical circulator and 3 dB coupler (C1) to generate backward-propagating SBS. The backward-propagating SBS oscillates inside the first loop and the secondary loop in the clockwise (CW) and counter clockwise (CCW) directions respectively, to generate another Brillouin Stokes in the opposite direction (counter clockwise inside the first loop). The first Stokes signal is re-injected into the other end of the PCF in a clockwise direction to act as a BP to generate the next Stokes. The cascading process continues to generate multi-wavelength lasing. In the secondary loop, the odd-order Stokes lines are blocked by the circulator and the even-order Stokes lines are allowed to oscillate and build-up their intensity. The oscillating light inside the secondary loop is extracted from the laser system by using 90/10 coupler where 10% power is used for monitoring and measurement purpose while the 90% power is circulated back into the laser cavity. The output spectrum is characterized by OSA with a resolution of 0.015 nm. The experiment is carried out for two different lengths of PCF; 50 m and 100 m. The experiments are also repeated with the conventional single ring cavity system, which is obtained by disconnecting the secondary loop and monitoring the output at port 3 of the optical circulator for comparison purpose.

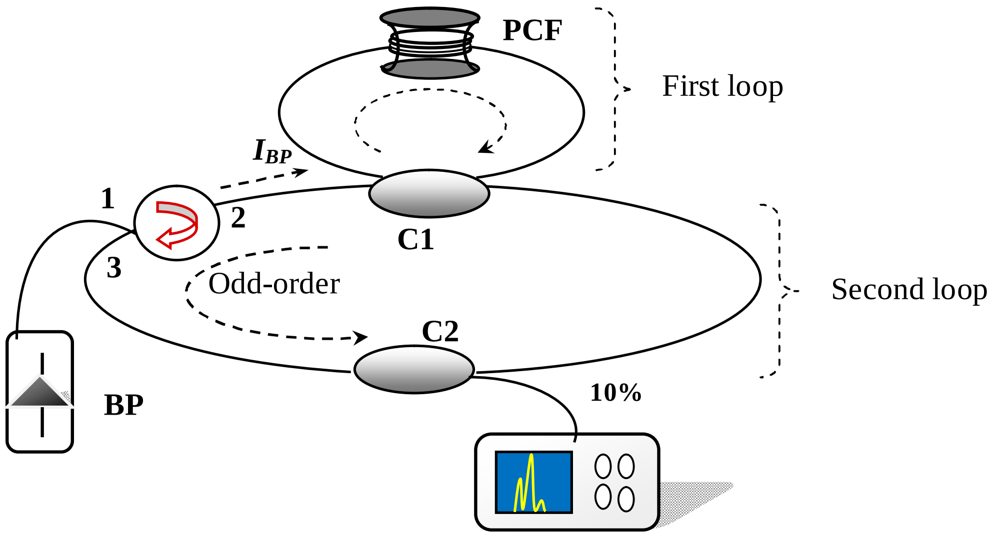

Figure 5. 6: Configuration of the figure-of-eight PCF-based BFL.

Figure 5.7 shows the output spectra of the BFL with a single-ring cavity and a figure-of-eight configuration at two different lengths of PCFs; 50 m and 100 m. In the experiment, the BP power is fixed at 15.3 dBm. In the conventional set-up of single ring cavity, only the first Stokes travelling in the clockwise direction is obtained from the OSA as shown in Figure 5.7.Due to this fact, the single-ring cavity cannot provide sufficient nonlinear gain to assist in cascading process for multiple Stokes generation. It is found that the signals to noise ratios of 23.4 and 24.1 dB are achieved by the BFL with 50 m and 100 m PCF, respectively. In case of the figure-of-eight configuration as shown in Figure 5.7, the BP generates the first Stokes, which has a higher peak power compared to the conventional configuration at a wavelength shifted by 0.08nm from the BP. The backward propagating Stokes generates the second Stokes which propagates in the opposite direction (counter clockwise direction in this setup). If the threshold condition is satisfied, this will generate a cascading Brillouin effect as a comb of lines. As shown in Figure 5.6, the oscillated signals in clockwise direction (odd order of Stokes lines) in the first cavity can be routed from C1 to port 3 of the circulator to oscillate in the second loop in the counter clockwise direction. The circulator functions to ensure unidirectional oscillation in the second loop. The output of the proposed BFL is observed from the 10% port of the output coupler and the remaining power is re-injected into the first cavity and act as a BP for the next even-order Stokes lines. As shown in Figure 5.7, the spacing between two consecutive odd-order Stokes lines is observed to be approximately 0.16 nm (~ 20 MHz in 1560 nm region). The anti-Stokes lines are also observed at wavelengths shorter than the BP, which occurs when various Stokes waves interact with the pump wave through the FWM process. At the BP of 15.3dBm and PCF length of 100 m, 7 lines are observed with the line spacing of 0.16 nm. Only 3 lines are observed with a shorter PCF length of 50 m.

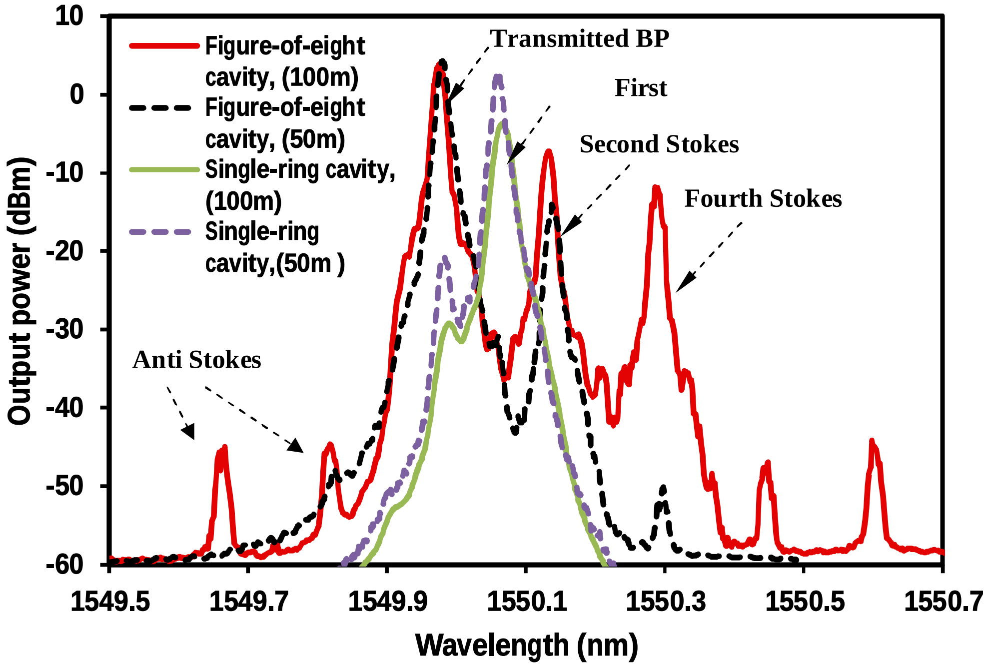

Figure 5. 7**:** Output spectra of the BFL with single ring cavity and figure-of-eight configurations at PCF lengths of 50 m and 100 m. The BP power is fixed at 15.3 dBm.

Figure 5.8 shows the measured peak power for the Stokes at different BP powers for two different lengths of 50 m and 100 m PCF in the proposed figure-of-eight MWBFL configuration. The threshold power is defined as the BP power where the resonator starts to generate laser via SBS and below this threshold power, only spontaneous scattering emission is oscillating in the resonator. As shown in the figure, the peak power increases with the BP power. With PCF length of 100 m, the threshold powers for the 2nd, and 4th order Stokes lines are obtained at about 6.5 dBm and 13.6 dBm respectively. The 2nd Stokes of the conventional ring laser has a threshold power of larger than the maximum BP power of 15.3 dBm and therefore only the 1st Stokes is observed in Figure 5.7. However, with the addition of the secondary cavity in the proposed figure-of-eight cavity we managed to reduce the threshold pump power and thus generate additional Stokes lines without the need to add any linear or nonlinear gain media in the configuration. It was also found that the Stokes power begin to saturate as the BP power increases above a certain level. For instance, with 100 m long PCF, the second Stokes line saturates as the threshold for the fourth Stokes is reached. This is due to the power transfer from the second Stokes to the fourth Stokes, which occurs when the BP power is approximately at 12.1dBm. The threshold power is also observed to be lower when a longer PCF is used.

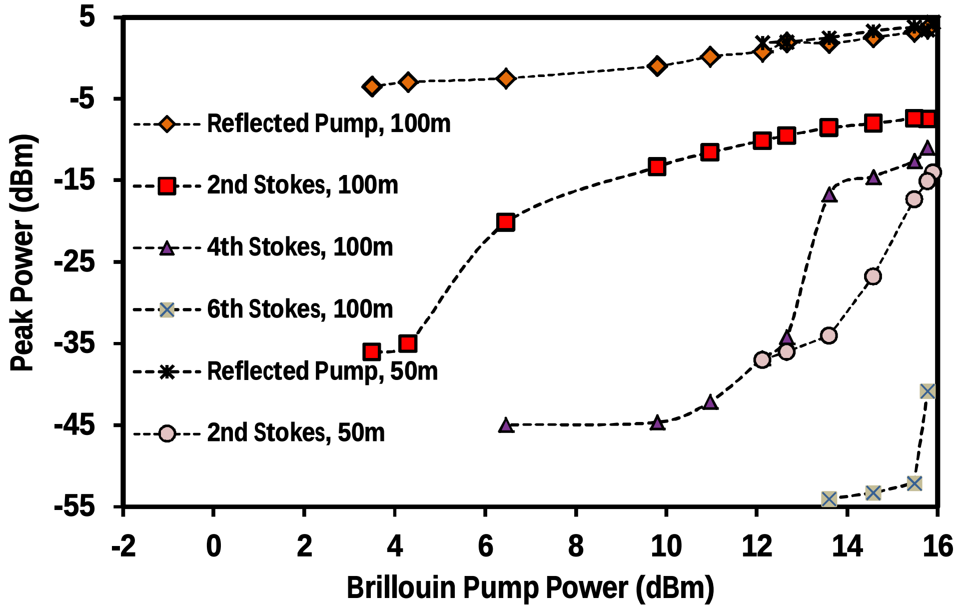

Figure 5.8: Brillouin Stokes power as a function of BP power for the proposed figure-of-eight BFL.

Figure 5.9 illustrates the output spectra of the proposed BFL as the BP wavelength is varied from 1520 nm to 1600 nm. It is found that the output spectrum is maintained over the 80 nm of tuning range. This is attributed to the multiple wavelength operation of the proposed BFL which is solely dependent on the SBS in the PCF but not much dependent on the operating wavelength. As shown in the Figure 5.9, at least 3 even-order Brillouin Stokes lines are obtained at BP power of 12 dBm. This result shows that the proposed BFL has a remarkable advantage that it can provide multi-wavelength operation in a broad band tuning range as long as the BP with the fixed power can be launched into the setup. The stability of the multi-wavelength operation is also investigated since it plays a vital role for practical applications.

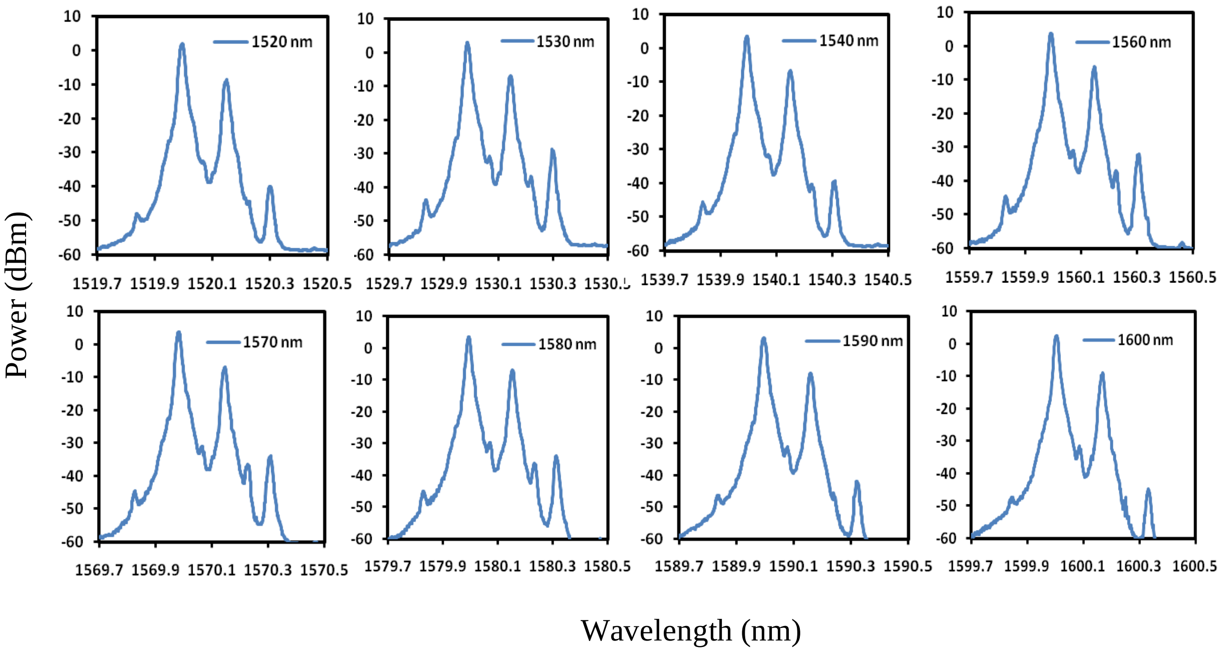

Figure 5. 9: Output Spectra of the tunable MWFBL with 3 Brillouin Stokes lines with 0.16 nm line spacing and over 80 nm tuning range.

Figure 5.10 depicts the spectral evolutions of the proposed multi-wavelength BFL against time. In the experiment, the output spectral is repeatedly scanned for every 20 min. The multi-wavelength BFL lases stably with power fluctuations of less than 0.5 dB for more than 3 hours.Temperature variations and mechanical vibrations were small as the experiment was conducted in a laboratory; thus the drift of the spectral profile was minimal. These results show that the proposed configuration has potentials for applications inthe future WDM optical communication networks.

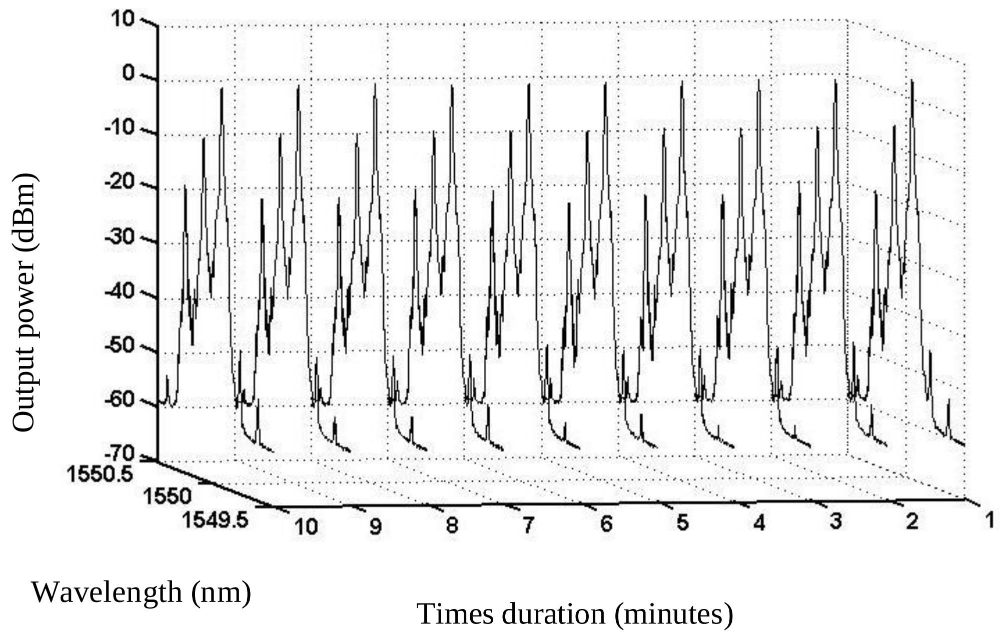

Figure 5.10:Spectral evolutions of the proposed figure-of-eight cavity multi-wavelength BFL against time. (The laser spectra scanned every 20 minutes).

5.4 BEFL with a hybrid gain medium

It was concluded in chapter 3 that multi-wavelength operation cannot be achieved by using only 50 m long PCF. In this section, a 1480 nm pumped Bi-EDF is incorporated in the previous resonator to assist multi-wavelength Brillouin laser generation with 50 m long PCF. This hybrid laser is called Brillouin Erbium Fibre Laser (BEFL). The configuration of the proposed BEFL is illustrated in Figure 5.11. This ring cavity resonator consists of an optical circulator, a 3dB coupler, a 50 m long PCF and 49 cm long Bi-EDF, which is pumped by 1480 nm laser diode via WSC coupler. The BP and 1480 nm pump have maximum powers of 6.1 dBm and 125 mW, respectively. The BP is launched into the PCF via port 1 through port 2 of the optical circulator and 3dB coupler to generate backward-propagating SBS, which oscillates inside the resonator to generate the Brillouin Stokes at wavelength downshifted by 0.08 nm (10 GHz) from the BP wavelength. The backward-propagating Stokes oscillates inside the ring cavity in the clockwise direction to generate another Brillouin Stokes in the opposite direction (counter clockwise). Based on this set up by which the clockwise propagated signals (the odd orders stokes lines) are tapped out via the port 3 of the circulator. The even order Stokes acts as a BP to generate the odd order Stokes and allows multi-wavelength generation using cascading process.

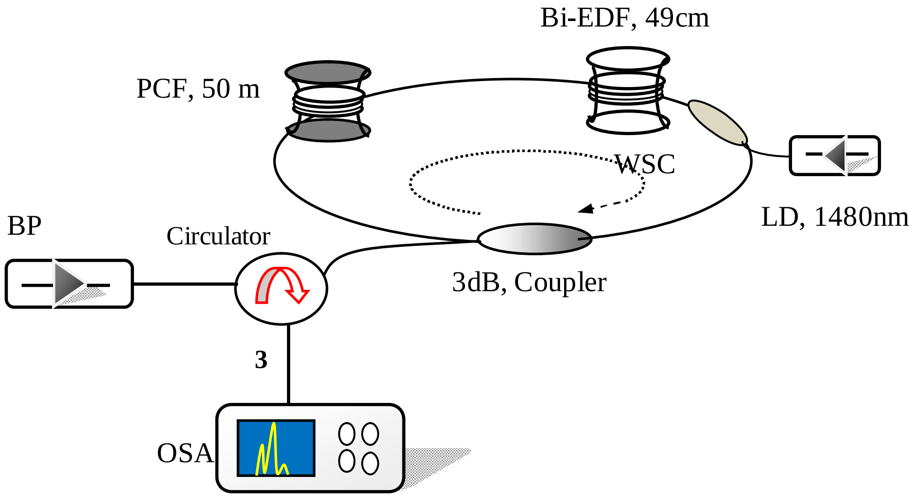

Figure 5. 11: Configuration of the BEFL.

Figure 5.12 shows the output spectra of the BEFL at different 1480 nm pump power. In the experiment, the BP power is fixed at 6.1 dBm and the1480 nm pump power is varied from 19 mW to 125 mW. This Bi-EDF gain amplifies the BP signal that oscillating inside the cavity and passing through 50 m long PCF to generate the first Stokes in the clockwise direction. The first Stokes acts as a pump to generate another Stokes in an opposite direction and this process is repeated to produce even and odd order of Stokes lines. The oscillating signals in clockwise direction, which mainly consists of odd order of Stokes lines are routed to the port 3 of circulator and being monitored by OSA. As shown in Figure 5.12, the number of Stokes increases as the pump power increases and the spacing between two consecutive odd Stokes lines is about 0.16 nm (~ 20 MHz) in 1560 nm region.

The Rayleigh scattered light from even order Stokes lines are also observed in the figure, which shows a significantly reduced peak power compared to the Stokes power. The anti-Stokes lines are also observed in the output spectrum due to the interaction among various Stokes waves and the pump wave via the FWM process. At the maximum 1480 nm pump power of 125 mW, at least three BEFL lines are obtained with line spacing of 0.16 nm. The signal to noise ratio of approximately 21 dB is also achieved for the three odd Stokes lines.

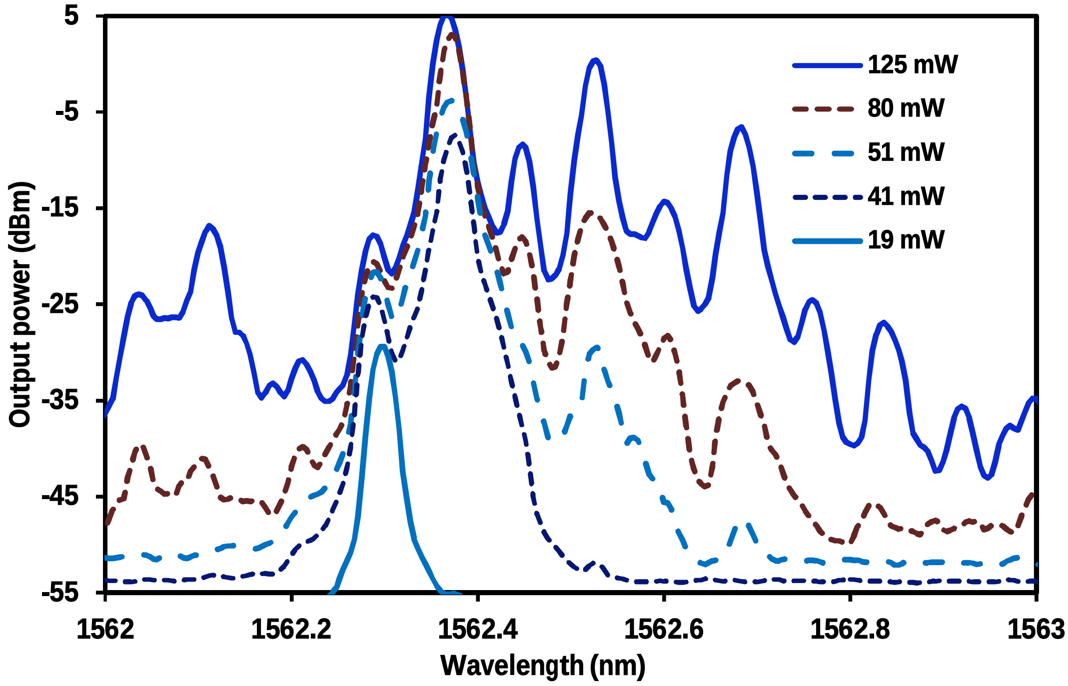

Figure 5. 12: Output spectra of the common ring cavity ring MWBFL of Bi-EDF and PCF hybrid vs different pump power.

Figure 5.13 shows the measured peak power of the Stokes against 1480 nm pump power. As shown in the figure, the peak power increases with the pump power with the thresholds for the 1st, 3rd, 5th, and 7th Stokes lines are obtained at about 31, 41, 63, and 80 mW respectively. The Stokes lines saturate as the 1480 nm pump power is further increased since the pump energy is used to generate next Stokes. For instance, the first Stokes line saturates as the threshold for the second Stokes is reached. This is due to the power transfer from the first Stokes to the second Stokes, which occurs when the BP power is approximately at 41 mW. The actual power transfer can be observed from Figure 5.13 due to invisibility of the even order Stokes lines in the output spectrum.

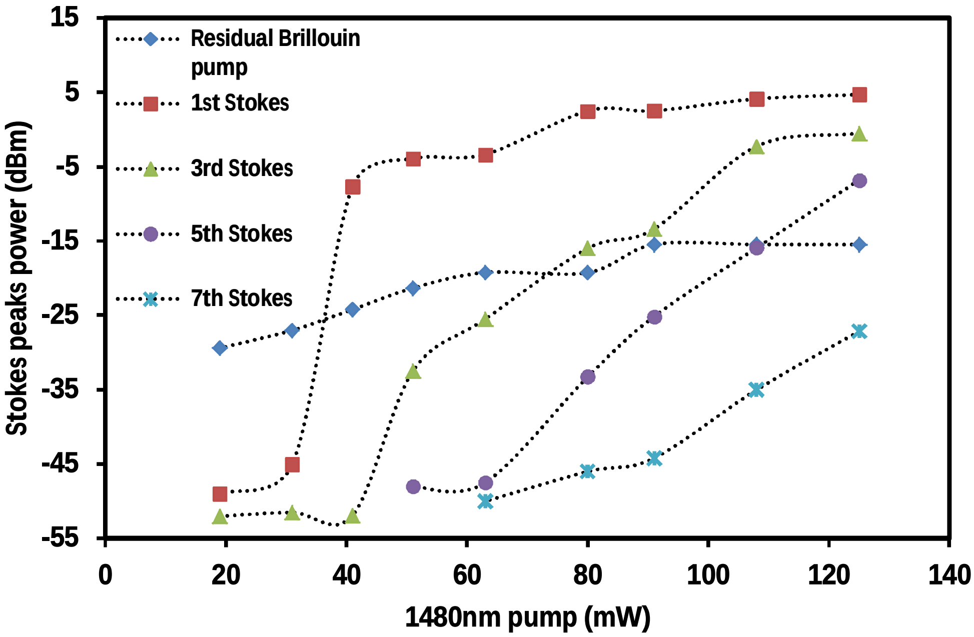

Figure 5. 13: Brillouin Stokes power against 1480 nm pump power for the BEFL.

5.5 Multi-wavelength fibre laser operating in L-band region

In our previous sections, various multi-wavelength lasers have been reported using a SBS effect. However, the spacing of this laser is fixed at 0.08 nm or 0.16 nm, which is very narrow for WDM applications. In this work, a multi-wavelength laser is demonstrated with a larger channel spacing using a FWM effect instead of SBS. To make the device very compact, a Bi-EDF is used as the nonlinear gain medium. As concluded in the previous chapter, 49 cm long Bi-EDF cannot effectively support the FWM process, a 215 cm long

Bi-EDF is used in this study and therefore the operating wavelength of the proposed multi-wavelength Erbium-doped fibre laser (EDFL) is in long wavelength band (L-band) region. The effect of different pumping schemes on the performance of the laser is also investigated. Figures 5.14 (a) and (b) show the configuration of the multi-wavelength EDFL with forward and backward pumping schemes respectively. Both ring resonators consist of a piece of Bi-EDF, tWSC couplers, two isolators, a polarization controller (PC) and a 10 dB output coupler. The 215 cm long Bi-EDF is pumped by a 1480 nm laser diode via the WSC to provide an amplified spontaneous emission (ASE) in L-band region. Two optical isolators are used to ensure a unidirectional operation of the proposed EDFL. A PC has been used to control the polarization and the birefringence inside the cavity, which in turn control the number of line generated, channel spacing and the peak power. The total cavity length of the ring resonator is approximately 7 m. The output of the proposed laser is tapped from the 10% port of the output coupler. The experiment is also repeated with the shorter length of Bi-EDF (49 cm) for comparison purpose. The used two isolators inside the ring cavity can probably be replaced with one higher isolation component.

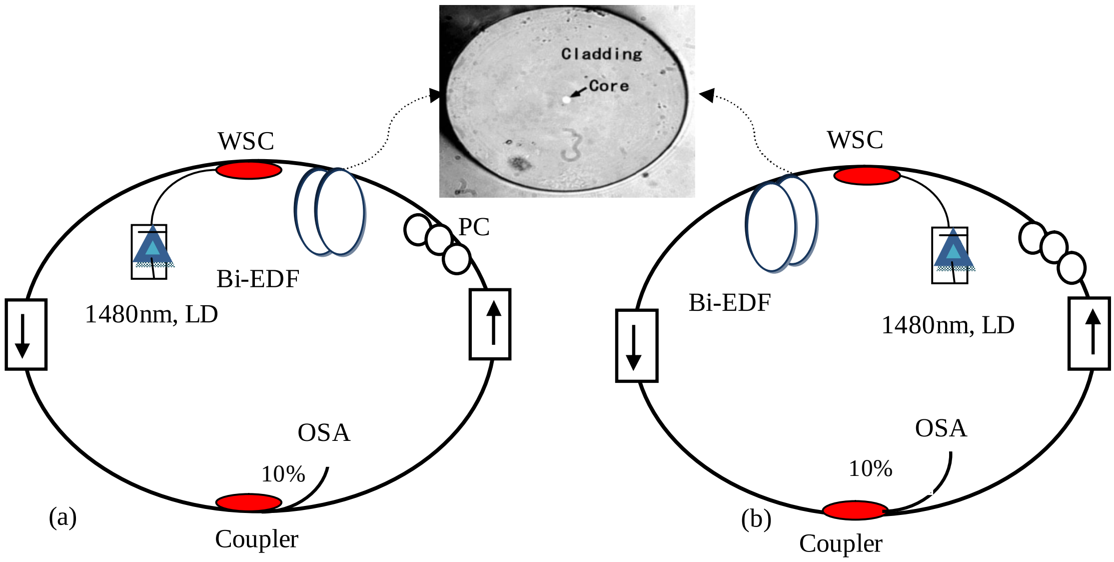

Figure 5. 14: Configurations of the multi-wavelength ring EDFL with (a) backward pumping and (b) forward pumping scheme.

Figure 5.15 compares the output spectrum of the proposed EDFL for different pumping scheme. The 1480 nm pump power is fixed at 147 mW. As shown in the figure, the laser comb is generated at wavelength region of approximately 1613.5 and 1615.5 nm for the forward and backward pumping respectively. The operating wavelength of the EDFL is determined by the Bi-EDF gain spectrum which covers the L-band region from 1560 to 1620 nm as well as the cavity loss. The multi-wavelength comb is generated in the region where the difference between Bi-EDF's gain and cavity loss is the largest. The forward pumping provides a slightly higher gain at shorter wave-length and therefore the operating wavelength of the EDFL moves to a shorter wavelength with the forward pumping. However, the backward pumping generates a higher number of lines compared to the forward pumping. This is attributed to the backward pumping which provides a lower noise in the laser cavity and thus enhances a FWM interaction.

As shown in Figure 5.15, with a backward pumping, the EDFL generates a multi-wavelength laser comb with 17 lines with a channel spacing of 0.41 nm at 1480 nm pump power of 147 mW. The multi-wavelength laser generation with a constant spacing involves erbium amplification and FWM effect processes in the Bi-EDF. The Bi-EDF generates an ASE when it is pumped by a 1480 nm laser. The ASE oscillates in the ring cavity to generate multiple waves due to interference between the longitudinal modes. The waves are amplified and get interact in the Bi-EDF section to create new photons at different frequencies by annihilating photons from these waves.

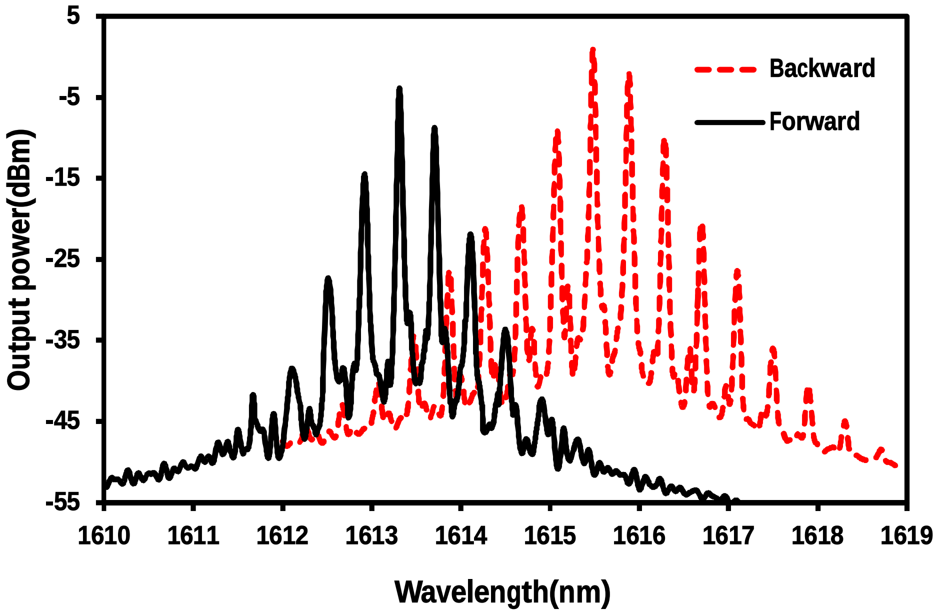

Figure 5. 15: Output spectra of the proposed multi-wavelength EDFL with forward and backward pumping schemes.

Figure 5.16 shows the output spectrum of the EDFL configured with 49cm long Bi-EDF at various 1480 nm pump powers. As shown in the figure, the EDFL operates in 1568 nm region which is within amplification region of the 49cm long Bi-EDF. The number of Stokes is significantly lower compared to that of the L-band EDFL. The signals interact longer in the 215 cm Bi-EDF and therefore the number of lines is higher with this fibre compared to that of EDFL with 49 cm Bi-EDF.

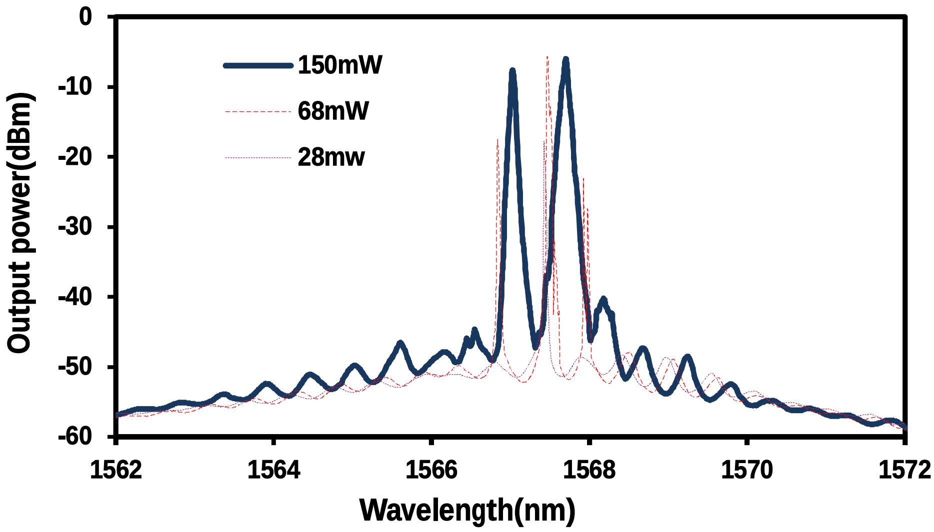

Figure 5.16: Output spectra of the proposed EDFL at various 1480 nm pump power for 49 cm Bi-EDF length.

Figure 5.17 illustrates the peak power of the best 4 lines of laser comb against 1480 nm pump power. The peak power as well as the number of generated lines is observed to increase as the 1480 nm pump power increases. It is also observed that the pump threshold for all lines is roughly 110 mW. At this pump power, the Bi-EDF provides an efficient gain to allow the higher order FWM Stokes to be generated by the assistance of nonlinear gain in the Bi-EDF. Below 1480 nm pump power, the erbium gain is very low and cannot sufficiently compensate for the loss inside the laser cavity and thus no wavelength comb is observed. The number of lines is limited by the availability of the 1480 nm pump power, fibre nonlinearity, and polarization filtering effect in the ring cavity laser as well as the length of the gain medium in the ring resonator. The multi-wavelength output was observed to be stable at room temperature with only minor fluctuations observed according to large temperature variances.

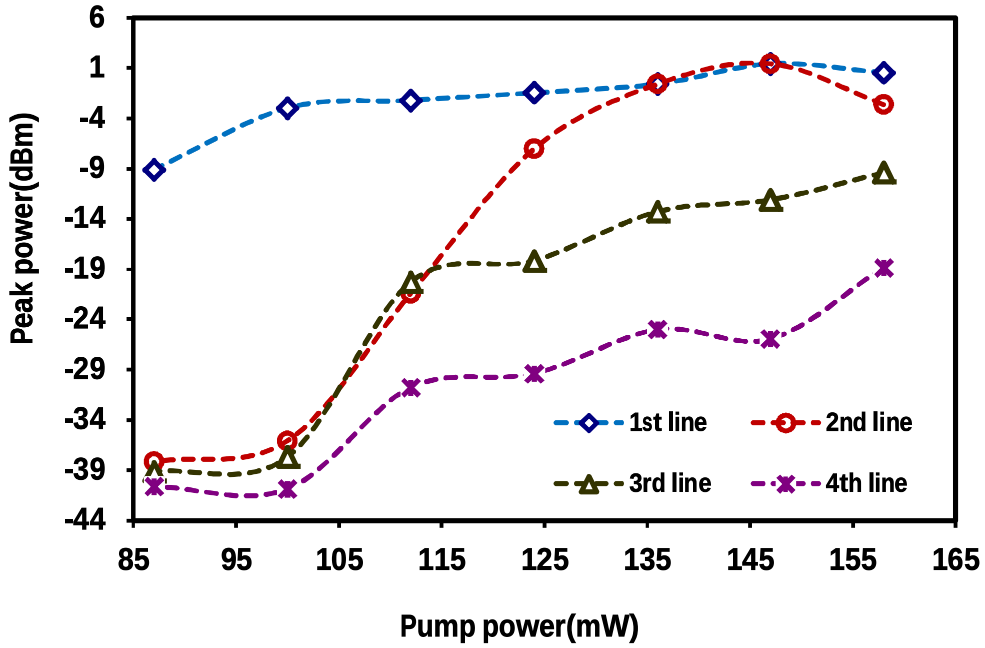

Figure 5. 17: Peak power of the EDFL lines against 1480 nm pump power.

5.5 FWM-based multi-wavelength EDFL with a PCF

As previously discussed, a Bi-EDF has a very high nonlinear characteristic which is suitable for use in compact nonlinear devices. In this section, a FWM-based multi-wavelength laser is demonstrated using a hybrid gain medium, which combines a Bi-EDF and PCF. It was demonstrated in sections 5.2 and 5.3 that a multi-wavelength laser operating in C-band region can be achieved by using a short length of PCF. Here, a FWM-based multi-wavelength EDFL is experimentally demonstrated using a 100 m long PCF in conjunction with a 49 cm long Bi-EDF in a ring configuration. FWM effect is used to suppress the mode competition by transferring the energy into different frequency components. The number of channels and wavelength spacing of the proposed multi-wavelength laser can be flexibly controlled by changing the ratio of the output coupler in the ring configuration.

The schematic diagram of the experimental set-up for the proposed multi-wavelength EDFL is shown in Figure 5.18. The main components are the forward pumped Bi-EDF, a 100 m long of PCF, an isolator, a PC and optical output coupler. The Bi-EDF is pumped by a 1480 nm laser diode with the maximum power of 140 mW to produce ASE operating in 1550 nm region. The ASE oscillates in the ring cavity to generate laser, by which its operation can be control by the external laser. The laser beam from a TLS is injected via an optical circulator to the ring cavity to control the operating wavelength as well as to realize a stable simultaneous multi-wavelength oscillation via FWM process. The TLS signal interacts with the oscillating free running laser in the opposite direction to enhance the phase matching condition and generate FWM Stokes signals. An optical isolator is used to block the TLS signal from oscillating in the cavity and to ensure unidirectional operation of the laser. A PC is used to control the polarization state in the cavity and thus maximize the FWM effect. The output of the EDFL is tapped out from the coupler with a larger portion of the light is allowed to oscillate in the ring cavity. The output spectrum is measured using the OSA.

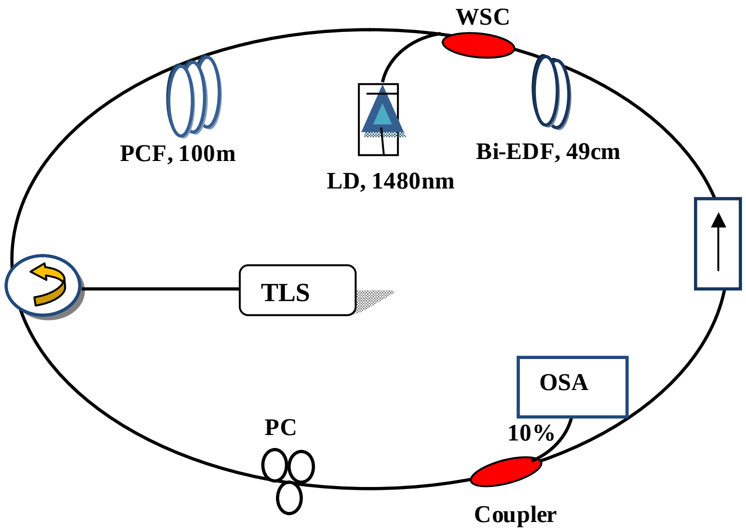

Figure 5. 18: Configuration of the FWM-based multi-wavelength laser with a hybrid gain medium.

Since the conventional EDFLs are homogeneously broadened, different oscillating wavelengths compete to emerge as the dominant wavelength. In the proposed EDFL, the Bi-EDF is mainly used to provide gain while the PCF is employed to suppress the mode competition in the laser cavity so that the simultaneous multi-wavelength operation can be achieved with assistance from the seed signal. Figure 5.19 shows the output spectrum of the laser without the seed TLS signal, which shows a peak wavelength at around 1561 nm. Inset of Figure 5.19 shows the free running spectrum of the Bi-EDF laser which was obtained by removing PCF in the cavity. This figure also demonstrates a random laser oscillation in 1561 nm region. Therefore, in this work, a TLS wavelength is set at 1561 nm.

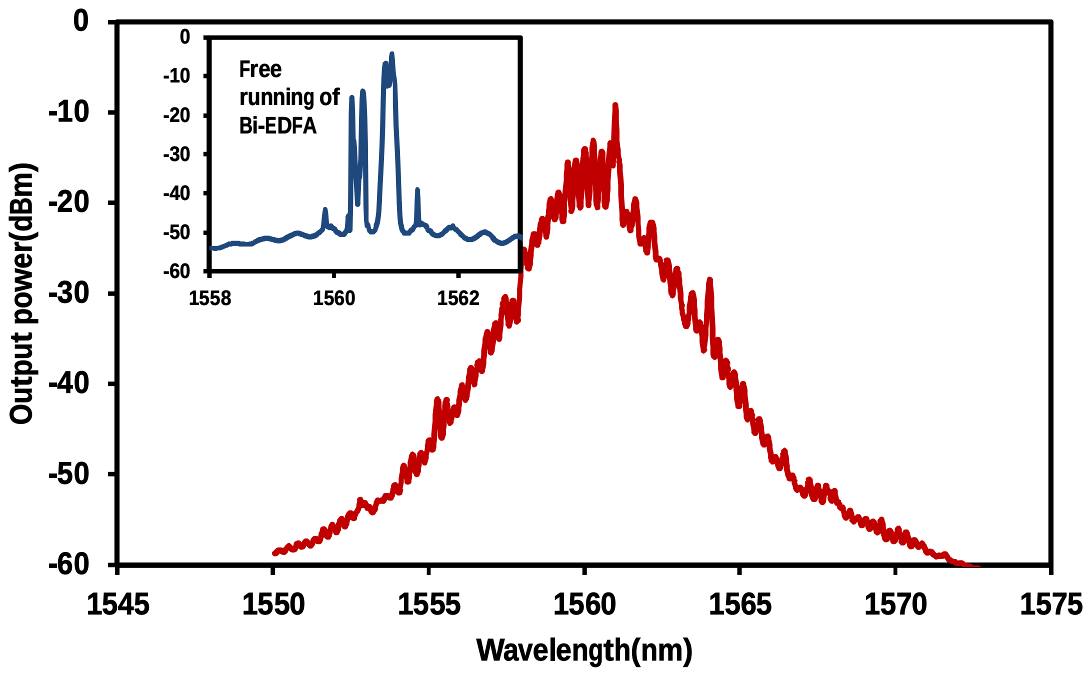

Figure 5. 19: Free running spectrum of the hybrid laser without seed signal. Inset shows the free running Bi-EDF laser.

Figure 5.20 shows the output spectrum of the proposed FWM-based multi-wavelength laser with a seed signal at 1561 nm for various 1480 nm pump powers. In the experiment the 10 dB output coupler is used and the TLS power is fixed at the maximum value of 5.5 dBm. As shown in the figure, at least 5 oscillating laser lines are obtained with a channel spacing of 2.15 nm at the maximum 1480 nm pump power of 140 mW. The signal to noise ratio of these lines is observed to be more than 20 dB. With the use of highly nonlinear PCF in the ring cavity, a wave with stronger energy can transfer part of the energy into another wave with weaker energy via FWM processes (Zhang *et al.*, 2006). This can effectively increase the stability and uniformity of the output multi-wavelength lines due to the self-stability function of FWM effect (Zhang *et al.*, 2006). By adjusting the PC to obtain a proper polarization state, the FWM effect can be maximized and the mode competition in the EDF can be further reduced.

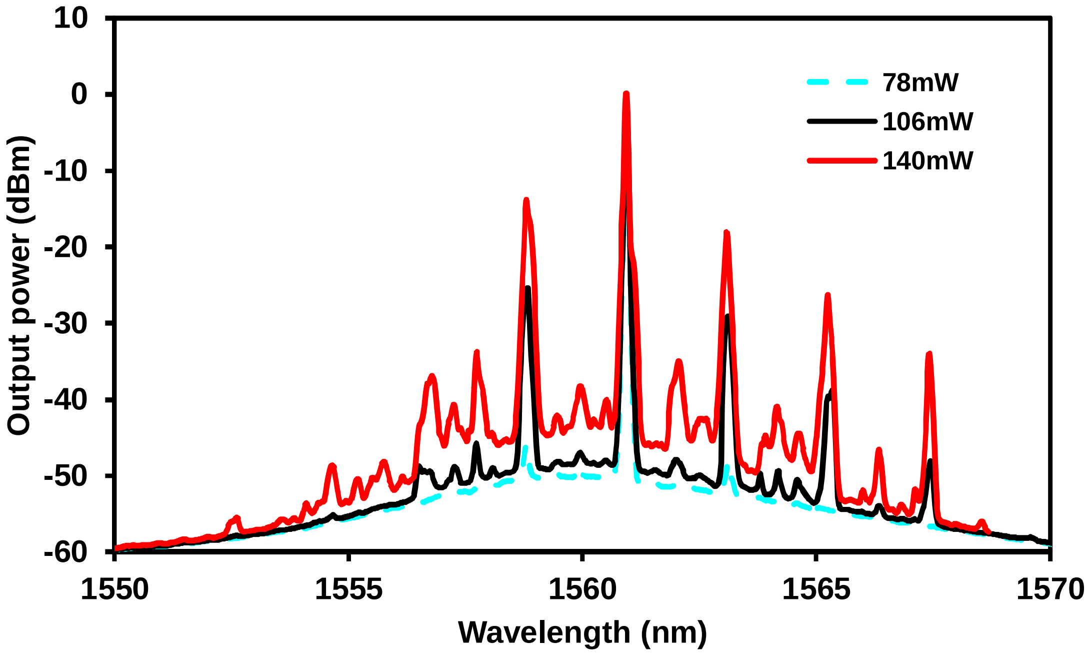

Figure 5. 20: The output spectrum of the multi-wavelength laser at different 1480 nm pump power employing 10 dB coupler as the output coupler.

The number of lines and its flatness are expected to be improved if the FWM effect can be maximized. The FWM efficiency is proportional to the product of γPL, where γ the nonlinear coefficient of the PCF, P is the optical power passing through the PCF and L is the effective length of the PCF. As mentioned earlier, the effectiveness of the FWM can be enhanced by using a longer length of PCF, and/or using a fiber with larger γ, and/or using higher gain and/or a larger saturation power EDFA to get a high cavity power P. In this case we try to incorporate longer length of nonlinear gain media and also more value of γ to enhance the FWM efficiency. It is also observed in Figure 5.20 that the number of oscillating laser lines increases with the 1480 nm pump power, which verifies the above expectation. It is also expected that when a coupler with a different coupling ratio is used, the bandwidth and the spacing between laser output lines will change. Figure 5.21 shows the laser output spectrum at different output couplers. As shown in this figure, the FWM lines of spacing of 1.15, 2.15, and 0.57 nm are dominant with the use of 80/20, 90/10, and 95/5 couplers, respectively. The optimum coupling ratio with the highest signal to noise ratio is obtained with the 90/10 or 10 dB coupler. This may be attributed to the oscillating laser power in the laser cavity, which has been optimized so that the product of γPL is largest in the cavity. The use of 90/10 coupler allows 90% of the light to oscillate in the cavity and thus provide the optimum gain to compensate for the loss in the cavity. Furthermore, the special ratio of coupler can generate sufficient phase matching which also depends on the other factors inside the cavity such as cavity loss and polarization.

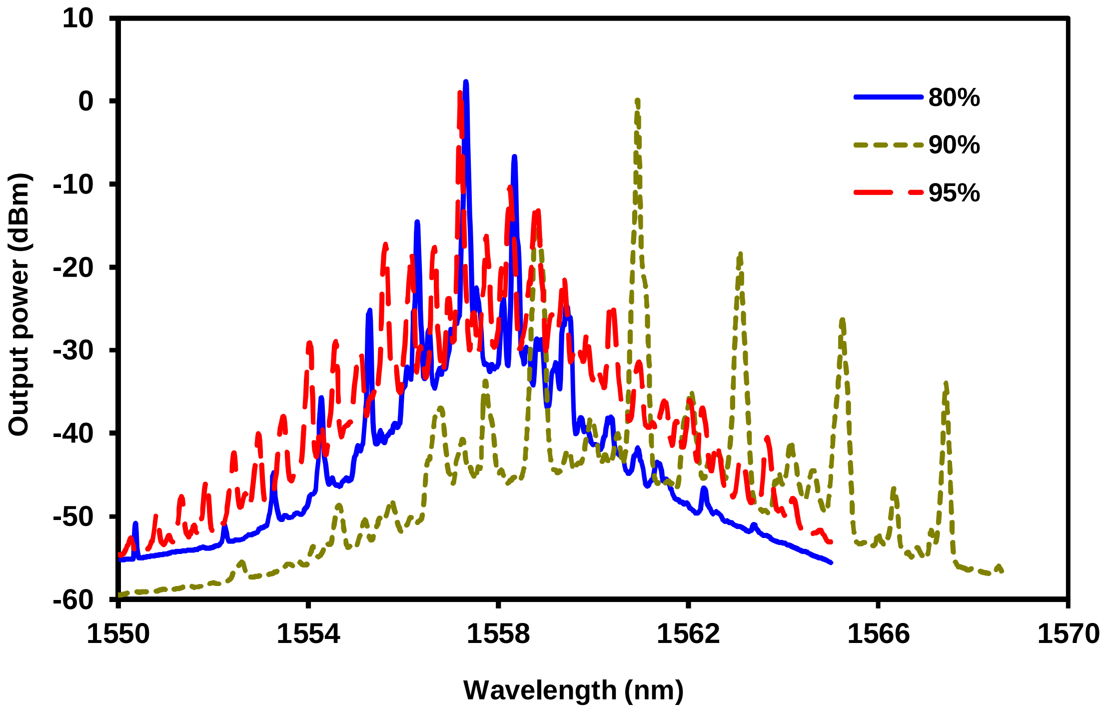

Figure 5. 21: Output spectrum of the FWM-based multi-wavelength laser at different output coupler ratios.

The stability of the multi-wavelength operation is of vital importance for practical applications. Figure 5.22 shows the spectral evolutions of the proposed EDFL with PCF in terms of time. In the experiment, the output spectrum is repeatedly scanned for every10 min. The multi-wavelength EDFL lases stably with power fluctuations of less than 0.5 dB over 2.5 hours. There are two main factors that contribute to the operation instability in the conventional EDFL. They are mode competition in the laser cavity and the drift of the spectral profile as a result of the thermal fluctuation. In the proposed set-up, a 100 m long PCF is used to reduce the mode competition inside the ring cavity via the nonlinear effect. Therefore, multi-wavelength operation may be self-stabilized by taking the combination of PCF and Bi-EDF as a promising candidate for nonlinear and linear gain media. In addition, temperature variations and mechanical vibrations were small as the experiment was conducted in a laboratory; thus the drift of the spectral profile was minimal. These results show that the phase matching condition for FWM in the PCF has been enhanced using a seed signal and a suitable state of polarization in the ring laser cavity. The number of channels and wavelength spacing can be controlled by varying the output coupler ratio. Therefore, the proposed configuration is suitable for multi-wavelength generation. The laser also has a potential in wavelength conversion application for optical communication networks.

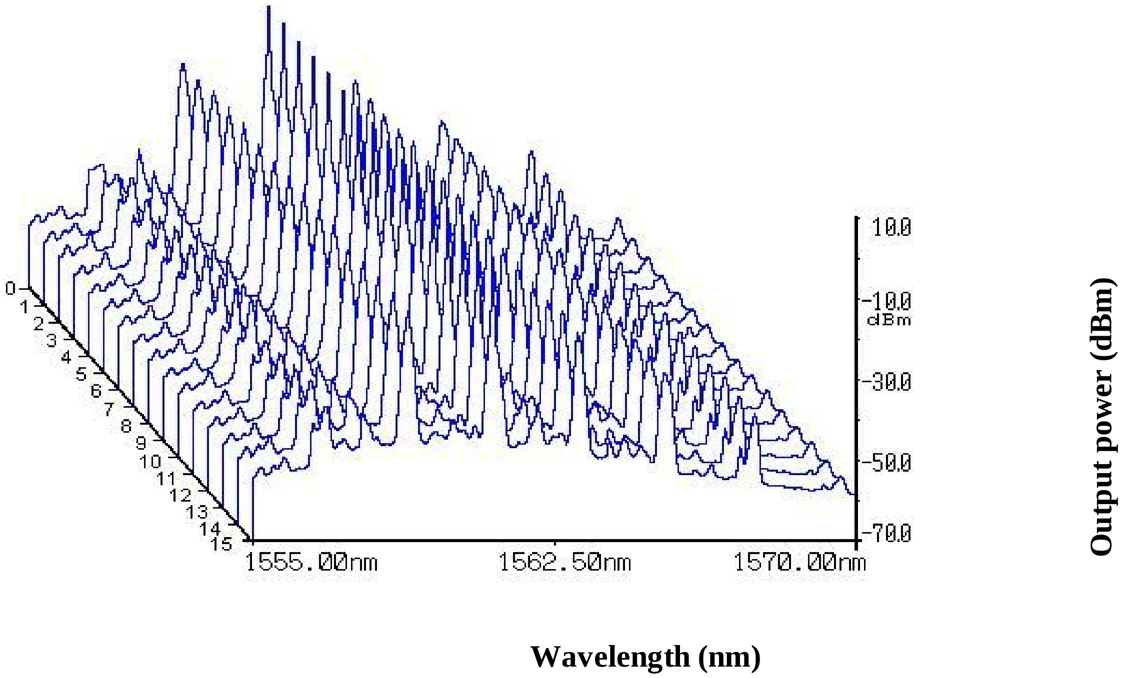

Figure 5. 22: The EDFL output spectrum against time.

5.6 FWM-based multi-wavelength EDFL operating in L-band region

In this section, we investigate the performance of the FWM-based multi-wavelength EDFL with combination of the 49 cm and 215cm long highly nonlinear Bi-EDF as the gain medium. This configuration incorporates two 1480 nm pumps with power of 150 mW and a broadband FBG operating in C band region. The combination of these two gain media has successfully produced a FWM-based multi-wavelength laser operating with injection of a seed signal from a TLS. This laser operates in L-band region due to the use a longer Bi-EDF with a total length of 264 cm. The experimental setup for the proposed new EDFL is illustrated in Figure 5.23. This ring cavity consists of a 49 cm long Bi-EDF, a 215 cm long Bi-EDF, two 1480 nm pump diodes, two WSC, an optical isolator and a TLS which acts as a BP.

The circulator is used to inject the BP into the ring cavity as well as to direct the propagation of Brillouin Stokes line in clockwise direction. The optical isolator is used to ensure a unidirectional operation of the EDFL. A PC has been used to control the polarization and the birefringence inside the cavity, which in turn control the number of line generated, channel spacing and the peak power. A two-stage Bi-EDF amplifier is used to provide an amplification in L-band region. A broadband FBG with a center wavelength of 1545 nm and bandwidth of 40 nm is placed in between the Bi-EDF sections. The FBG functions to allow the BP to reach the second stage and to suppress the backward ASE from the second stage. The output of the laser is extracted from the ring cavity by using a 10 dB coupler while allowing 90% of the power to circulate back into the cavity.

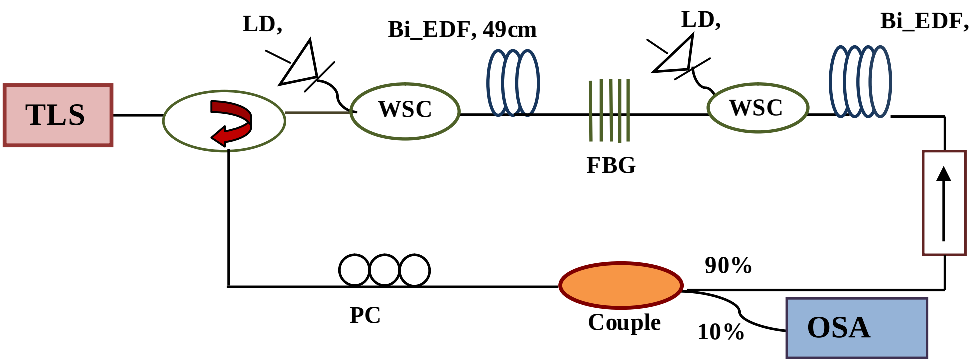

Figure 5. 23**:** Configurations of FWM-based EDFL operating in L-band region.

Figure 5.24 shows the output spectrum of the EDFL at various total 1480 nm pump power. As shown in this figure, a comb spectrum with at least 7 lines with a constant spacing of 0.5 nm is obtained at the maximum pump power. The number of lines increases with the pump power. The strongest line has a peak power of approximately - 5 dBm for total pump powers at 300 mW. The multi-wavelength laser generation with a constant spacing is due to the interaction between the seed signal and the oscillating EDFL via a FWM process. In this process, photons from these waves are annihilated to create new photons at different frequencies. Brillouin Stokes lines are also observed in the output spectrum, which occurs due to the interaction of oscillating light with acoustic waves or vibration phonons. The Brillouin Stokes generation is more pronounced at a higher 1480 nm pump power as shown in Figure 5.24. The long Bi-EDF used (264 cm) provides sufficient Brillouin gain to assist in Stokes generation. The numbers of FWM and SBS lines are limited by the availability of the 1480nm pump power, fibre nonlinearity, polarization filtering effect in the ring cavity laser and the length of the ring cavity laser.

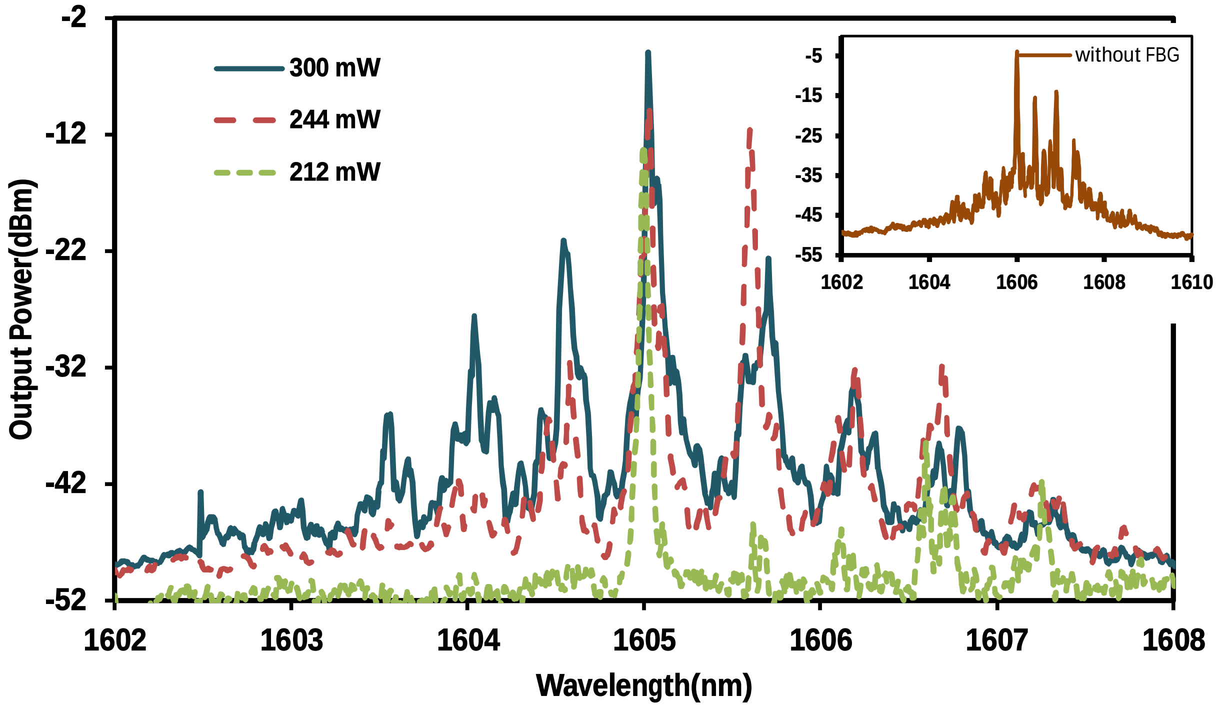

Figure 5. 24: Output spectrum of the EDFL at various 1480 nm total pump power. Inset shows the output spectrum of the EDFL configured without the FBG

The multi-wavelength generation is due to oscillating Bi-EDF laser lines which interacts each other to create new photons at other frequency via FWM process. Without the FBG, only a random laser lines with inconsistent spacing is observed as shown in the inset of Figure 5.24. The broadband FBG reflects the C-band ASE and allows it to intensify and oscillates in the anti-clockwise direction. The ASE suppress the erbium gain as well as the nonlinear gains in the ring cavity and thus disturbs the multi-wavelength generation process.

CHAPTER SIX: CONCLUSIONS AND FUTURE SCOPE OF WORK

6.1 Conclusions

This thesis concentrated on a thorough study on the use of photonic crystal fibre (PCF) and Bismuth-based Erbium-doped fibre (Bi-EDF) for nonlinear fibre laser applications. Various configurations on the continuous-wave (CW) single-wavelength and multi-wavelength fibre lasers have been proposed and demonstrated using either PCF or/and Bi-EDF as a nonlinear gain medium. Nonlinear effects such as the stimulated Brillouin scattering (SBS) and four-wave mixing (FWM) are used in the fibre lasers for generating stimulated fibre laser and multi-wavelength comb lines either through a Brillouin fibre laser (BFL), Brillouin/Erbium fibre laser (BEFL) or FWM-based fibre laser. The aim of these works is to produce a compact and efficient nonlinear fibre lasers using a highly nonlinear fibre. This study involves three main parts; nonlinear characterization of the nonlinear fibres, development of compact nonlinear fibre lasers and advanced configurations of a compact multi-wavelength fibre laser.

Nonlinear Characterization of PCF and Bi-EDF

In chapter 3, a new approach has been described to calculate SBS threshold power provided by a piece of PCF. In this investigation, threshold pump power has been evaluated against fibre length and incident pump power by considering 1% criterion as well as the pump depletion. It is observed that the simulated results are in a good agreement with experiment. The Brillouin threshold gain was also calculated to be varying from 14 to 18 depending on the PCF length. The gain and noise figure characteristics of the Bi-EDFA were also experimentally and theoretically investigated. In the theoretical analysis, the rate and power propagation equations are solved to examine the effect of the fibre length on the bandwidth of the gain spectra. The Bi-EDFA operates in C-band region with the use of 0.49 m long Bi-EDF and the operating wavelength slowly shifts to the L-band region as the length of gain medium increases. The optimum length for the Bi-EDFA to operate in C-band is theoretically around 0.5 to 0.8m. The nonlinear effect inside a piece of 0.5 long Bi-EDF was also experimentally investigated. It is observed that this length was not sufficient to demonstrate both SBS and FWM effects in a common basic configuration without looping.

A simple technique for simultaneous measurements of the nonlinear and dispersion properties of the PCF was presented using a FWM process. A theoretical analysis simulates the experimental conditions and is exploited to determine nonlinear Kerr coefficient, chromatic dispersion and nonlinear phase shift with high accuracy. The nonlinear Kerr coefficient γ and chromatic dispersion are calculated to be about 43 $(\mathrm{Wkm})^{-1}$ and 6.05 ps /nm km respectively at 1560nm for the 100m long PCF. The nonlinear figure-of-merit is obtained at around 0.737 (W^{-1}) that shows that the PCF offer a significant performance in compact nonlinear devices due to its special structure based on air and silica.

Compact nonlinear fibre lasers

In Chapter 4 compact nonlinear fibre laser configurations employing PCF or Bi-EDF were presented. Firstly, a single wavelength conventional BFL is demonstrated using three different length of PCFs as the gain medium. At PCF length of 100 m, the BFL has a peak power of 0dBm which translates to 10% power conversion efficiency with a side mode suppression ratio (SMSR) of more than 30 dB. The spacing between the BP and the Stokes is measured to be approximately 0.08 nm. However the threshold of the BFL is measured to be approximately 9.4 dBm, which is much less compared to the BFL configured with 50 even 20m long PCF. In this study, the Brillouin gain spectrum obtained by both PCF and SMF were also compared. The frequency shift of Brillouin scattering achieved by PCF is around 9.75 GHz whereas it is around 10.83 GHz by employing SMF. This change is probably attributed to the higher amount of Ge_2O_3 is doped in the PCF than the SMF. In order to reduce the threshold power of SBS laser, a new configuration was demonstrated by rearranging the components of the BFL to reduce the cavity loss. The laser thresholds for the conventional and the proposed new BFL are obtained at around 12.7 and 10.4 dBm, respectively and the new BFL has a SMSR of around 31.5 dB, which is nearly 6.3 dB higher compared to the conventional BFL.

To reduce the length of the gain medium of BFL, a single wavelength BEFL is proposed and successfully demonstrated using only a 49-cm Bi-EDF as the gain medium. The BEFL is achieved by reducing and optimization of the cavity loss in the ring configuration. At the BP power of 6 dBm and 1480-nm pump power of 144 mW, the BEFL operates at 1550.49 nm, which is upshifted by nearly 0.09 nm from the BP with a peak power of approximately -4 dBm and an SMSR of 14 dB. The BP wavelength is also tunable within a wavelength range from 1558.8 nm to 1560.0 nm. The generated BEFL has a narrow linewidth, as well as low relative linewith noise and frequency noises, which makes it suitable for sensing applications. To improve the performance of the BEFL, an isolator and PC are included in the enhanced configuration. The enhanced BEFL operates at 1563 nm region to achieve a SMSR of 29 dB when the BP and 1480 nm pump power are fixed at 6 dBm and 144 mW, respectively.

A compact nonlinear fibre laser is also demonstrated based on FWM effect using 49cm long Bi-EDF. By deploying the ring cavity, the EDFL is able to generate a laser comb with more than 5 lines and peak powers above –35 dBm. The channel spacing of 0.5 nm is obtained with the PC in the cavity. The incorporation of broadband FBG in the cavity reduces the noise and enhances the FWM interaction to make the multi-wavelength generation to be more efficient.

Multi-wavelength nonlinear laser generation utilizing advanced configurations

In chapter 5, many new configurations of multi-wavelength fibre laser were demonstrated using either SBS or FWM effect. Firstly, a stable room temperature multi-wavelength lasing oscillation was experimentally demonstrated by exploiting SBS in a short length of PCF in conjunction with dual-pass configuration. Nearly 7 Brillouin Stokes lines with a constant spacing of 0.08 nm are achieved by 15.7 dB BP power and 100 m long PCF. Four anti-Stokes lines are also obtained due to four wave mixing and bidirectional operation. Depending on the BP wavelength and FBG region used, the proposed configuration can work at any wavelength which is the advantage compared to other schemes. When the pump power exceeds the SBS threshold power, it is also revealed that the previous stokes line starts to saturate and thus a flat output lines can be achieved. In order to generate multiwavelength laser with different order of Brillouin spacing, a figure-of-eight configuration is proposed using a 100 m length of PCF. With a BP of 15.3 dBm, at least 4 even-order BFL lines are obtained with a line spacing of 0.16 nm. The anti-Stokes lines are also obtained due to FWM processes. It was found that the output spectrum can be tuned by at least 80 nm, depending on the availability of BP source. The multi-wavelength BFL operates stably with power fluctuations of less than 0.5 dB for more than 3 hours.

In a BEFL, Bi-EDF acts as both nonlinear and linear gain medium. In this study, a 50m long PCF is incorporated as additional nonlinear gain medium PCF besides the 49 cm long Bi-EDF inside the ring BEFL to generate double-spacing Brillouin Stokes lines. With BP and 1480 nm powers of 6 dBm and 125 mW respectively, 4 odd-order lines are obtained with a line spacing of 0.16 nm, which is comparable with the previously proposed figure-of-eight BFL. The thresholds for the 1st, 3rd, 5th, and 7th odd order Stokes lines are obtained at about 31, 41, 63, and 80 mW respectively. To increase the number of lines and channel spacing, a multi-wavelength EDFL was then demonstrated using a piece of 215 cm long Bi-EDF via FWM process in a ring configuration. The proposed FWM-based EDFL is able to generate up to 17 lines with a constant channel spacing of 0.41 nm at 1615.5 nm region using 147 mW of 1480 nm pump power. However, the number of lines reduces to two with the use of 49 cm of Bi-EDF. The proposed multi-wavelength EDFL is stable at room temperature and also compact due to use of only a very short length of gain medium.

A hybrid multi-wavelength EDFL was also experimentally demonstrated at room temperature based on FWM effect using a 100 m long PCF and a forward pumped 49 cm long Bi-EDF. At maximum 1480 nm pump power of 147 mW, 5 lines are stably produced with nearly 2.15 nm spacing between the lines and a signal to noise ratio of more than 20 dB. The phase matching condition for FWM in the PCF has been enhanced using a seed signal and a suitable state of polarization in the ring laser cavity. The number of channels and wavelength spacing can be controlled by varying the output coupler ratio.

It is concluded that a multi-wavelength generation can be easily achieved in a very short length nonlinear fibres such as PCF and Bi-EDF. BFL can obtain a wavelength spacing of either 0.08 or 0.16 nm. If a larger spacing is required, a FWM-based nonlinear laser can be used. The proposed multi-wavelength fibre lasers have many possible applications such as WDM network, sensor and etc.

6.2 Recommendations for future works

For future work, SBS and FWM effects on other types of PCF should be studied. The composition and geometrical structure of different PCF can be tailored to achieve a lower threshold and the maximum gain for both SBS and FWM effects. Since the numbers of channels in the proposed PCF based BFL is limited due to the insufficient incident pump power, the comb generation can be further investigated using more enhanced configurations such as hybrid of two stages or including an amplifier in the structure to boost up the BP. The study should also concentrate on reducing further the length of used nonlinear fibre or to replace the Bi-EDF and PCF with other enhanced rare earth dopant fibres likes Zirconia-Yttria doped fibre that can maintain high flat gain per length coefficient of compact amplifiers.

Furthermore, the multi-wavelength generation should also be investigated using another type of nonlinear effect such as stimulated Raman scattering (SRS). The use of Raman gain to replace Erbium gain in the hybrid BFL or FWM-based laser can be also experimented. Additionally, the compact multi-wavelength fibre laser can be improved with the present of suitable Fibre Bragg Grating (FBG). Highly nonlinear fibres such as Chalcogenide fibre or Bismuth based PCF can also be used as a gain medium. In future work, theoretical works on high efficiency BFL should also be directed towards further improvement of the proposed linear and ring BFL cavities. This investigation should also concentrate on the four-wave mixing and the simulation of close loop BFL configurations which seems to be important factors in determining the threshold condition in the BFL generation. As an active significant area of research in nonlinear fibre optics, it seems that BFLs, MBFLs, and MBEFLs remain as an important issue of the future.